UNIVERSITEIT VAN PRETORIA
UNIVERSITY OF PRETORIA
YUNIBESITHI YA PRETORIA

Department of Mechanical and Aeronautical Engineering

Thermodynamic optimisation of an open-air solar thermal Brayton cycle with fixed temperature constraints

by

Eugene Jansen
27301576

Submitted in partial fulfilment of the requirements for the degree

MASTER OF ENGINEERING (Mechanical)

February 2014

Abstract

Title:	Thermodynamic optimisation of an open-air solar thermal Brayton cycle with fixed temperature constraints
Author:	E. Jansen
Student number:	27301576
Starting date:	8 January 2012
Study leaders:	Dr T Bello-Ochende and Prof JP Meyer

This project mainly focused on the implementation of the second law of thermodynamics relating to the design of heat-exchanging components in an open-air solar thermal Brayton cycle. These components include one or more regenerators (in the form of cross-flow heat exchangers) and the receiver of the parabolic dish where the system heat was absorbed. The generation of entropy is under close investigation since the generation of entropy goes hand in hand with the destruction of exergy, or available work. This phenomenon is caused by two factors, namely the transfer of heat across a finite temperature difference and also the friction that is caused by the flow of a working fluid in a system consisting of components and ducts. The dimensions of some components were used to optimise the cycles under investigation. Entropy Generation Minimisation (EGM) was employed to optimise the system parameters by considering their influence on the total generation of entropy. Various assumptions and constraints were considered and discussed to aid in the solution process, making it simpler in some cases and more feasible in others. The total entropy generation rate and irreversibilities were determined by considering all of the individual components and ducts of the system, and their respective inlet and outlet conditions such as temperature and pressure. The major system parameters were evaluated as functions of the mass flow rate to allow for proper discussion of the system performance. Ultimately, conclusions and recommendations were made, which state the optimum system to be used in this type of solar application, where the amount of net power output is the main driving factor.

Acknowledgements

Honour to Him through Whom all things are possible.

Table of Contents

List of Figures

List of Tables

List of Symbols

English Symbols

Symbol	Meaning	Unit
A	Area	m^2
a	Height of channel/tube	m
b	Width of channel/tube	m
C	Specific heat	J/kg.K
C_w	Ratio of internal to external irreversibilities	
c	Specific heats ratio	
D	Diameter	m
d	Change in	
e	Energy	J
f	Friction factor	
Gr	Grashof number	
H	Total height of regenerators	m
h	Convection coefficient	$W/m^2.K$
h	Enthalpy	J
I	Irreversibility	W
I	Radiation	W/m^2
$\dot{I}$	Irreversibility	W
k	Gas constant	
k	Conduction coefficient	W/m.K
L	Length	m
MT	Micro-turbine number	
m	Mass	kg
$\dot{m}$	Mass flow rate	kg/s
NTU	Number of transfer units	
Nu	Nusselt number	
n	Number of plates/channels	
Pr	Prandtl number	
P	Pressure	Pa
p	Perimeter	m
Q	Heat transferred	J

$\dot{Q}, q$	Heat transfer rate	W
R	Universal gas constant	J/mol.K
Re	Reynolds number	
R_f	Fouling factor	
r	Pressure ratio	
S	Entropy	J/K
$\dot{S}, \dot{s}$	Entropy rate	W/K
s	Entropy	J/K
T	Temperature	K
t	Time	s
t	Thickness of regenerator plates	m
U	Overall heat transfer coefficient	$W/m^2.K$
u	Energy	J
V	Volume	m^3
v	Specific volume	m^3/kg
W	Work	J
$\dot{W}$	Work (rate)	W
X	Exergy	J
$\dot{X}$	Exergy rate	W

Subscripts

Subscript	**Meaning**
a	Absorbed
a	Aperture
aa	Indication of state or position
atm	Atmospheric
CV	Control volume
c	Cross-sectional
circ	Circular
comp	Compressor
D	Diameter
D	Destruction
drop	Drop in value
e	Exit

F	Fuel
gen	Generated
H	High value
H	Hot side
h	Hydraulic
hot	Hotter stream
i	Inlet
in	Inlet
L	Loss
L	Low value
loss	Loss in value
max	Maximum
min	Minimum
net	Net value (When W_{net}= second law of thermodynamics)
net1	First thermodynamic law net value
out	Out
P	Products
p	Constant pressure
p0	Constant pressure
plate	Only 1 channel
rec	Receiver
rect	Rectangular
reg	Regenerator
s	Ideal state
surr	Surroundings
sys	System
T	Measured
T	Temperature
T0	Temperature at earth's surface
th	Thermal
tot	Total
turb	Turbine
v0	Constant volume
w	Wall

0	Ambient
1	Inlet of cycle
1,2,…	Indication of state or position
10	Outlet of cycle
23, 45…	Denotation of duct 2-3, 4-5, etc.
'	Ideal state
∞	Environmental

Superscripts

Superscript	**Meaning**
c	Cold stream
D	Diameter
h	Hot stream
rev	Reversible cycle
solid	Solid material
*	Sun

Greek Symbols

Symbol	**Meaning**	**Unit**
β	Receiver tilt angle	°
δ	Change	
ε	Effectiveness	%
ε	Exergetic efficiency	
η	Efficiency	%
ρ	Density	kg/m^3
ψ	Flow availability	W

Glossary

Aperture	An opening or hole through which light travels.
Closed cycle	A cycle in which the same working fluid leaving the last section of the cycle enters the cycle again at the inlet.
Entropy generation minimisation (EGM)	The process of evaluating all entropy generation processes and individually optimising each system to eventually create an optimised whole when combined.
Entropy	A thermodynamic property used to determine the energy not available for work during a thermodynamic process.
Exergy	In thermodynamics, exergy is the maximum useful work available.
Heat exchanger	A device that transfers heat across a temperature gradient, between two streams that are in thermal contact.
Ideal cycle	A cycle in which the maximum result possible is found due to the absence of losses and irreversibilities.
Irreversibility	Characteristic allocated to a process which cannot be undone once it has run its course.
Isentropic	When a process occurs from start to end without an increase in the entropy, the process is known as being isentropic.
Isothermal	A process which occurs at a constant temperature.
Modularity	The degree to which a system's components may be combined and separated. In context, it describes a system that can be easily integrated into existing set-ups or systems.

Organic fluid	A high molecular mass fluid used in heat transfer processes.
Open cycle	A cycle in which the working fluid leaves the cycle at the outlet and is exhausted/ejected into the ambient.
Pressure ratio	The ratio between the outlet and inlet pressures of components or sections in a system.
Real (non-ideal) cycle	A cycle that includes all known losses and irreversibilities, which produces real, feasible results.
Receiver	The focal point in a solar collector where the sun's rays are focused and the heat and radiation are received.
Regeneration	The process of transferring lost heat to a cold stream before it is used, to improve efficiency.
Regenerator	See 'Heat Exchanger'.
Scalability	The ability of a system or design to be made larger or smaller to provide the same scale of results as the scale at which the original system was altered.
Scattering	The occurrence of the sun's rays being reduced to a smaller finite value by the time it reaches the solar collector. The radiation of the sun is scattered by particles in the air such as water and other impurities.
Selective coating	A coating that is put on solar receivers to increase their efficiency. These coatings have high solar absorbance, low thermal emittance and they are thermally stable, thereby extracting more energy from incident solar radiation.
Solar collector	A device that captures and uses the heat and radiation from the sun's rays. It consists of a dish (or similar) collector and a receiver.

1 Introduction

1.1 Background

The world is entering an age where energy alternatives can make or break populations due to the increasing load that is being set on current energy options. It is a well-known fact that in the next few generations, the world's inhabitants will face serious problems as coal and oil reserves will decrease and the demand for energy will continually increase. For this reason, it is more than acceptable to consider alternative ways of generating electricity, the emphasis of which is the magnitude or capacity that should be covered by energy supplies. Of all the new solutions being considered, sustainable energy systems are the most worthwhile since the reward will be highest. Currently, a major drawback of sustainable energy generation systems is the enormous initial capital needed to properly develop and construct these systems. These systems include wind, tidal, geothermal, solar power and biomass systems. Any one of these systems can prove to be invaluable to modern-day society; however, all of the systems are subject to certain boundary conditions and operating parameters. It is for this reason that solar power seems a viable candidate for further detailed study.

Many parties consider solar technology to be in its pre-adolescent years. However, the sun's rays were utilised to light fires as far back as the seventh century B.C. In the present age, mankind is in possession of some buildings and vehicles such as cars, aircraft and boats that are powered by solar energy. From The History of Solar [1] as presented by the United States of America (U.S.A) Department of Energy, a simple timeline is set up to explain and discuss the evolution of solar power. From this timeline, the major contributors will be emphasised. As mentioned, as far back as the seventh century B.C., mirrors and glass were used to light fires and burn simple objects, such as ants. It is said that the well-known Greek scientist, Archimedes, used an array of polished bronze shields to focus sunlight and set fire to wooden ships from the Roman Empire. Even though no proof exists that this feat did indeed occur, an experiment was conducted by the Greek Navy in 1973, with which a wooden ship was set alight from 50 metres away [1].

As for the history of solar collectors, a Swiss scientist known as Horace de Saussure was credited with the development of the world's first solar collector in 1767. This is the same collector that was used by Sir John Herschel to cook food when he was on expedition to South Africa in the 1830s. An artists' representation of this solar cooker can be found online at [2].

In the 1860s, French mathematician August Mouchet proposed an idea for solar-powered steam engines. In the two decades that followed, he and his assistant, Abel Pifre, constructed what is

believed to be the first solar-powered engines and used them for a variety of applications. These engines were the predecessors to the modern-day parabolic dish collectors [1].

As for the analysis of the whole process, in 1953, Dr. Dan Trivich of the Wayne State University made the first theoretical calculations to determine the efficiencies of various materials in different bandwidths based on the spectrum of the sun [1].

After the paper of photoelectric effect by Albert Einstein in 1905, the majority of work conducted and progress made in solar power up to the 1970s, were in the field of photovoltaic cells [1].

In 1969, the sheer size of solar projects was reborn with the Odeillo solar furnace that can be found in Odeillo, France. This furnace consisted of among others, a parabolic mirror that spanned eight stories high [1].

The U.S.A. Department of Energy, along with an industry consortium, started operating Solar One, seen in Figure 1.1, which is a central receiver system with a 10MW capacity. The project proved the feasibility of such a system, which is also known as a power tower system, and also the feasibility of other concentrating solar power technologies [1].

Figure 1.1 Solar One, Barstow, California [3]

In 1986, the world's largest (at that time) solar thermal facility, located in Kramer Junction in California, was commissioned. This solar field was made up of many rows of mirrors that concentrated the sun's rays and the energy therein onto a system of pipes, which circulated a specific heat transfer fluid. The working fluid turned to steam through the transfer of the collected heat, and the steam was subsequently used to interface with a conventional turbine, with which electricity was generated [1].

An upgrade to Solar One, named Solar Two, was commissioned in 1996. The improved central receiving plant demonstrated how solar energy can be stored efficiently and this brought about the possibility of power being available even when the sun is not shining [1].

To date, many further smaller improvements and investigations have been made to solar power systems, be it solar power towers, parabolic dish collectors or parabolic trough collectors. The extent to which improvements and calculations have been made concerning these systems, leads to the feasibility of further study of these systems [1].

1.2 Motivation

Currently, the majority of the world's energy supply is generated from fossil fuels. The problem, however, is that fossil fuel supply is decreasing, the prices are increasing, the dependence on imports is putting a strain on the global market as only a few countries have significant fossil fuel supplies and so doing control the world economy to some extent. The level of toxic gases being released into the atmosphere as a result of the burning fossil fuels is also a major concern. In today's age, the trend of design is to go green; to decrease the negative effect current processes have on the environment. Solar energy has become just like many other systems, a source of renewable energy whose main advantage is that it does not draw on finite resources that may become too expensive to collect. Solar power proves to be more advantageous than current forms of electricity generation, and has enjoyed much attention in the last couple of years [4].

First of all, solar power alternatives have reduced dependencies on fossil fuels. Even though the sunshine depends on time of day, season and year, a properly sized solar power system can provide a decent stream of energy in the long term. The environmental advantages associated with solar power speak for themselves. Solar power systems have the ability to match peak-time output with peak-time demand meaning solar power can be used to aid the existing power grids when peak loads are experienced. The modularity and scalability mean that the application of solar power technologies is readily scalable and versatile. Solar power plants can be used in many different locations, which reduces the required investment in transport and production. The main problem with location is that a solar farm should be as close to an electric grid as possible, to ease the integration of the different electricity supplies [4].

Previous research and discussions, as above, show that solar power systems are more than a viable replacement for current electricity generation methods. Even though the substitution of one system for another will not happen for many more decades, the need exists for in-depth research into solar power.

1.3 Previous investigations

When considering both the second law of thermodynamics and entropy generation, many different investigations have already been done to date.

Chen et al. [5] compared efficiencies of the Brayton cycle and other cycles and found that the Brayton cycle is worth studying. It was found that Brayton cycles that are combined with regeneration have higher cycle efficiencies than the Brayton cycles that do not. Likewise, a Brayton cycle with a low pressure ratio has a higher efficiency than a Brayton cycle with a higher pressure ratio. Counterflow heat exchangers should be used as regenerators as suggested by Shah [6] and the regenerative Brayton cycle is recommended for solar thermal applications as discussed by Kreith and Kreider [7]. Counterflow heat exchangers find numerous applications in regenerative heating associated with the Brayton cycle [8]. When considering turbo machinery, the micro-turbines from Honeywell are suggested by Shah [6].

The Brayton cycle requires large receivers or cavity receivers due to lower gas heat transfer coefficients, which means the amount of heat that is transferred per volume of working fluid, is not as much as with a Rankine cycle. According to Stine and Harrigan [9], a black solar receiver placed at the focus of a parabolic dish concentrator can be sized such that it absorbs the maximum amount of heat. When selecting a receiver mounted in a cavity and with selective coatings, the convective losses can be reduced by reducing the thermal losses due to radiation. These selective coatings include compositions such as Luz Cermet, Lux Black Chrome, Solel Uvac, Schott and Goal [10]. Shuai et al. [11] investigated many different cavity geometries. Prakash et al. [12] found that thermal losses (energy loss through conduction, convection and radiation) and optical losses (energy loss occurring in the atmosphere, typically but not limited to scattering, pollution and other impurities in the air, transmittance and receiver absorption) from an open-cavity receiver were less than the losses of other receiver types, such as linear omnidirectional receivers [13], volumetric pressurised receivers [14] and solar particle receivers [15]. Reddy and Sendhil Kumar [16] found that the modified cavity receiver was better suited for solar dish collector systems. Reddy and Sendhil Kumar also numerically investigated the natural convective heat loss [17], an inclusion of the contribution of radiation losses [16] and an improved model for natural convection heat loss for the modified cavity receiver [18].

Bejan [8] states that the irreversibilities of convective heat transfer are due to the heat transfer across a non-zero temperature difference, and fluid friction. Yilmaz et al. [19] included the losses due to heat exchange with the environment for a heat exchanger. Bejan [8] proposed ways of reducing irreversibilities in heat exchangers. He also showed that three main features cause irreversibilities in a solar receiver, namely the sun receiver heat exchange, receiver ambient heat loss and the internal irreversibility in the receiver.

Bejan [20] showed that the optimal receiver temperature for maximum power per unit area can be determined in three ways, namely by maximising the net power output, by minimising the

entropy generation rate or by maximising the exergy streaming. According to the Gouy-Stodola theorem, the maximisation of exergy output is equivalent to the minimisation of entropy generation. Entropy generation minimisation (EGM) has been used in various internal flow optimisation studies. Entropy generation and the minimisation thereof have been expressed for numerous heat exchangers and heat transfer surfaces as discussed by Le Roux et al. [21]. Hesselgreaves [22] suggests the use of the ε-NTU method for calculating the outlet temperatures and the total heat transfer from the hot fluid to the cold fluid. Heat exchanger optimisation via EGM has been used in numerous applications.

Narenda et al. [23] and Jubeh [24] performed exergetic analyses in solar thermal applications. These analyses were done for a solar thermal Rankine heat engine and a regenerative Brayton cycle with isothermal heat addition and isentropic compressor and turbine. Many authors discussed the importance of the optimisation of the system as a whole, instead of optimising components individually [21]. It is important to consider the individual optimisation of components within a cycle as it is sure to give a proper breakdown of all applicable areas of concern, meaning all the phases or parts in a cycle where improvements can be made to lower the sum of all the losses within the cycle. However, as a researcher, one cannot help but wonder if this process would be time and resource consuming. Therefore a simpler method of cycle optimisation can also be considered. The comparison between the two aforementioned optimisation strategies should give a good overview of the cycle's operational characteristics.

It is very important to note that the work covered in this dissertation follows that of the work of Le Roux, Bello-Ochende and Meyer, which is summarised in Le Roux et al. [21]. Thus there are similarities in the background work considered and the methodology behind the optimisation of the systems. The importance lies therein that the systems considered in this dissertation are more complex than those of Le Roux et al. [21], and contain clear differences and improvements. These differences and improvements brought about by the new systems are closely considered and discussed in this dissertation.

1.4 Objectives

A solar thermal power cycle is under investigation and the system needs to be optimised in terms of its components so that the net power extracted from the cycle is at a maximum. To accomplish this, the second law of thermodynamics as well as entropy generation minimisation (EGM) must be applied. In a Brayton cycle with a micro-turbine, compressor, solar receiver and regenerators, the entire system is solved as a whole instead of each separate component being investigated. The micro-turbine is chosen to operate at its highest efficiency and the regenerators'

dimensions will be optimised to ensure that the result of the maximum net power/work output supplies a set of fixed, optimal dimensions for the components under investigation. As far as the solar collector is concerned, a modified cavity receiver will be used as explained in more detail later on.

As part of this dissertation, the cycle that will be investigated is the solar thermal Brayton cycle with a few modifications. The cycle will consist of a primary and secondary loop with a compressor and turbine present in each of the loops. The heat is transferred from the primary to the secondary cycle by means of a regenerator. The excess heat present in the outlet air of the secondary cycle is transferred to another point in the secondary cycle by means of a second regenerator.

Standard micro-compressors and micro-turbines are used in the analysis, which makes the regenerators' dimensions more important. Optimisation is carried out by considering the points at which the gradients of the parameter functions equal zero. Ultimately, recommendations and conclusions will be made concerning the two systems that are investigated.

2 Literature study

2.1 Introduction

The first step in any engineering analysis is to get a proper understanding of the problem at hand and of the best methods known with which the said problem can be solved. In this chapter, an in-depth literature study is conducted to investigate every last detail of the project. This enables the engineer to synthesise proper methods with which the system can be solved. Thermal power systems are investigated to find the theoretical best choice. The second law of thermodynamics, entropy generation and exergy for thermal cycles are investigated. Solar collectors are discussed since the collector is the single most important component of the system at hand. Again exergetic analysis procedures are investigated. Since this dissertation is as much about the optimisation as anything else, the irreversibilities and losses that are present in the system are also discussed.

2.2 Thermal power cycles

2.2.1 The Brayton cycle (air-standard cycle)

2.2.1.1 The ideal and non-ideal cycle

The Brayton cycle is regarded as the backbone of power generation. Usually, the Brayton cycle consists of a compressor, combustion chamber and a turbine. The Brayton cycle can be either an open or closed cycle.

Fresh air from the ambient enters the compressor where its temperature and pressure are increased. The high-pressure air then proceeds to the combustion chamber where it is saturated with a combustor, which aids in the constant pressure burning of the air. The high-temperature air then proceeds to the turbine where it passes through a series of blade formations and where the air expands to atmospheric pressure through a row of nozzle vanes. This causes the turbine blades to spin, which, in turn, leads to the rotation of a shaft in a generator. This rotation through an electromagnetic coil then generates current. For an open cycle, the exhaust gases that leave the cycle are not re-circulated. For a closed cycle, the turbine outlet gases become the compressor inlet gases [25].

The Brayton cycle is ideally a simple gas turbine cycle. Figure 2.1 shows the basic set-up of the Brayton cycle.

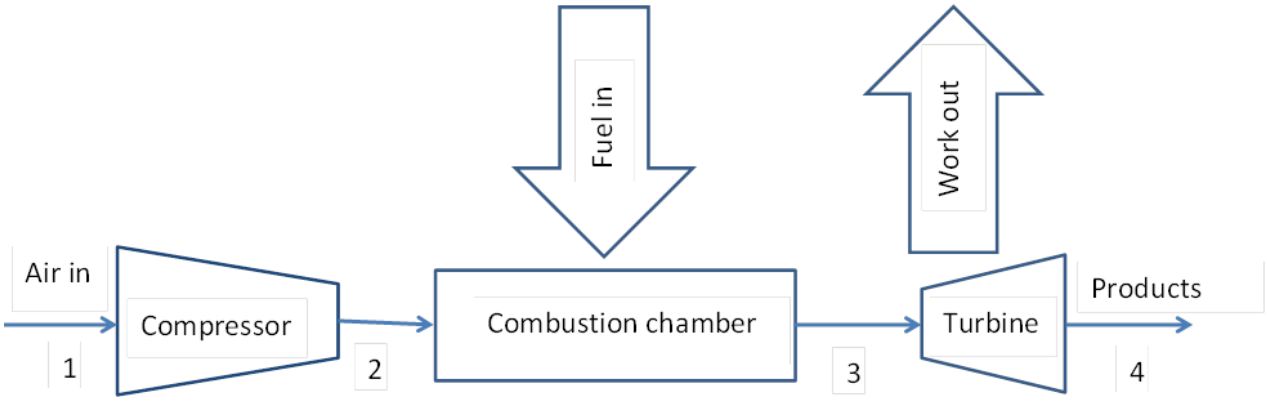

Figure 2.1 The air standard Brayton cycle

The numbering in Figure 2.1 was included in order to help explain the T-s and P-v diagrams in Figure 2.2.

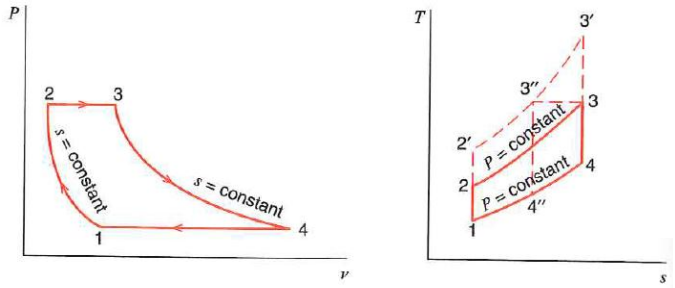

(a) (b)

Figure 2.2 Properties of the air standard Brayton cycle [26]. a) Pressure as a function of the specific volume (P-v diagram) and b) Temperature as a function of entropy (T-s diagram).

In Figure 2.2 it is noted that the pressure at the inlet and outlet of the cycle has the same value, which makes perfect sense as the air entering the system is at atmospheric pressure and the air then exits the system at atmospheric pressure once again. Also the flow through the combustion chamber occurs at constant pressure. This is a major characteristic of an ideal cycle. The entropy stays constant for the flow through the compressor and the turbine respectively. In Figure 2.2.b) the standard Brayton cycle is represented by 1-2-3-4-1. When the pressure ratio of the cycle is increased, the T-s diagram changes to 1-2'-3'-4-1. The aforementioned cycle has a higher heat supply while still rejecting the same amount as the first cycle; therefore it has a greater efficiency. The maximum temperature in the cycle also increased from 3 to 3'. Unfortunately, this maximum temperature cannot be increased without being constrained by the cycle material properties. If this maximum temperature is fixed at the original value as at point 3, the cycle will be 1-2-3"-4"-1, in which case the cycle has a higher efficiency than the original cycle, as the temperature at point 2' is much higher than at point 2. The ideal cycle was evaluated in full detail by Sontagg, Borgnakke and Van Wylen [26].

However, for this project, the non-ideal cycle is more important as it includes irreversibilities. These irreversibilities occur in the compressor, turbine, combustion process and all ductwork, and are influenced by the pressure drop in the flow passages between all of the hardware in the Brayton cycle as well as the combustion chamber. When the irreversibilities are taken into account, the T-s diagram changes to that in Figure 2.3 as below:

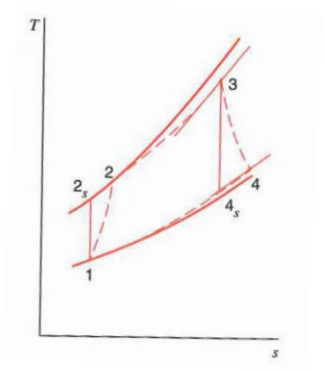

Figure 2.3 Effect of irreversibilities on the gas turbine cycle [26]

The influence of irreversibilities is apparent when Figures 2.2 and 2.3 are compared. In Figure 2.3 the simple (ideal) cycle is now denoted by 1-2s-3-4s. When compared to the actual (real) cycle, represented by 1-2-3-4, it shows that the latter does not consist of constant entropy processes through the compressor and turbine, but rather experiences losses which reduces the overall cycle efficiency. When considering the cycle, it is known that the compressor work is very large when compared to the turbine work. Considering this, it is also known that both compressor and turbine efficiencies should be more than at least 60% to ensure that the entire system overall efficiency is more than zero (0%) [26].

2.2.1.2 The Brayton cycle with regeneration

Even though the cycles already discussed function to some extent, it is the function and purpose of an engineer to improve the efficiencies of these cycles to the maximum values possible. A regenerator improves the efficiency of the gas turbine cycle. Figure 2.4 is a simple schematic diagram to show the integration of a regenerator into the Brayton cycle (or simple gas turbine cycle).

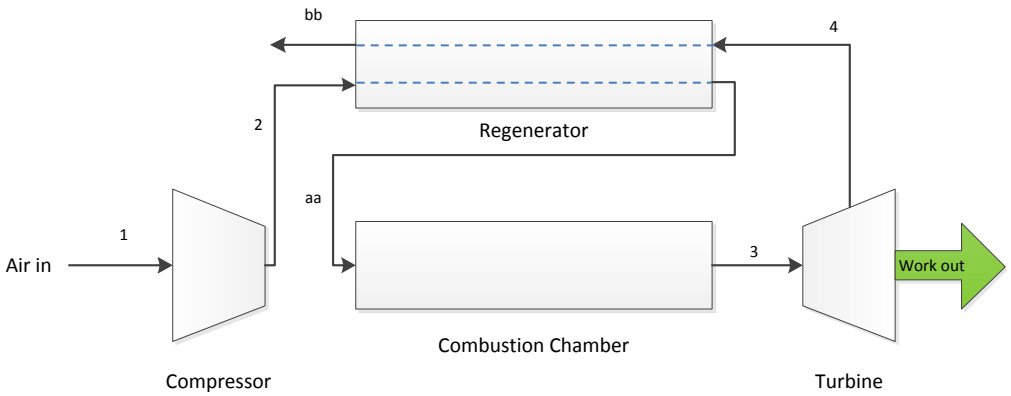

Figure 2.4 Brayton cycle with regenerator

Since the regenerator acts as a cross-flow heat exchanger between the flows coming from the compressor and the turbine, it is easy to realise that the efficiency can be increased when the area of the heat exchanger is increased. However, it is known that with an increase in this area, the pressure drop will also increase, resulting in higher losses. Thus, an optimum configuration for heat exchanger area must be found to ensure the best overall efficiency for the cycle under discussion [27].

2.2.2 The Rankine cycle

The Rankine cycle is also known as the Clausius-Rankine cycle. The working fluid in a conventional Ranking cycle is steam; however organic fluids can be used instead of steam; in which case the cycle is called an Organic Rankine cycle. Some of these working organic fluids are silicone oils, hydrocarbons and fluorocarbons. [27].

The internal components of the organic cycle are exactly the same as those of the normal Clausius Rankine cycle and can be seen in Figure 2.5.

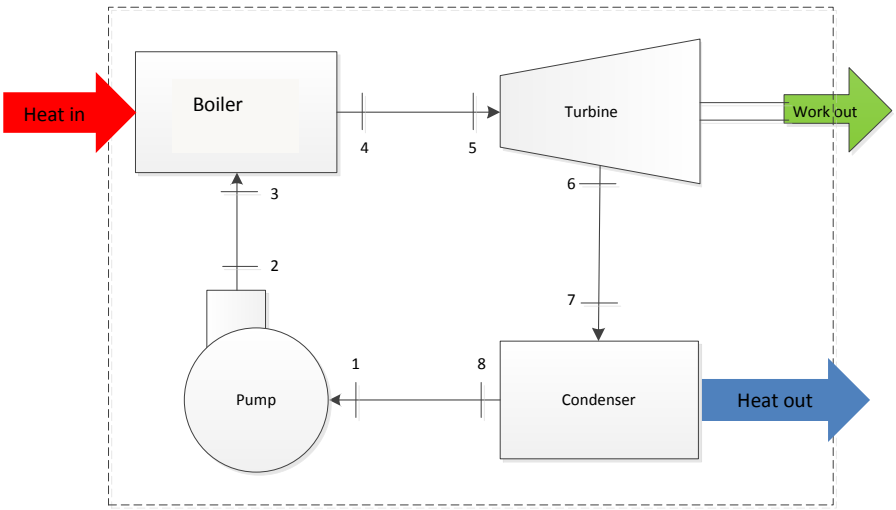

Figure 2.5 The basic Rankine cycle

At present, the organic Rankine cycle is mainly used for electricity production from biomass and geothermal heat. Power generation scales typically vary from 500 kW to 1,500 kW with electric efficiencies in the order of 10 to 12% when a regenerator is employed. Organic Rankine cycles are also suitable for waste-heat recovery and power production from solar thermal heat. These applications are yet to be investigated in detail and are subjects of further study. When considering the organic Rankine cycle, it is known that when linked with reverse osmosis, the cycle is a favourable choice for seawater desalination [27]. The main advantage of the organic Rankine cycle is that it is best suited in cases where power needs to be produced from low-temperature heat, which makes it a promising choice for the concentrated solar system that is under investigation in this dissertation.

A performance analysis was done by Müller and Fréchette [28] on the Brayton and Rankine microsystems. Even though the sheer size of the investigation was not the same as in normal investigations, the recommendation for the Rankine cycle set-up is applicable. The said recommendation is for a Rankine cycle to have a pump, turbine, condenser and heat source, which normally is a boiler, but can also be a solar collector.

A similar recommendation is made by Kapooria et al. [29] and Spliethoff and Schuster [27]. In the work of Spliethoff and Schuster [27], however, a second configuration of the Rankine cycle is suggested, where a regenerator is integrated into the cycle. This configuration is shown in Figure 2.6.

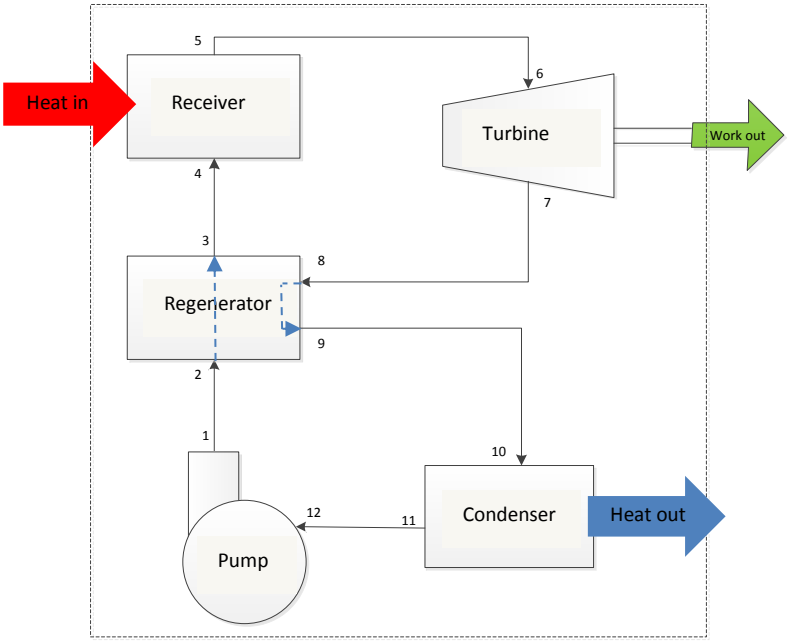

Figure 2.6 The Rankine cycle with a regenerator

As can be seen in Figure 2.6, the stream exiting the turbine is rerouted to the regenerator where it can transfer heat to the stream moving between the pump and the heat source, which in this case is the receiver.

In Kapooria et al. [29], an alternative configuration is recommended. This configuration is known mainly as a reheat cycle. This entails a few differences from the original Rankine cycle such as a two-stage turbine, and the stream moving back to the heat source in between the two turbines. Figure 2.7 illustrates this point.

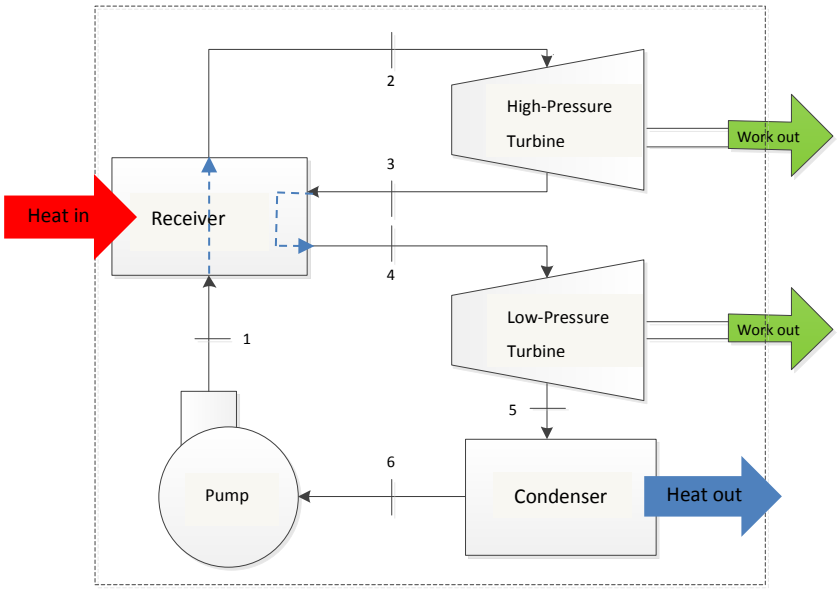

Figure 2.7 The Rankine reheat cycle

In Sonntag et al. [26], the cycle as in Figure 2.5 is suggested as an easy-to-solve cycle when considering the ideal Rankine cycle. A reheat cycle is also suggested as it has been proved to take advantage of the increased efficiency with higher pressures. This cycle is illustrated in Figure 2.7. A regenerative Rankine cycle, as in Figure 2.6, is also discussed. A Rankine cycle with an integrated open feedwater heater enjoys attention in the text as well. The purpose of the feedwater heater in the cycle is to extract some of the vapour after the partial expansion in the turbine, and so doing further increase the cycle's efficiency.

2.2.3 The Stirling cycle

The Stirling engine utilises the Stirling cycle and is currently used in specialised applications such as submarines or as auxiliary power generators for yachts, in which case, it is important to have quiet operation. The cycle uses an external heat source such as fossil fuels or solar power. The Stirling cycle runs without emissions provided that heat is not provided to the cycle by means of burning

fossil fuels. Unlike an internal combustion engine, no explosions take place inside the engine, thus making it very quiet [30]. Figure 2.8 shows a schematic diagram of the components of a Stirling engine.

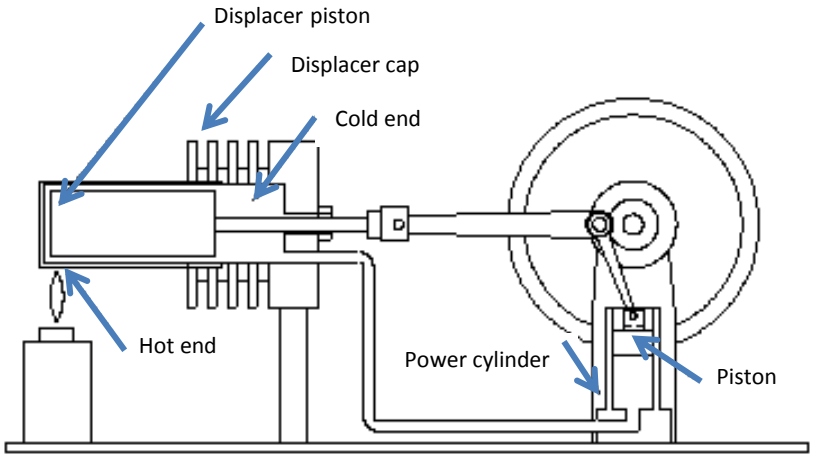

Figure 2.8 Schematic diagram of a Stirling engine [31]

The process in Figure 2.8 is as follows: the hot end is used to heat gas which in turn expands and moves a displacer piston towards the cold end of the displacer cap. The movement of the displacer piston in turn creates linear movement of a piston inside the power cylinder. This linear movement is translated to rotational movement by means of a crank linkage system. The rotational movement is connected to the displacement piston by means of another linkage. This completes the Stirling cycle.

Stirling engines are widely used and this is evident in an article discussing the usage of a Stirling engine/solar dish technology in what is possibly the largest solar power generation field in the U.S.A. up to date [32].

Bowyer [33] describes how Stirling engines are proposed for small solar power applications, typically, those whose power generation ranges from 10 to 100 kW in magnitude. This means they can be designed to have the same efficiency as the ideal Carnot cycle.

Whilst comparing Stirling engines to the main focus of their study, namely ORC's, Spliethoff and Schuster [27] suggest that the Stirling cycle efficiency ranges from 11 to 15%. As for the Stirling engine itself, its efficiency in solar applications vary with different concentrators, different size concentrators, different topographical locations, different cycles etc. There are thus too many external influences on the Stirling engine efficiency to allow the feasible assumption of a typical efficiency value.

Stine and Harrigan [9] suggest that the Stirling engine has a high cycle efficiency potential, which leads to their preferred use in low power ranges, typically 10 to 100 kW. Some disadvantages

are known for the Stirling engine such as the losses brought about by the sinusoidal piston motion, dead volume and also the lack in regeneration. Another cause of inefficiency in the Stirling cycle is that not all gas in the engine participates in the cycle. Stine and Harrigan also describe the four processes of an ideal Stirling engine as seen in Figure 2.9.

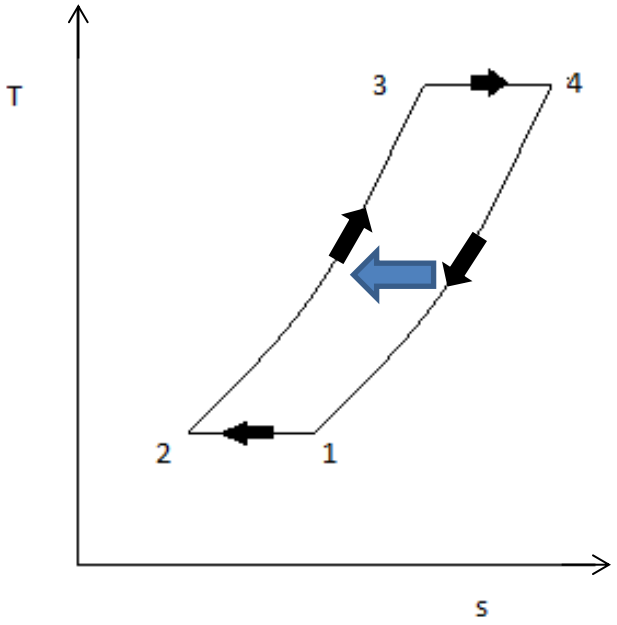

Figure 2.9 The processes for an ideal Stirling cycle

These processes consist of two constant-temperature and two constant-specific volume stages. Isothermal compression takes place from 1 to 2, where after constant-volume heat addition occurs with no work being done as shown by 2 to 3. Following this is a constant-temperature expansion process from 3 to 4 where work is done by the working fluid as heat is added. Finally, constant-volume heat rejection occurs from 4 to 1 where once again no work is done. The Stirling cycle is also regenerative from 4-1 to 2-3 as indicated by the blue arrow. Because more work is done by expanding an amount of gas at a higher temperature than at a lower temperature, the Stirling engine produces a net amount of work. By eliminating the need to transfer heat from sources at temperatures other than the cycle's maximum and minimum temperatures, the regenerative Stirling cycle will have the same efficiency as a Carnot cycle. The only difference between the Stirling and Carnot cycles is that there is no heat transfer from 2 to 3 and from 1 to 4 in the Carnot cycle.

As suggested by Martini [34], the effect of the dead volume is to decrease the work done per cycle. This work done has an almost linear relationship to the dead volume in the engine. To determine the cycle efficiency and influence of dead volume on the Stirling engine involves a numerical analysis, for which Martini [34] and Urieli and Berchowitz [35] can be studied for specific examples.

2.2.4 Comparison of power generation cycles

When considering the three different power cycles described, a simple comparison can be made to aid in the assessment of the applicability of each cycle to the problem at hand. This helps the author choose a feasible cycle, and helps the reader realise why the respective choice was made.

Table 2.1 Comparison of power cycles

Power cycle	Advantages	Disadvantages	Efficiency range [27]	Power generation scale [27]
Brayton	• Can use air as working fluid • High efficiency • Small and large scale • Low-pressure ratios when regeneration is used	• Irreversibilities occur due to pressure losses • Large compressor work compared with turbine work • Large receivers for sufficient heat input	16-52 %	1 - 1, 000 MW (When used in conventional steam power plants)
Rankine	• Low operating temperatures • Commonly used cycle • Suitable for waste-heat recovery	• Needs a condenser (size becomes an issue) • Increased efficiency at the cost of higher pressures	10-16 %	0.2 - 2 MW
Stirling	• Low noise • High cycle efficiency • Small power applications	• Numerous inefficiencies due to sinusoidal piston motion, defective regeneration and dead volume	11-15 %	0.02 - 0.08 MW

The efficiency and power generation ranges shown in Table 2.1 are taken from Spliethoff and Schuster [27]. The efficiencies shown are for the specific power ranges given. When

comparing the power generation cycles it helps to use quantative weighing to allocate a numerical value to the comparisons. This weighing can be seen in Table 2.2. A simple scoring system is employed where only yes or no answers count. In the event of a yes, a single point is awarded, and where a no is given, no point is awarded.

Table 2.2: Quantative weighing for power cycles under investigation

Advantages	**Brayton**	**Rankine**	**Stirling**
Can use air as working fluid	1	0	0
High efficiency	1	0	1
Small and large scale	1	0	1
Low-pressure ratios when regeneration is used	1	0	0
Low operating temperatures	0	1	0
Commonly used cycle	0	1	0
Suitable for waste-heat recovery	0	1	0
Low noise	0	0	1
Small power applications	1	0	1
Total advantages	**5.00**	**3.00**	**4.00**
Disadvantages			
Irreversibilities occur due to pressure losses	1	1	1
Large compressor work compared to turbine work	1	1	0
Large receivers for sufficient heat input	1	1	1
Needs a condenser (size becomes an issue)	0	1	0
Increased efficiency at the cost of higher pressures	1	1	0
Numerous inefficiencies due to sinusoidal piston motion, defective regeneration and dead volume	0	0	1
Total disadvantages	**4.00**	**5.00**	**3.00**
NET RESULT	**1.00**	**-2.00**	**1.00**

In Table 2.2, both the Brayton cycle and Stirling engine scored a net point value of 1. However, when considering the advantages, the Brayton cycle scored the most points of all the cycles. Even though there is no substantial difference in the allocated points in Table 2.2, The Brayton cycle seems to be a viable choice for further investigation.

2.2.5 Conclusions

From Tables 2.1 and 2.2, the Brayton cycle will be the best choice for the problem at hand. This is mainly due to the low pressure ratios, the types of applications possible and the fact that air can be used as the working fluid which significantly reduces the installation and running costs of the cycle.

The disadvantages are not forgotten and do pose problems. However, the irreversibilities due to pressure losses and receiver size can be optimised by numerically solving the cycle as a whole. The Rankine cycle is used in too large applications to be considered in this investigation. The Stirling engine is a strong contender, however the losses due to dead volume and piston motion is undesirable, as they cannot be easily minimised.

2.3 Solar power

2.3.1 Justification for solar power

As discussed by Roos [36], the availability of current carbon sources will decrease and a needed limit will be enforced. Concentrated solar power projects can easily be scaled up once proven sufficient. As the capacity of solar farms and the supply of solar energy increase, the cost of solar power will come down. This cost is expected to fall below that of natural gases in the next few years.

Kalogirou [37] discusses the relevance of solar power as an alternative energy source on the basis of environmental problems such as acid rain, ozone layer depletion and global climate change. The major problem with renewable energy technologies is that they are generally diffused and not fully accessible. The benefits arising from the operation of solar systems can be put into three main categories: energy saving, job creation and the decrease of environmental pollution. Solar thermal systems are non-polluting and offer significant protection to the environment. The main advantage of employing solar energy is the reduction it brings to greenhouse gas pollution.

2.3.2 The economics of concentrated solar power

Zamfirescu et al. [38] show the feasibility of concentrated solar generators at the hand of an economic investigation. The analysis was performed in Ontario, Canada, and a base investment of about CN$ 10,000 was set. It was shown that with a government subsidy this investment, and taking interest into account, can be repaid in 21.6 years. If certain realistic deductions, such as electricity buy back and reduction in $C0_2$ tax is taken into account, the initial investment can be repaid in only 11.3 years. Zamfirescu et al. [38] also show that the savings brought about by the use of a concentrated solar generator is made up by approximately 7 % carbon tax deduction, 30 % less electricity production and 63% due to the reduction in the natural gas heating capacity. One of the main factors behind the hesitant implication of concentrated solar generators is the lack of conversion efficiency that can compete, in terms of economics, with the better established power plants such as fossil fuel power plants, nuclear power, hydroelectricity, etc.

2.3.3 Influence of weather on solar power production

One of the major drawbacks of a solar power generation system is the exposure to the main source of energy, the sun. Naturally, any meteorological occurrence such as cloud cover, rain, snow and wind will decrease the amount of solar radiation absorbed by the solar collector; therefor the receiver temperature will be lower which leads to a lower system efficiency and also lower net power output. This problem can be addressed in a couple of ways. One such way is to use biofuel or natural gas backup systems to produce energy when a solar plant experiences a decrease in power generation [37]. Another way to address the problem is by means of solar generation prediction from weather forecasts using machine learning as explained by Sharma et al [39]. They explain that by using weather data and setting up proper weather prediction models, the available solar radiation can be predicted to a certain degree. This helps to lower the intermittent and uncontrollable nature of solar energy supply, subsequently bettering the integration of solar power generation into existing electricity grids.

In Duffie and Beckman [13] some typical heat loss coefficients are given for convective heat loss when considering wind effects. They state that free and forced convection equations must be considered and compared in order to make a proper conclusion. It appears that horizontal and vertical collectors under free-convection conditions (no wind) will have convection heat transfer coefficients of minimum 5 W/m^2K. If the scenario is changed and wind effect is added, e.g. a 5 m/s wind, the convective heat loss coefficient goes up to 10 W/m^2K when e.g. a characteristic length of 8 m is used. Thus wind increases the heat transfer coefficient at the collector, so doing removes heat from the focal point which will lead to less power generation.

2.3.4 Solar irradiance

Solar irradiance is the amount of solar radiant energy falling on a certain earth surface area per unit time. According to Stine and Harrigan [9] the solar radiation falling directly on earth is anywhere from 451 up to 1,135 W/m^2. Fluri [40] states that the solar irradiation in the northern parts of the Northern Cape, South Africa, is more than 8 and 6kWh/m^2 in December and June respectively. Most areas in South Africa receive on average between 4.5 and 6.5 kWh/m^2 per day [41]. For a steady-state analysis of a high irradiance location in South Africa, at noon, an assumed solar irradiance of 1,000 W/m^2 would be acceptable.

2.3.5 Different types of solar collectors

There are a number of ways in which a working fluid, such as air, can be heated by using the energy extracted from concentrated solar rays. Some of these methods use parabolic dish collectors, parabolic trough collectors and tower power collectors [36].

2.3.5.1 Parabolic dish collector

Reddy and Sendhil Kumar compare various receivers [17] and investigate natural convection heat loss for simple [18] and fuzzy focal solar dish collectors [17]. In all their papers concerning the receiver discussions, the solar dish is always the type of collector being used. Reddy and Sendhil Kumar [18] states that a solar parabolic dish collector is an attractive method to concentrate direct beam radiation and convert it to thermal energy in a useful form for electrical power generation.

Roos [36] states that dish technology is a mature and cost-effective technology since large utility projects that use parabolic dishes are now under development. An advantage of the parabolic dish collector is its high efficiency. It demonstrates the highest solar-to-electric conversion efficiency and it has the potential to become one of the least expensive sources of renewable energy. Another advantage is its flexibility. It is modular as it may be deployed individually for remote applications or grouped together for small-grid system, e.g. power for villages.

A parabolic dish collector is shown in Figure 2.10.

Figure 2.10 Parabolic dish collector with receiver for Stirling engine [36]

Kalogirou [37] shows that parabolic dish collectors can achieve temperatures in excess of 1,500 °C. The major advantages of parabolic dish collectors are 1) that they are the most efficient of all collector systems when they are always pointing towards the sun, 2) they have high concentration ratios and thus are also very efficient at thermal energy absorption and power conversion and 3) they can function independently or as a part of a system due to their modular collectors and receivers.

2.3.5.2 Parabolic trough collector

As discussed by Odeh et al. [42], parabolic trough collectors are employed in the largest solar electric generation system, in unison with synthetic oil as working fluid in the collecting loop. A parabolic trough collector is shown in Figure 2.11.

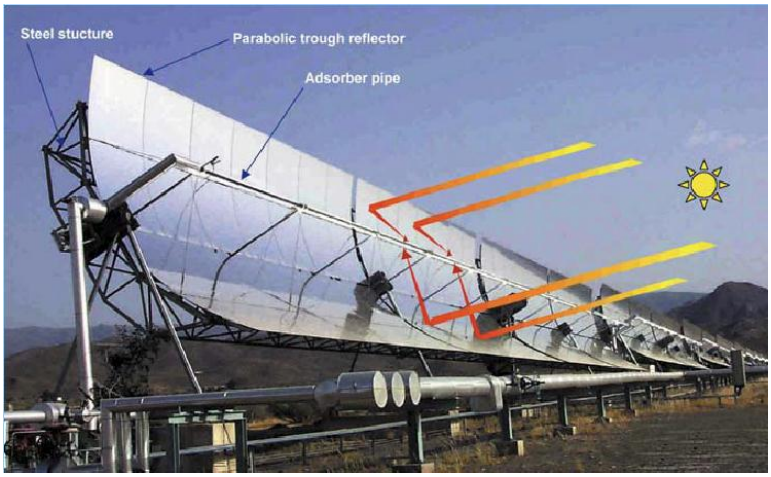

Figure 2.11 Parabolic trough collector [36]

Parabolic trough collectors or PTCs can effectively produce heat at temperatures ranging from 50 to 400 °C. PTCs are constructed from a parabolic bent sheet of reflective material. At the focal line of this trough is a black metal tube with a glass tube housing to reduce heat losses. This trough functions by focusing parallel rays onto the central tube. Inside the central tube, the working fluid passes and receives the transferred heat. Single-axis tracking is sufficient with the collaboration of long collector troughs. PTC systems are the most advanced in the solar collecting field due to the higher experience and advances in commercial industry of the manufacturing and marketing of these systems [36], [37].

Investigations into the performance of parabolic through collectors are available [43].

2.3.5.3 Heliostat/power tower

Consider Figure 1.1 where Solar One is shown. Solar One is a prime example of a power tower-type solar field. It operated from 1982 to 1986 in Barstow, California, and was used to show the feasibility of harnessing the sun's energy to generate electricity. Solar Two was later built to improve the thermal storage capacity of the system in Solar One. Figure 2.12 shows Solar Two; with a central receiver and a number of heliostats positioned around it.

Figure 2.12 Solar Two [44]

The orientation of the heliostats is such that they all concentrate their beams on a single disk on the central tower. As discussed by Kalogirou [37], this type of field is good in applications where high inputs of radiant energy are present. The heliostats are normally slightly curved so that larger amounts of energy can be directed onto the receiver. The energy is used to produce steam at high temperature and pressure. The list of advantages of solar receivers is extensive, and includes: 1) the minimisation of thermal energy transport requirements, 2) high efficiency in collecting energy and converting it to electricity due to high concentration ratios, 3) ability to store thermal energy and 4) benefits from economies of scale due to their physical size. When analysing the system, the selection of heat transfer fluid, thermal storage medium and power conversion cycle defines the plant. The working fluid can be water/steam or an organic fluid such as liquid sodium, molten nitrate salt and other similar fluids. These systems normally utilise steam Rankine cycles, however, there have been newer designs that use air as the working fluid and either a Rankine or an open Brayton cycle both of which use ceramic bricks for thermal storage.

2.3.5.4 Comparison of solar collector types

Each collector types is summarised in Table 2.2 to give a clear understanding of how they measure up to one another. The efficiencies of these collector types are not listed, since they are made up of efficiencies such as thermal, optical and conversion efficiencies, and vary greatly between different types of applications, like the power cycle they are used in, the geographic location they are placed in and the atmospheric conditions they are exposed to.

Table 2.2 Comparison of solar collector types

Type of Collector	Advantages	Disadvantages	Temperature range	Power generation scale
Parabolic Dish	• Mature • High efficiency • Flexibility • Modular	Amount of energy extracted not as much as other larger collectors	~1,000 °C	25 kW per dish typically
Parabolic Trough	• Most proven • Highest experience collector	• Lower temperatures generated at receiver • Size • Cost	~ 400 °C	>50 MW for large scale operation. ~1 MW for ORC

Heliostat/Power Tower	• Minimises transport requirements • High efficiency • Ability to store thermal energy	• Only for high inputs of radiant energy • Size • Cost	~700 °C	>30 MW Typically

2.3.5.5 Conclusions

From the preceding discussion, the best collector type to be integrated in the system under consideration is the parabolic dish collector. Some of the other collector types pose advantages in their own respect, however, it is required that the solar thermal system should be small and modular, which ultimately makes the parabolic dish collector the best choice. According to Reddy and Sendhil Kumar [18], a collector consisting of a parabolic concentrator and a modified cavity receiver is the optimal choice.

2.4 Thermodynamics

It is important to get a good understanding of some basic terms before the work in this report becomes too detailed.

2.4.1 The second law of thermodynamics

The second law of thermodynamics was set up to supply a method which acknowledges that processes sometimes occur in only one direction, meaning that with the second law of thermodynamics comes an understanding of irreversible processes. Heat engines and refrigerators can be solved in terms of the second law of thermodynamics, with which second law efficiencies are defined. For the heat engine, this efficiency is known as the thermal efficiency, and for the refrigerator, it is called the coefficient of performance. There are two classic statements of the second law known as the Kelvin-Planck statement and the Clausius statement. The Kelvin-Planck statement is: “It is impossible to construct a device that will operate in a cycle and produce no effect other than the raising of a weight and the exchange of heat with a single reservoir.” The Clausius statement further describes this law as follows: “It is impossible to construct a device that operates in a cycle and produces no effect other than the transfer of heat from a cooler body to a hotter body.” [26]

The work produced in a system can be written as:

$$W = W_{rev} - T_0 S_{gen} \quad [2.4.1\text{-}1]$$

When the reversible system work, denoted W_{rev}, is substituted in equation 2.4.1-1, the system work output can be written as:

$$W = \sum \left(1 - \frac{T_0}{T}\right) q_{CV} + h_{tot,i} - h_{tot,e} - T_0(s_i - s_e) - T_0 S_{gen} \quad [2.4.1\text{-}2]$$

Equation 2.4.1.-2 represents the second law of thermodynamics work output for a control volume [26], where $T_0 S_{gen}$ represents the destruction of exergy.

An early statement of the second law of thermodynamics is that heat always flows downhill. In a more scientific sense, if two or more bodies are in thermal contact, the energy of heat will always flow from higher to lower values. This second law of thermodynamics also states that the entropy never decreases but always increases (also called entropy generation).

2.4.2 Entropy and entropy generation

It is safe to say that there is another factor other than enthalpy that influences the reactions in thermochemistry. This factor is called entropy.

It should be noted that when speaking of entropy, it is important to recall that entropy can be described as follows: when we require a higher efficiency, we require a lower increase in total entropy. Also the change in entropy of an irreversible system can be associated with a change of state from a less probable to a more probable state. Putting this differently, entropy is the thermodynamic property that can be used to determine the energy not available for work in the process [26].

Sonntag et al. [26] show how the entropy equations for a system are found. The first step in considering entropy is to consider the inequality of Clausius, which states:

$$\oint \frac{\delta Q}{T} \leq 0 \quad [2.4.2\text{-}1]$$

In the inequality of Clausius, the inequality sign holds for irreversible systems and the equality sign holds for reversible systems.

Entropy change occurs in a reversible process according to equation 2.4.2-2 where isothermal heat transfer occurs from the high-temperature reservoir to the working fluid.

$$S_2 - S_1 = \int_1^2 \left(\frac{\delta Q}{T}\right)_{rev} \quad [2.4.2\text{-}2]$$

The entropy change in an irreversible process is larger than the change in a reversible process for the same δQ and T. This is now written as equality below:

$$S_2 - S_1 = \frac{\delta Q}{T} + \delta S_{gen} \quad [2.4.2\text{-}3]$$

provided that the last term, which is for the generated entropy, is always positive or equal to zero.

The entropy change for an ideal gas can be determined by considering the thermodynamic property relation and the ideal gas relations:

$$Tds = du + Pdv \quad [2.4.2\text{-}4]$$

$$du = C_{v0}dT \; and \; \frac{P}{T} = \frac{R}{V} \quad [2.4.2\text{-}5]$$

This brings about the entropy change for an ideal gas as:

$$s_e - s_i = C_{p0} \ln\left(\frac{T_e}{T_i}\right) - R \ln\left(\frac{P_e}{P_i}\right) \quad [2.4.2\text{-}6]$$

By employing equations 2.4.2-3 and 2.4.2-6, the entropy generation of a system can be minimised. Sonntag et al. [26] also show that when considering a control volume, such as the case in this dissertation, the entropy generation can be calculated by taking the change of entropy for a control mass in rate form, and adding the mass flow rates in and out of the system:

$$\frac{dS_{CV}}{dt} = \sum \dot{m}_i \dot{s}_i - \sum \dot{m}_e \dot{s}_e + \sum \frac{\dot{Q}_{CV}}{T} + \dot{S}_{gen} \quad [2.4.2\text{-}7]$$

This equation accounts for any system that will result in a subset of this equation when the second law of thermodynamics is employed. It also solves for the transient case, where the amount of entropy change and generation per unit time change as the time domain changes. When the system is set as steady, and no inlet or outlet mass flow rates exist, this equation simplifies greatly. It must be understood that solar radiation is not steady since it fluctuates and is intermittent. Due to the nature of the study at hand, the steady state system will not be covered.

2.4.3 Exergy and exergy generation

The main thing to remember when considering exergy and all it entails is that exergy and entropy are linked. The destruction of exergy, which is also the destruction of available energy, will increase as entropy is generated. Entropy generation occurs in the presence of heat transfer, and entropy can never decrease. Thus as heat transfer occurs, the destruction of exergy will increase. The trick with any thermodynamic analysis (2nd law) is to minimise the rate of increase and magnitude of both the entropy generation and destruction of exergy. Once this has been mastered, the solution will be optimised.

Availability is a term used more widely in conjunction with the irreversibility of a system. The availability can be seen as the amount of work a system can potentially achieve at its original state.

Sonntag et al. [26] derive the change in exergy with time according to the different terms relating to the heat transfer together with those relating to the flow and by grouping them together show that:

$$X = m(e - e_0) + P_0 m(v - v_0) - T_0 m(s - s_0) \qquad [2.4.3\text{-}1]$$

where the subscript 0 refers to the dead state at which there is no kinetic energy.

When the rates of change are employed in equation 2.4.3-1 and using some further mathematical manipulation, an equation can be set up with which the total system exergy can be calculated per change in time:

$$\frac{dX}{dt} = \sum \left(1 - \frac{T_0}{T}\right) \dot{Q}_{CV} - \dot{W}_{CV} + P_0 \frac{dV}{dt} + \sum \dot{m}_i \psi_i - \sum \dot{m}_e \psi_e - T_0 S_{gen} \qquad [2.4.3\text{-}2]$$

Equation 2.4.3-2 is made up of the following terms:

$\sum \left(1 - \frac{T_0}{T}\right) \dot{Q}_{CV}$ = Transfer by heat

$-\dot{W}_{CV} + P_0 \frac{dV}{dt}$ = Transfer by shaft and boundary work

$+\sum \dot{m}_i \psi_i - \sum \dot{m}_e \psi_e$ = Transfer by flow in which ψ represents the flow availability, which is made up of enthalpy and entropy terms

$-T_0 S_{gen}$ = Exergy destruction

Equation 2.4.3-2 contains terms that will be used in the final exergy evaluation or entropy generation minimisation of the system [26].

Zamfirescu and Dincer [52] show that the exergy of incident solar radiation at the receiver can be determined as:

$$X_{incident} = \eta . I_{T0} \qquad [2.4.3\text{-}3]$$

Where η is the conversion effectiveness and I_{TO} is the total normal radiation at the receiver. The conversion effectiveness, which is essentially exergy based efficiency, can be calculated as:

$$\eta = 1 - \frac{T_0 I_{SC}}{T_{T0} I_{T0}} \qquad [2.4.3\text{-}4]$$

I_{SC} is the radiation measured at the solar collector and T_{T0} is the temperature at the earth's surface. The total normal radiation can be determined as:

$$I_{T0} = I_T \cos \theta_i \qquad [2.4.3\text{-}5]$$

With I_T the measured radiation and θ_i the incidence angle in degrees.

In Bejan [53], it is shown that exergetic efficiency, also known as second law efficiency, effectiveness or rational efficiency, is a parameter that can be used for thermodynamic performance evaluation. It provides a measure of performance from a thermodynamic perspective. An equation is introduced where a fuel and a product is used to analyse a certain thermodynamic system.

$$\varepsilon = \frac{\dot{X}_p}{\dot{X}_F} = 1 - \frac{\dot{X}_D + \dot{X}_L}{\dot{X}_F} \qquad [2.4.3\text{-}6]$$

In equation 2.4.3-6 the exergetic efficiency, ε, is found by dividing the exergy rate of the products, $\dot{X}_p$, by the exergy rate of the fuel, $\dot{X}_F$. Furthermore in equation 2.4.3-6, $\dot{X}_D$ is the rate of exergy destruction and $\dot{X}_L$ is the rate of exergy loss.

Bejan [53] states that exergetic efficiency is ordinarily more meaningful and feasible than any other efficiency based on the first or second laws of thermodynamics, even the thermal efficiency of a power plant, isentropic efficiency of a compressor or turbine and effectiveness of a heat exchanger. Yilmaz et al. [15] deliberates and compares the performance criteria for both exergy and entropy analyses and states that exergetic efficiency, which is said to give a degree of thermodynamic perfection, is of little or no use for individual components such as heat exchangers. It is mentioned that its use may even lead to false conclusions.

2.5 Irreversibilities

Irreversibility is brought about mainly by the losses present in any cycle. In Figure 2.3, losses occur from points 1 to 2 and from points 3 to 4 as these processes do not occur at constant entropy. Since physical losses occur, it is impossible for the system to go back to its original configuration after completing one cycle. For this reason, it is said the system is irreversible. This reiterates the basic theory of the second law of thermodynamics [26].

It is shown that the irreversibility increases as the highest temperature in the cycle increases and decreases as the heat transfer rate increases. This is caused by the dependency on entropy and the difference in values for entropy change as the temperature and heat transfer increase.

According to Sonntag et al. [26], the irreversibility of a real process can be written as:

$$I = T_0(s_e - s_i) - \frac{T_0}{T_H}q \qquad [2.5\text{-}1]$$

Equation 2.5-1 is shown to be equal to:

$$I = T_0 S_{gen} = W^{rev} - W \qquad [2.5\text{-}2]$$

with W^{rev} the same as W_{rev} and already shown in equations 2.4.1-1 and 2.4.1-2. From this it can be said that the irreversibilities of a real process and the exergy destruction are similar, especially when comparing equations 2.4.3-2 and 2.5-2.

2.6 Losses

2.6.1 Receiver losses

Reddy and Sendhil Kumar [16] discuss the three mechanisms which are responsible for the heat loss from the receiver. These are: 1) conductive heat loss from receiver, 2) radiative heat loss through the receiver aperture and 3) convective heat loss through the receiver aperture. From

these mechanisms, the natural convection heat loss contributes a substantial amount of the total energy loss. In conventional receivers, the convection heat loss can be 10 - 12 % of the absorbed energy, whereas the natural convection heat loss in fuzzy focal solar dish receivers may be higher. Reddy and Sendhil Kumar [17] show some indicative magnitudes for radiative and conductive heat loss compared to the total heat loss experienced by an insulated or non-insulated receiver. For the insulated receiver they show at small inclinations (e.g. 0° to 45°) of the receiver, the radiative heat loss can be 31-36% of the total heat loss while conductive heat loss will only be 3.5-4.5 % of the total heat loss. Thus for this specific scenario and range of inclination the convective heat loss can be 59 - 65 % of the total heat loss. It is also shown that as the inclination angle increases, the impact of the conductive and radiative heat losses increase while the impact of the convective heat losses decrease. When a receiver is not properly insulated, the largest component of all the losses experienced is the radiative losses.

2.6.2 Turbine and compressor losses

It is at this point already known that any actual cycle differs from its ideal. This difference exists due to the presence of losses in the real cycle. The major losses are attributed to the turbine, pipes and compressor. Turbine losses arise as a result of the flow through the turbine blades and passages within the turbine itself. The large positive turbine work is reduced by the isentropic turbine efficiency. The heat transfer to the surroundings should also be noted but is of less importance.

Compressor and pump losses are caused mainly by the irreversibility of the fluid flow. Compressor losses are similar to pump losses and are much smaller than the turbine losses due to the associated work that is much smaller [26].

2.6.3 Pipe and duct losses

Pipe or duct losses are a result of the frictional effects and heat transfer to the surroundings caused by the flow of the working fluid. If this flow process were to be discussed with the aid of a T-s diagram, it will be noted that the frictional effects cause an increase in the entropy. The heat transfer to the surroundings, which happens at constant pressure for every respective pipe or duct section, decreases the entropy. However, both the pressure drop and the heat transfer decrease the availability or exergy of the working fluid [26].

2.7 Conclusions

Thermal power cycles were discussed. From the discussion, the Brayton cycle with regeneration is the best choice. It was found that the modified cavity receiver, as suggested by Reddy and Sendhil Kumar [16], was the best choice for a receiver to use with the Brayton cycle. The sun's rays

are focused by means of a parabolic dish. An exergetic analysis will be completed for the chosen power cycles. The generation of entropy was investigated and possible minimisation strategies were described. The origin of irreversibilities and losses was investigated and will be included in the numerical analysis of the systems.

3 Problem definition

3.1 Introduction

In this chapter, the cycle to be used is described and analysed. The objective function for the cycle is formulated. The individual components and their respective entropy generation rates are identified. As is shown, the total entropy generation can be found when adding the entropy generation rates of the individual components of the system. By doing an exergy analysis, the total entropy generation rate is linked to the net power output.

The geometries of the solved components are shown and the objective function is written in terms of these geometries. The assumptions and constraints are listed for the objective function.

3.2 Cases under consideration

3.2.1 The theoretical double open-air solar thermal Brayton cycle

As described by Le Roux et al. [21], there are four different cases that can be considered when looking at the regenerative Brayton cycle. A detailed discussion can be found in Le Roux et al. [21]. From this discussion, a regenerative Brayton cycle with an added solar heat exchanger will be investigated. A simple sketch of this system is shown below.

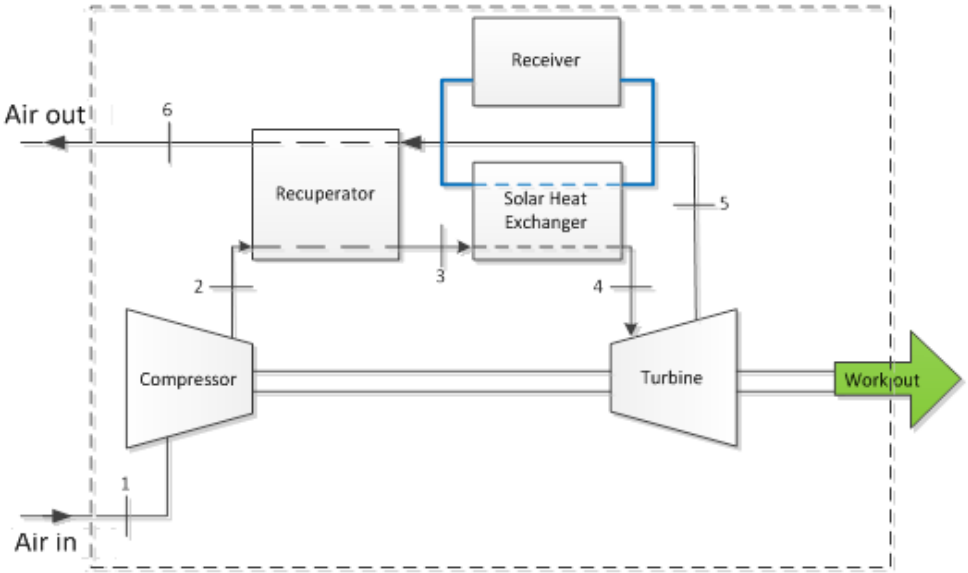

Figure 3.1 Theoretical double open-air solar thermal Brayton cycle

The cycle shown in Figure 3.1 consists of a primary and secondary cycle. The primary cycle is a closed cycle linking the receiver to the solar heat exchanger. The working fluid in the cycles is air. The secondary cycle is open, which means the air enters the cycle from the surroundings and exits the cycle to the surroundings. No radiator is required as the air that enters the cycle is at

atmospheric temperature. The system is also said to be indirect since the primary cycle captures the sun's heat and uses a heat exchanger to transfer heat from one fluid line to the next. The physical appearance of this cycle is discussed in the remainder of this chapter.

3.2.2 The real double open-air solar thermal Brayton cycle

The cycle in Figure 3.1 is an ideal cycle and will not be used as is. Figure 3.2 shows the cycle that will be used. A compressor is added to the primary cycle. This compressor must be present to promote flow in the cycle. It is this flow which will bring about the transfer of heat from the receiver to the first regenerator. Regenerator 1 (the solar heat exchanger in Figure 3.1) is so named since the two regenerators will be dimensioned similarly and the numbers are only needed to distinguish their position in the system. The addition of a turbine in the primary cycle is also clearly visible. This addition is to combat the large compressor work that will be present in the cycle due to two compressors being used. The turbine subsequently produces its own power. For the sake of simplicity, the same type of compressor will be used in both the primary and secondary cycle. The two turbines will also be the same type, all of which will be taken as off-the-shelf components, again for simplicity.

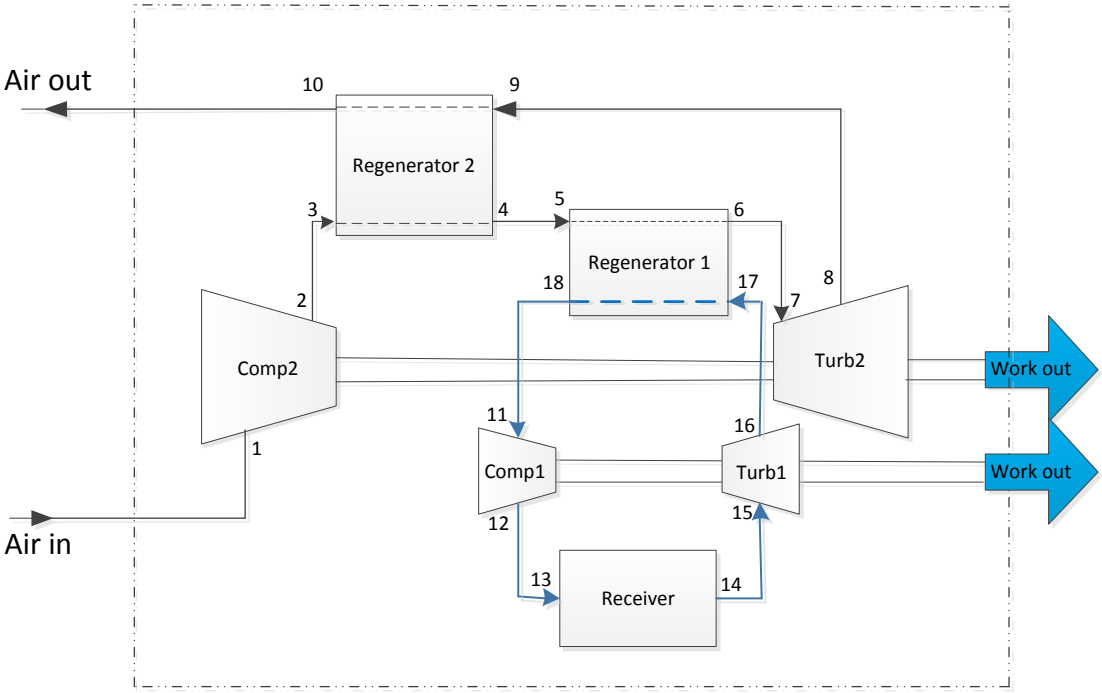

Figure 3.2 The double open-air solar thermal Brayton cycle

3.3 Physical model

3.3.1 The open-air solar thermal Brayton cycle

3.3.1.1 Choice of cycle configuration

As discussed earlier, a comparison was made in Le Roux et al. [21], between four different cycles. The chosen configuration is as presented in Figure 3.2.

3.3.1.2 Choice of collector

As discussed earlier in this report, the Brayton thermal cycle is slightly modified to include a solar collector rather than a combustion chamber. This replacement is made due to the costs and sheer size applicable to the operation of current combustion chambers. Even though solar collectors are still far from functioning optimally, they pose the possibility of increasing the overall efficiency of the Brayton cycle as a whole. Also solar collectors have no harmful exhausts when the working fluid is air.

As mentioned, the parabolic dish collector will be used in conjunction with the Brayton cycle.

3.3.1.3 Choice of receiver

A modified cavity receiver is suggested by Reddy and Sendhil Kumar [18]. The numerical analysis that was conducted showed that the maximum and minimum convection heat loss occurs at $\beta = 0$ and $\beta = 90°$, this suggests the receiver aperture facing sideways (at $\beta = 0$) and facing straight downwards (at $\beta = 90°$). When closely considering the receiver, an area ratio (ratio of inner-wall area to aperture area) of 8 is suggested. This is the ratio at which the minimum heat loss is found. This ratio applies to the modified cavity receiver with which the research was conducted. The inner surface of the receiver is made up of closely wound copper tubing that is bunched very tightly to form a continuous hemispherical surface. The working fluid is pumped through these tubes where heat transfer can occur from the higher-temperature cavity volume to the tubing. Le Roux et al. [21] further discussed the geometry of the cavity receiver as well as the sizing of the aperture.

In Reddy and Sendhil Kumar [16], a comparison is made between three different types of receivers to investigate the effects of natural convection heat loss. The receivers discussed are a cavity receiver, semi-cavity receiver and a modified cavity receiver. The orientation of the receiver apertures was altered from being directly sideways to facing directly downwards. It was shown how this orientation influences the amount of natural convection heat loss considerably. In all three cases, it was found that the losses were the least when the receiver apertures faced directly downwards. When considering the three receiver types, it was found that the modified cavity receiver was the preferable choice as it supplied the minimal natural convection heat loss.

The optimisation of the receiver dimensions will be included in the numerical analysis of the system.

3.3.1.4 Regenerators

The function of the regenerators is to act as heat exchangers with which heat is transferred from one fluid flow line to another. Cross-flow regenerators are chosen as the two fluid streams spend the maximum possible time in 'contact' in order for heat transfer to occur. This allows the maximum amount of heat to be transferred between the two air-flow streams. In Regenerator 1 in Figure 3.2, the flow coming out of Regenerator 2 is heated by the flow coming out of Turbine 1. In Regenerator 2 the flow coming out of Compressor 2 is heated by the flow coming out of Turbine 2. Regenerators decrease the amount of energy or heat lost due to the finite temperature difference between the two air-flow streams. An optimisation of the regenerator is conducted by Le Roux et al. [21]. A similar optimisation will be carried out as part of this investigation for the system as presented in Figure 3.2.

3.3.1.5 Compressor and turbine cross-dependencies

Since the entire system is to be optimised, the mass flow rate through the system depends on the turbine, which in its own right depends on the compressor. Garret by Honeywell [45] contains the turbine maps with which the system can be solved. It can be seen that the turbine efficiency, the mass flow rate and the pressure ratio are all closely linked to one another. When the turbine pressure ratio is set as a parameter, it fixes the mass flow rate and the turbine efficiency as parameters.

As discussed in Le Roux et al. [21], where compressor maps were utilised, the highest possible compressor efficiency that can be achieved is on the island in the middle of a compressor map. This value will be found between low and high mass flow rate values and between low- and high-pressure ratio values. They further show that an optimum pressure ratio exists for each specific turbine, which would give the maximum net power output for the system, if the said system consisted of its optimised geometry.

3.4 Mathematical model

3.4.1 Brayton cycle efficiencies

When Figure 2.1 comes under investigation, it is known that the efficiency of the air-standard Brayton cycle is found as shown by Sonntag et al. [26]:

$$\eta_{th} = 1 - \frac{Q_L}{Q_H} = 1 - \frac{C_p(T_4 - T_1)}{C_p(T_3 - T_2)} = 1 - \frac{T_1\left({}^{T_4}/_{T_1} - 1\right)}{T_2\left({}^{T_3}/_{T_2} - 1\right)} \qquad [3.4.1\text{-}1]$$

In this cycle, it can be noted that:

$$\frac{P_3}{P_4} = \frac{P_2}{P_1} \quad [3.4.1\text{-}2]$$

Where 1 is the inlet and 2 is the outlet of the control volume. Furthermore:

$$\frac{P_2}{P_1} = \left(\frac{T_2}{T_1}\right)^{\frac{k}{k-1}} = \frac{P_3}{P_4} = \left(\frac{T_3}{T_4}\right)^{\frac{k}{k-1}} \quad [3.4.1\text{-}3]$$

$$\frac{T_3}{T_4} = \frac{T_2}{T_1} \therefore \frac{T_3}{T_2} = \frac{T_4}{T_1} \; and \; \frac{T_3}{T_2} - 1 = \frac{T_4}{T_2} - 1 \quad [3.4.1\text{-}4]$$

$$\eta_{th} = 1 - \frac{T_1}{T_2} = 1 - \frac{1}{(P_2/P_1)^{(k-1)/k}} \quad [3.4.1\text{-}5]$$

From the non-ideal T-s diagram in Figure 2.3, the efficiencies of the compressor and turbine can be defined in relation to the isentropic processes:

$$\eta_{comp} = \frac{h_{2s} - h_1}{h_2 - h_1} \quad [3.4.1\text{-}6]$$

$$\eta_{turb} = \frac{h_3 - h_4}{h_3 - h_{4s}} \quad [3.4.1\text{-}7]$$

By using the above equations in conjunction with the text from [26], the cycle with all the irreversibilities taken into account can be properly analysed.

From Figure 2.4, the efficiency of the regenerator can be shown to be the following, when taking C_p to be constant:

$$\eta_{reg} = \frac{h_{aa} - h_2}{h_{aa'} - h_2} = \frac{T_{aa} - T_2}{T_{aa'} - T_2} \quad [3.4.1\text{-}8]$$

3.4.2 Entropy generation in the system as a whole

As discussed by Bejan [8], and also in section 2.4.2, it is possible to minimise entropy generation as follows:

$$S_2 - S_1 = \int_1^2 \frac{\delta Q}{T} + S_{gen} \quad [3.4.2\text{-}1]$$

$$s_2 - s_1 = C_{p0} \ln\left(\frac{T_2}{T_1}\right) - R \ln\left(\frac{P_2}{P_1}\right) \quad [3.4.2\text{-}2]$$

The above two equations are used in the derivation of the entropy generation for each of the individual components of the system. These derived equations can be found later on in this section.

As explained in Sonntag et al. [26], the balance of entropy for a control volume is defined as:

$$\frac{dS_{CV}}{dt} = \sum \dot{m}_i s_i - \sum \dot{m}_e s_e + \sum \frac{\dot{Q}_{CV}}{T} + \dot{S}_{gen} \quad [3.4.2\text{-}3]$$

From Bejan [20], it is possible to account for the irreversibilities that accompany the transition from solar radiation into mechanical power. Firstly, consider a photon gas system as depicted in [20]. For adiabatic free expansion, the first law of thermodynamics is used to provide an estimate of the final equilibrium state. Ultimately, the increase in entropy, or known otherwise as the entropy generation, is as follows:

$$S_{gen,1-2} = S_1 \left(\frac{T_1}{T_2} - 1 \right) > 0 \quad [3.4.2\text{-}4]$$

It is of course possible to consider entropy generation for the Brayton cycle as a whole. In Sonntag et al. [26], a proper discussion is found for the entropy change in irreversible processes. This entropy change is formulated as:

$$dS = \frac{\delta Q}{T} + \delta S_{gen} \quad [3.4.2\text{-}5]$$

under the condition that the entropy generation is larger than zero as in equation 3.4.2-4. This internal generation of entropy can be caused by friction, unrestrained expansion and the internal transfer of energy over a finite temperature difference. External irreversibilities can be attributed to the heat transfer over finite temperature differences as δQ is transferred from a reservoir or by mechanical transfer of work. The principle of the increase of entropy for a control volume is known as:

$$\frac{dS_{net}}{dt} = \frac{dS_{CV}}{dt} + \frac{dS_{surr}}{dt} = \sum \dot{S}_{gen} \geq 0 \quad [3.4.2\text{-}6]$$

The total internal entropy generation rate is equal to the sum of the internal entropies of each of the system's individual components. The open-air Brayton cycle's components are:

- compressors
- regenerators
- turbines
- receiver.

Below is a brief discussion of each of the components and the relevant entropy generation rate equation allocated to each of them. In each case, the equations in Section 2.4.2 are used and derived for each of the specific components.

3.4.2.1 Compressor

The derived equation used to calculate the compressor's entropy generation rates is in terms of the temperatures and pressures at the inlet and outlet of the compressor itself. These temperatures and pressure can be determined by using the isentropic compressor efficiency.

$$\dot{S}_{gen,comp} = \dot{m}C_{p0}\, ln\left(\frac{T_e}{T_i}\right) - \dot{m}R\, ln\left(\frac{P_e}{P_i}\right) \quad [3.4.2\text{-}7]$$

3.4.2.2 Regenerator

Each regenerator has two inlets and two outlets. In the equation below, stream 1-2 is the cold stream and stream 3-4 is the hot stream.

$$\dot{S}_{gen,reg} = \frac{\dot{Q}_{loss,reg}}{T_0} + \dot{m}C_{p0}\, ln\left(\frac{T_2T_4}{T_1T_3}\left(\frac{P_2P_4}{P_1P_3}\right)^{\frac{1-k}{k}}\right) \quad [3.4.2\text{-}8]$$

According to Ordóñez and Bejan [46], the equation above must be altered to account for the entropy generated due to the discharge of the regenerator in an open cycle. This new improved equation is now:

$$\dot{S}_{gen,reg} = \frac{\dot{Q}_{loss,reg}}{T_0} + \dot{m}C_{p0}\, ln\left(\frac{T_2T_4}{T_1T_3}\left(\frac{P_2P_4}{P_1P_3}\right)^{\frac{1-k}{k}} + \frac{T_4 - T_0}{T_0}\right) \quad [3.4.2\text{-}9]$$

The above equation, however, depends on the original definition of the control volume and where its boundary crosses the system boundary under discussion.

In Figure 3.2 the boundary of the C.V. excludes the discharge of the regenerator. It is assumed that T_{10} is so close to the outlet of the regenerator that it cannot be seen as a discharge that influences the generation of entropy for the regenerator. For this reason, the influence of the regenerator discharge on the entropy generation of the regenerator itself is neglected in this analysis.

3.4.2.3 Turbine

The derived equation used to calculate the turbine's entropy generation rate is also in terms of the temperatures and pressures at the inlet and outlet of the turbine itself, as was the case with the compressor. These temperatures and pressures can be determined by using the isentropic turbine efficiency.

$$\dot{S}_{gen,turb} = \dot{m}C_{p0}\, ln\left(\frac{T_e}{T_i}\right) - \dot{m}R\, ln\left(\frac{P_e}{P_i}\right) \quad [3.4.2\text{-}10]$$

3.4.2.4 Receiver

The receiver entropy generation rate is determined with the main assumption that the working fluid is an ideal gas, which is a reasonable assumption since air is the working fluid in the open-air Brayton cycle. Following this and the use of the sun's temperature, T^*, and using the sun as a source of exergy that causes heat generation $\dot{Q}^*$ at the absorbing surface, the equation to be used is:

$$\dot{S}_{gen,rec} = -\frac{\dot{Q}^*}{T^*} + \frac{\dot{Q}_0}{T_0} + \dot{m}C_{p0}\, ln\left(\frac{T_e}{T_i}\right) - \dot{m}R\, ln\left(\frac{P_e}{P_i}\right) \quad [3.4.2\text{-}11]$$

Various approaches for the sun's temperature are discussed in the analysis of solar plants. Some authors prefer to have the T^* equal to some magnitude close to 6,000 K as with Zamfirescu and Dincer [52] while other authors suggest a smaller value such as is the case with Bejan [20] where T^* = 2,470 K to account for the influence that scattering will have on the generation of entropy. Furthermore, $\dot{Q}_0$ represents the rate of heat generation before any losses occur. This can be seen as the heat generation rate close to the sun's surface.

3.4.3 Irreversibilities

As given in Hartley [47], the general equation for irreversibility is a function of the mass flow rate, the ambient temperature, the entropy generation rate in the system and also the heat generation rate in the system. This is shown analytically as follows:

$$\dot{I} = T_0\left(\dot{m}\left(\frac{ds_{sys}}{dt}\right) + \sum_{i=0}^{n}\frac{\dot{Q}_i}{T_i}\right) \quad [3.4.3\text{-}1]$$

For an adiabatic process, the heat transfer term in the general irreversibility equation tends to zero, which then leads to the irreversibility being:

$$\dot{I} = T_0\left(\dot{m}(s_{exit} - s_{inlet})\right) \quad [3.4.3\text{-}2]$$

If, however, the process is non-adiabatic, which then leads to the integration of the original equation as there is only one thermal reservoir, an equation can be set up, which represents the heating and heat exchanger processes.

$$\dot{I} = T_0\left(\dot{m}(s_{exit} - s_{inlet}) + \frac{\dot{Q}_i}{T_i}\right) \quad [3.4.3\text{-}3a]$$

When equation 3.4.3-3a is considered, the term in brackets can be replaced by the entropy generation rate of the system, so that the equation becomes:

$$\dot{I} = T_0\dot{S}_{gen} \quad [3.4.3\text{-}3b]$$

Equation 3.4.3-3b can be used to calculate the internal irreversibility of each of the components in the cycle by using the entropy generation rate of each of those components respectively.

When considering irreversibility, it is important to be able to illustrate the total irreversibility of a cycle. In this case, the total internal irreversibility is simply the sum of all the irreversibilities of all the processes for the Brayton cycle:

$$\dot{I}_{cycle} = \dot{I}_{compressors} + \dot{I}_{combustion} + \dot{I}_{turbines} + \dot{I}_{heatexchangers} \quad [3.4.3\text{-}4]$$

$\dot{I}_{cycle}$, as shown in equation 3.4.3-4, is representative of the internal irreversibility of the cycle. To find these internal irreversibilities, the entropy generation rates are used unchanged for each component and multiplied by the ambient temperature, T_0.

This process is shown in the equations below.

$$\dot{I}_{internal} = \dot{I}_{compressors} + \dot{I}_{turbines} + \dot{I}_{regenerators} + \dot{I}_{receiver} \quad [3.4.3\text{-}5]$$

where:

$$\dot{I}_{compressors} = T_0\left(\dot{S}_{gen,comp1} + \dot{S}_{gen,comp2}\right)$$

$$\dot{I}_{turbines} = T_0\left(\dot{S}_{gen,turb1} + \dot{S}_{gen,turb2}\right)$$

$$\dot{I}_{regenerators} = T_0\left(\dot{S}_{gen,reg1} + \dot{S}_{gen,reg2}\right)$$

$$\dot{I}_{receiver} = T_0\left(\dot{S}_{gen,receiver}\right)$$

When considering the double Brayton cycle as in Figure 3.2, the external irreversibility is calculated as shown by le Roux et al. [21]:

$$\dot{I}_{external} = \dot{m}c_P(T_1 - T_{10}) - \dot{m}T_0c_P\left(\frac{T_1}{T_{10}}\right) \quad [3.4.3\text{-}6]$$

with subscripts 1 and 10 denoting the inlet and outlet temperatures of the entire cycle respectively. Equation 3.4.3-6 shows that at high external irreversibilities, the temperature at T_{10} should also be high, which means that the regenerator efficiency should be small (if considering equation 3.4.4-51).

3.4.4 Temperatures and pressures

Consider Figure 3.2. The objective function is a single function in which the entire system's losses are accounted for and with which the overall system can be accurately characterised. The temperature and pressure fields for Figure 3.2 need to be identified before an objective function can be properly set up. First of all, T_1 = 300 K and P_1 = 101,325 Pa, which are the ambient conditions as the air (working fluid) enters the system. The pressure drops in the ducts vary as a function of their expected lengths. Le Roux et al. [21] show that the unknown temperature and pressure fields can be determined for a simpler cycle. This process is slightly altered and employed here with the physical system being the main difference.

Turbine maps are used to find the ranges of optimum performance for a number of different turbines. From these maps, the turbine efficiencies are also taken. The two compressors are the same and two turbines are also the same, thus pressure drop and efficiency will not differ between them.

A function was created that calculates the temperatures, pressures, entropies and all other desired outputs for the system as found in Figure 3.2. First of all, the pressures for the secondary cycle are determined. This cycle goes from 1 to 10 and can be easily identified in Figure 3.2. The pressure at point 1 is, as mentioned, assumed to be equal to ambient:

$$P_1 = P_{atm} \quad [3.4.4\text{-}1]$$

Since the exact pressure ratio for the compressor is not known, the pressure of point 2 needs to be determined by some other means. Assume that P_{10} is also at ambient, thus:

$$P_{10} = P_1 = P_{atm} \quad [3.4.4\text{-}2]$$

From this, the pressure at point 9 is determined as:

$$P_9 = P_{10}(1 + Pdrop_{9-10}) \quad [3.4.4\text{-}3]$$

with:

$$Pdrop_{9-10} = \frac{f_{hot2}.L_{reg}.8.\left(\dot{m}_{plate2}\left(\frac{a}{b}\right)_{reg}\right)^2}{D_{h,reg}{}^5.\left(\left(\frac{a}{b}\right)_{reg}+1\right)^4.\rho_{hot2}.(1000P_1)} \quad [3.4.4\text{-}4]$$

The unknowns used in equation 3.4.4.-4 are all shown and explained in the list of symbols. Following equation 3.4.4-4:

$$P_8 = P_9(1 + Pdrop_{8-9}) \quad [3.4.4\text{-}5]$$

with:

$$Pdrop_{8-9} = 0.001\ Pa \quad [3.4.4\text{-}6]$$

When considering Turbine 2, the pressure ratio can be read off from the turbine map. This makes the calculation for P_7 remarkably easier:

$$P_7 = P_8.r \quad [3.4.4\text{-}7]$$

with r the pressure ratio of the turbine under discussion. The pressure drop in duct 6-7 is then used to determine the pressure at point 6 as:

$$P_6 = P_7(1 + Pdrop_{6-7}) \quad [3.4.4\text{-}8]$$

with:

$$Pdrop_{6-7} = 0.004\ Pa \quad [3.4.4\text{-}9]$$

The pressure drop through Regenerator 1 is similar to that of Regenerator 2, so:

$$P_5 = P_6(1 + Pdrop_{5-6}) \quad [3.4.4\text{-}10]$$

where:

$$Pdrop_{5-6} = \frac{f_{cold1}.L_{reg}.8.\left(\dot{m}_{plate1}\left(\frac{a}{b}\right)_{reg}\right)^2}{D_{h,reg}{}^5.\left(\left(\frac{a}{b}\right)_{reg}+1\right)^4.\rho_{cold1}.(1000.P_1.r.(1-P_{drop4-5}))} \quad [3.4.4\text{-}11]$$

An addition is made to the pressure drop in 5-6 since it is seen as a cold stream, which differs slightly from a hot stream such as 9-10. The pressure at point 4 is now determined by using the pressure drop in duct 4-5.

$$P_4 = P_5(1 + Pdrop_{4-5}) \quad [3.4.4\text{-}12]$$

where:

$$Pdrop_{4-5} = 0.004\ Pa \quad [3.4.4\text{-}13]$$

The pressure drop through the cold stream of Regenerator 2, namely 3-4 can be calculated as:

$$Pdrop_{3-4} = \frac{f_{cold2}.L_{reg}.8.\left(\dot{m}_{plate2}\left(\frac{a}{b}\right)_{reg}\right)^2}{D_{h,reg}{}^5.\left(\left(\frac{a}{b}\right)_{reg}+1\right)^4.\rho_{cold2}.(1000.P_1.r.(1-P_{drop2-3}))} \quad [3.4.4\text{-}14]$$

where:

$$P_{drop2-3} = 0.001\ Pa \quad [3.4.4\text{-}15]$$

Also using the pressure drop in duct 2-3, the pressure at point 2 is determined as:

$$P_2 = P_3(1 + Pdrop_{2-3}) \quad [3.4.4\text{-}16]$$

Now the pressure ratio for Compressor 2 can be written as:

$$\frac{P_2}{P_1} = r_{comp} \quad [3.4.4\text{-}17]$$

The second phase of the solution process is where the pressures in the primary (closed) cycle are calculated. The working fluid in the secondary cycle is also air. First of all, a pressure of atmospheric is assumed at the receiver outlet. This can be shown as:

$$P_{14} = P_{atm} \quad [3.4.4\text{-}18]$$

Atmospheric pressure is assumed at the receiver outlet since a (any) pressure value is needed for the optimisation algorithm to initiate its iterative loops. The choice is thus completely arbitrary. From this, the pressure at point 15 is calculated using the pressure drop in duct 14-15:

$$P_{15} = P_{14}(1 - Pdrop_{14-15}) \quad [3.4.4\text{-}19]$$

with:

$$Pdrop_{14-15} = 0.004\ Pa \quad [3.4.4\text{-}20]$$

The pressure drop through Turbine 1 is determined exactly as through Turbine 2, so:

$$P_{16} = P_{15}.r \quad [3.4.4\text{-}21]$$

The pressure drop in duct 16-17 is assumed to be:

$$Pdrop_{16-17} = 0.001\ Pa \quad [3.4.4\text{-}22]$$

so that the pressure at point 17 is determined as:

$$P_{17} = P_{16}(1 - Pdrop_{16-17}) \quad [3.4.4\text{-}23]$$

The pressure drop through the hot stream of Regenerator 1 is determined exactly the same as the hot stream of Regenerator 2.

$$Pdrop_{17-18} = \frac{f_{hot1}.L_{reg}.8.\left(\dot{m}_{plate1}\left(\frac{a}{b}\right)_{reg}\right)^2}{D_{h,reg}{}^5.\left(\left(\frac{a}{b}\right)_{reg}+1\right)^4.\rho_{hot1}.(1000P_1)} \quad [3.4.4\text{-}24]$$

From this, the pressure at point 18 is:

$$P_{18} = P_{17}(1 - Pdrop_{17-18}) \quad [3.4.4\text{-}25]$$

The pressure at point 11 is determined using the pressure drop in duct 18-11.

$$P_{11} = P_{18}(1 - Pdrop_{18-11}) \quad [3.4.4\text{-}26]$$

where:

$$Pdrop_{18-11} = 0.004\ Pa \quad [3.4.4\text{-}27]$$

The pressure drop in Compressor 1 is determined using the compression ratio found from the analysis of Compressor 2. A simple comparison can be written as:

$$\frac{P_{12}}{P_{11}} = \frac{P_2}{P_1} \quad [3.4.4\text{-}28]$$

From this:

$$P_{12} = \frac{P_2 . P_{11}}{P_1} \quad [3.4.4\text{-}29]$$

The pressure at point 13 is determined using the pressure drop in duct 12-13 such that:

$$P_{13} = P_{12}(1 - Pdrop_{12-13}) \quad [3.4.4\text{-}30]$$

where:

$$Pdrop_{12-13} = 0.001\ Pa \quad [3.4.4\text{-}31]$$

Finally, the pressure at the receiver outlet is recalculated by using the pressure drop in the receiver itself. Thus:

$$P_{14} = P_{13}(1 - Pdrop_{13-14}) \quad [3.4.4\text{-}32]$$

where:

$$Pdrop_{13-14} = 0.04\ Pa \quad [3.4.4\text{-}33]$$

The newly calculated value for the P_{14} is compared with the originally guessed value of P_{atm} and an iterative loop is used to ensure convergence of the two pressures within an error of 1e-3 %. At this point in the process, all the pressures for the double Brayton cycle as in Figure 3.2 are known. Phase 3 of the solution process starts off with solving the first couple of temperatures for the secondary cycle. T_1 is assumed to be equal to T_{atm} as already mentioned.

By using T_1, and the compressor pressure ratio, T_2 is solved to be:

$$T_2 = T_1 . \left(1 + \frac{K_{comp} - 1}{\eta_{comp}}\right) \quad [3.4.4\text{-}34]$$

where:

$$K_{comp} = r_{comp}^{\frac{k-1}{k}} \quad [3.4.4\text{-}35]$$

with k = 1.4. The temperature at the inlet of Regenerator 2 is determined using the temperature drop in duct 2-3.

$$T_3 = T_2 - T_{drop} \quad [3.4.4\text{-}36]$$

The temperature drops in all the ducts are assumed to be the same magnitude and equal to 2K.

For now, the focus of the analysis will shift to the primary cycle. The temperature for the outlet of the receiver is assumed to be a maximum value of 1,200 K. From this:

$$T_{15} = T_{14} - T_{drop} \quad [3.4.4\text{-}37]$$

By using the pressure ratio in Turbine 1, as read from the turbine maps, the temperature for the outlet of Turbine 1 is calculated as:

$$T_{16} = \frac{T_{15}}{1 - \eta_{turb}.\left(1 - \frac{1}{K_{turb}}\right)} \quad [3.4.4\text{-}38]$$

where:

$$K_{turb} = r^{\frac{k-1}{k}} \quad [3.4.4\text{-}39]$$

with k the same as before. The temperature drop in duct 16-17 is utilised to determine the temperature at point 17, the inlet of Regenerator 1.

$$T_{17} = T_{16} - T_{drop} \quad [3.4.4\text{-}40]$$

The inlet temperature for Compressor 1 is assumed a constant value of 700 K. This value can be varied at any time, and will change throughout the optimisation process. From this, the outlet temperature of Compressor 1 is determined by employing equation 3.4.4-41

$$T_{12} = T_{11}\left(1 + \frac{K_{comp} - 1}{\eta_{comp}}\right) \quad [3.4.4\text{-}41]$$

with K_{comp} shown in equation 3.4.4-35, and η_{comp} the compressor efficiency as taken from the turbine charts which can be found in Appendix II. The inlet temperature of the receiver is calculated by using the temperature drop in duct 12-13.

$$T_{13} = T_{12} - T_{drop} \quad [3.4.4\text{-}42]$$

Using the assumed value of the outlet temperature of the receiver, which will stay constant throughout the optimisation at the specified magnitude, the amount of heat absorbed at the receiver can be determined:

$$\dot{Q}_a = \dot{m}.c_p(T_{14} - T_{13}) \quad [3.4.4\text{-}43]$$

Originally, the work by Richard Petela [48] was used to determine the amount of energy absorbed by the receiver of the parabolic dish. It was found, however, that the results from the Petela process were not feasible as their magnitudes were not realistic. The reason for this is that the mathematical process incorporates parameters such as the sun's radius, the average distance between the earth and sun and even the parabolic dish diameter, but nowhere is the rest of the cycle being considered. This means that the same amount of energy is absorbed regardless of the set-up of the cycle. Thus the number of compressors, turbines, regenerators and even the size of the receiver tubes within the modified cavity receiver do not influence the amount of energy absorbed by the cycle in any sort of way. It was concluded for this reason that the process as suggested by Petela cannot be integrated in the optimisation algorithm that is used to solve for the open-air solar thermal Brayton cycle in this dissertation.

The secondary cycle temperatures are solved through an iterative process. To begin with, the temperature at point 4, the cold stream outlet of Regenerator 2, is assumed to be an arbitrary magnitude, i.e. 700 K. This value can be changed if needed. From this:

$$T_5 = T_4 - T_{drop} \quad [3.4.4\text{-}44]$$

By using the heat transferred in Regenerator 1, the outlet temperature for Regenerator 1 is determined as:

$$T_6 = T_5 + \frac{\dot{Q}_{reg1}}{\dot{m}c_p} \quad [3.4.4\text{-}45]$$

The inlet temperature for Turbine 2 is now determined as:

$$T_7 = T_6 - T_{drop} \quad [3.4.4\text{-}46]$$

By using the pressure ratio taken from the turbine map, the outlet temperature for Turbine 2 is calculated as:

$$T_8 = \frac{T_7}{1 - \eta_{turb}.\left(1 - \frac{1}{K_{turb}}\right)} \quad [3.4.4\text{-}47]$$

The temperature drop in duct 8-9 is used to determine the inlet temperature of the hot stream for Regenerator 2 as:

$$T_9 = T_8 - T_{drop} \quad [3.4.4\text{-}48]$$

By using the efficiency of Regenerator 2:

$$\eta_{reg2} = \varepsilon = \frac{\dot{Q}}{\dot{Q}_{max}} = \frac{T_{cold,out} - T_{cold,in}}{T_{hot,in} - T_{cold,in}} = \frac{T_4 - T_3}{T_9 - T_3} \quad [3.4.4\text{-}49]$$

The outlet temperature of the cold stream, point 4, is determined as:

$$T_4 = T_3 + \eta_{reg2}(T_9 - T_3) \quad [3.4.4\text{-}50]$$

It is at this point that the iterative loop for T_4 is repeated until the temperatures in the secondary cycle are solved to within an error of less than 1e-3 %. The efficiency or effectiveness of Regenerator 2 is employed to aid in solving T_{10}. The equation to perform this calculation is shown below:

$$T_{10} = T_9 - \eta_{reg2}(T_9 - T_3) \quad [3.4.4\text{-}51]$$

The value of T_{10} has no limit as it is an outlet temperature where waste heat exits the secondary stream. Naturally, the exit temperature must be kept as low as possible to ensure as little as possible heat is wasted in the overall heat transfer process.

The heat transfer rate from the hot to cold stream in Regenerator 2 is assumed to be a value that utilises the known T_3 and initially guessed T_4 value. This heat transfer rate can be shown as:

$$\dot{Q}_{reg2} = \dot{m}c_p(T_4 - T_3) \quad [3.4.4\text{-}52]$$

The final temperature to determine for the primary cycle is point 18, the outlet of Regenerator 1. This temperature is determined by using the efficiency or effectiveness of Regenerator 1.

$$T_{18} = T_{17} - \eta_{reg1}(T_{17} - T_5) \quad [3.4.4\text{-}53]$$

Now that the temperatures at the inlet and outlet of Regenerator 1 are known, the amount of heat that will be transferred to the cold stream can be determined as:

$$\dot{Q}_{reg1} = \dot{m}c_p(T_{17} - T_{18}) \quad [3.4.4\text{-}54]$$

The temperature of the Compressor 1 inlet temperature, T_{11}, is now recalculated from the outlet temperature of Regenerator 1 as:

$$T_{11} = T_{18} - T_{drop} \quad [3.4.4\text{-}55]$$

The iterative loop for the primary cycle is now continued until the inlet temperature of Compressor 1 converges to within an error of 1e-3 %. The structure of the optimisation procedure is included and properly discussed in Section 4.3.

3.4.5 The objective function

Since a major concern of this report is the exergy destruction or availability of exergy in the system, it is acceptable to now introduce the Gouy-Stodola theorem. This theorem states that the entropy generation in a system will be directly proportional to the lost available work for that same system [20]. For this reason, the sum of all the generated entropy rates in the system can be used to illustrate the maximum net power output. The entropy generation rates of the compressors, turbines, regenerators, ducts as well as the receiver can be included in the objective function. Scattering of the sun's radiation energy brings about a decrease in the solar radiation temperature. This loss leads to more entropy generation. According to Bejan [20], in order to ensure that the entropy generation rate due to scattering is negligible, the temperature of the sun, the sun being the main exergy source, must be assumed to be 2 470K.

Le Roux et al. [21] show that the objective function, being the maximum net power output obtainable from the system, can be written in terms of the temperature and pressure fields when the velocities and size at the inlet and outlet of the cycle are equal. Following a similar process, the discussion that follows was set up. When considering the entire C.V., it can be shown that the net power, or work, in the open air Brayton cycle can be illustrated as:

$$\dot{W}_{net} = \dot{W}_{turb} - \dot{W}_{comp} \quad [3.4.5\text{-}1]$$

and

$$\dot{W}_{net} = -T_0\dot{S}_{gen} + \left(1 - \frac{T_0}{T^*}\right)\dot{Q}^* + \dot{m}C_{p0}(T_{in} - T_{out}) - \dot{m}C_{p0}T_0 \ln\left(\frac{T_{in}}{T_{out}}\right) \quad [3.4.5\text{-}2]$$

The total entropy generation rate, $\dot{S}_{gen}$, is determined by adding the entropy generation rates of all the individual components in the cycle. These equations were discussed in each component's

respective section. Due to the complexity of the objective function, it is not shown as one single equation. Each separate entropy generation rate can now be added to the objective function.

$$\dot{W}_{net} = -T_0\left(\dot{S}_{gen,comp} + \dot{S}_{gen,reg} + \dot{S}_{gen,turb} + \dot{S}_{gen,rec} + \dot{S}_{gen,ducts}\right) + \left(1 - \frac{T_0}{T^*}\right)\dot{Q}^* + \dot{m}C_{p0}(T_{in} - T_{out}) - \dot{m}C_{p0}T_0\, ln\left(\frac{T_{in}}{T_{out}}\right) \quad [3.4.5\text{-}3]$$

where:

$$\dot{S}_{gen,comp} = \dot{S}_{gen,comp1} + \dot{S}_{gen,comp2} \quad [3.4.5\text{-}4]$$

$$\dot{S}_{gen,reg} = \dot{S}_{gen,reg1} + \dot{S}_{gen,reg2} \quad [3.4.5\text{-}5]$$

$$\dot{S}_{gen,turb} = \dot{S}_{gen,turb1} + \dot{S}_{gen,turb2} \quad [3.4.5\text{-}6]$$

$$\dot{S}_{gen,rec} = -\frac{\dot{Q}^*}{T^*} + \frac{\dot{Q}_0}{T_0} + \dot{m}C_{p0}\, ln\left(\frac{T_{12}}{T_{15}}\right) - \dot{m}R\, ln\left(\frac{P_{12}}{P_{15}}\right) \quad [3.4.5\text{-}7]$$

$$\dot{S}_{gen,ducts} = \dot{S}_{gen,23} + \dot{S}_{gen,45} + \dot{S}_{gen,67} + \dot{S}_{gen,89} + \dot{S}_{gen,1213} + \dot{S}_{gen,1415} + \dot{S}_{gen,1617} + \dot{S}_{gen,1811} \quad [3.4.5\text{-}8]$$

A generic equation can be set up to solve for each of the ducts' entropy generation rates. The inputs to this equation are the inlet and outlet to each duct, i.e. 2 and 3.

$$\sum_{i=2,4,6,8,12,14,16,18} \dot{S}_{gen:i,i+1} = \frac{\dot{Q}_{loss}}{T_0} + \dot{m}C_{p0} \ln\left(\frac{T_{i+1}}{T_i}\right) - \dot{m}R \ln\left(\frac{P_{i+1}}{P_i}\right) \quad [3.4.5\text{-}9]$$

The above equation holds for all ducts, where *i* and *i+1* must be seen as inlet and outlet points of each respective duct. The heat loss in each duct is assumed to be constant and fixed; therefore, it is not influenced by the duct under consideration. The major factor influencing the entropy generation rate in the ducts is the temperatures at the start and end of each duct.

3.4.6 Regenerator efficiency

Included in this section is the method with which the efficiencies for both regenerators are determined so that these efficiencies can be included in the overall optimisation algorithm. Depicted in Figure 3.3 is the regenerator design to be used.

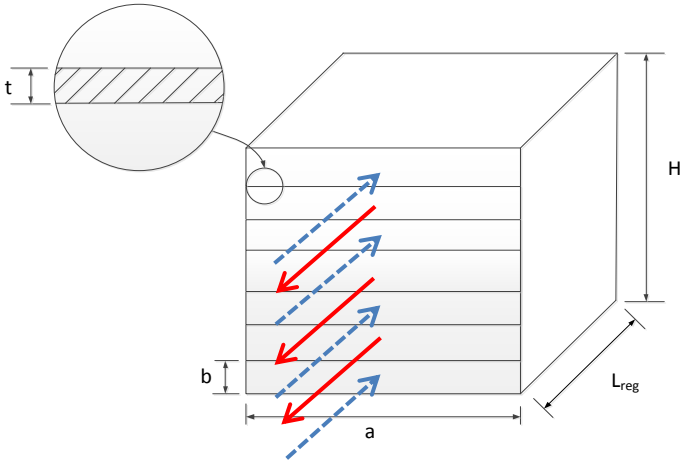

Figure 3.3 The plate-type regenerator to be used

As a start, some fixed parameters are defined. These include the total height of the regenerator, set to 1m to ensure simplicity, also the thickness of the plate between subsequent channels and the thermal conductivity to be used for the regenerators. Thereafter, a temperature is assumed for the cold and hot streams of the regenerator respectively, and at these temperatures, the Prandtl number, thermal conductivity, constant-pressure-specific heat and the dynamic viscosity of the two streams are used as inputs. The total mass flow rate of the cycle is also used as input for this function.

The mass flow rate per channel is determined with:

$$\dot{m}_{channel} = \frac{2\dot{m}}{n} \qquad [3.4.6\text{-}1]$$

with:

$$n = \frac{H}{t+b} = \frac{H}{t + D_{h,reg}\left(\left(\frac{a}{b}\right)_{reg} + 1\right) / \left(2\left(\frac{a}{b}\right)_{reg}\right)} \qquad [3.4.6\text{-}2]$$

with H, t and b as defined in Figure 3.4.

The next step is to determine the Reynolds number for each of the fluid streams (in a rectangular channel) with the following equation, which is in terms of the regenerator parameters:

$$Re = \frac{4\dot{m}_{reg}\left(\frac{a}{b}\right)_{reg}}{\mu D_{h,reg}\left(\left(\frac{a}{b}\right)_{reg} + 1\right)^2} \qquad [3.4.6\text{-}3]$$

The first Petukhov equation [49] is used to determine the friction factor as:

$$f = (0.79\ln(Re) - 1.64)^{-2} \qquad [3.4.6\text{-}4]$$

It is at this point in the process that the Gnielinski equation [50] is used to determine the Nusselt number as it is expected that small Reynolds numbers will be present in each channel of the regenerators since the mass flow rates are small.

$$Nu_D = \frac{Pr(Re - 1000)(f/8)}{1 + 12.7(f/8)(Pr^{2/3} - 1)} \qquad [3.4.6\text{-}5]$$

From which the convection heat transfer coefficients of both the hot (h_h) and cold (h_c) streams can be determined by using equation 3.4.6.-6:

$$h = \frac{kNu_D}{D_{h,reg}} \qquad [3.4.6\text{-}6]$$

Once the hot and cold streams are solved separately, the overall heat transfer coefficient is determined with:

$$U = \left(\frac{1}{h_c} + 2R_f + \frac{L_{reg}}{k_{solid}} + \frac{1}{h_h}\right)^{-1} \quad [3.4.6\text{-}7]$$

Çengel [51] suggests a fouling factor (R_f) of 0.004 when air is used as the working fluid. The area per plate in the regenerator is determined with:

$$A_{plate} = D_{h,reg} L_{reg} \left(\left(\frac{a}{b}\right)_{reg} + 1\right)\left(1 + \left(\left(\frac{a}{b}\right)_{reg}\right)^{-1}\right) \quad [3.4.6\text{-}8]$$

The total number of heat transfer units in the regenerator (NTU) is then determined as:

$$NTU = \frac{UA_{plate}}{\dot{m}_{plate} c_p} \quad [3.4.6\text{-}9]$$

Where $\dot{m}_{plate} = \dot{m}_{channel}$. Equation 3.4.6-9 can be used for both hot and cold streams.

The ratio between cold and hot constant-pressure specific heats is calculated as:

$$c = \frac{c_{p,c}}{c_{p,h}} \quad [3.4.6\text{-}10]$$

Where $c_{p,c}$ is the constant-pressure specific heat for the cold stream, and $c_{p,h}$ is the constant-pressure specific heat for the hot stream. Both of whom are read off from property tables at the various stream temperatures. Finally, the heat exchanger efficiency is determined by using the suggestions from Stine and Harrigan [9] and Çengel [51], which state that the effectiveness and efficiency for a regenerator are defined in the same way, thus:

$$\eta_{reg} = \varepsilon = \frac{1 - exp\big(-NTU(1-c)\big)}{1 - c.exp\big(-NTU(1-c)\big)} \quad [3.4.6\text{-}11]$$

The efficiency that is determined for each regenerator is again inserted in the main optimisation algorithm to ensure that the temperatures and pressures for the cycles are determined as accurately as possible.

3.4.7 Interpolation for mass flow rate from pressure ratio

A simple yet effective interpolation equation was derived with which each turbine choice's optimal mass flow rate can be calculated by using all the data given in the turbine maps and also a certain pressure ratio, which is an input parameter to the optimisation scheme. The maximum and minimum pressure ratios and mass flow rates for a given turbine were used as shown in Table 3.1.

Table 3.1 Interpolation for operation mass flow rate

Pressure ratio (r)	Mass flow rate ($\dot{m}$)
r_{min}	$\dot{m}_{min}$
$r_{operation}$	$\boldsymbol{\dot{m}_{operation}}$
r_{max}	$\dot{m}_{max}$

By employing simple interpolation, it can be derived that:

$$\frac{\dot{m}_{operation} - \dot{m}_{min}}{r_{operation} - r_{min}} = \frac{\dot{m}_{max} - \dot{m}_{min}}{r_{max} - r_{min}} \quad [3.4.7\text{-}1]$$

where:

$$\dot{m}_{operation} = \left(\frac{\dot{m}_{max} - \dot{m}_{min}}{r_{max} - r_{min}}\right)\left(r_{operation} - r_{min}\right) + \dot{m}_{min} \quad [3.4.7\text{-}2]$$

It was found that the relationship between the specified operation pressure ratio and the mass flow rate of operation is purely linear as can be seen in the example below.

Consider Turbine 60 which is the largest turbine in the list in Appendix II. The maximum and minimum mass flow rates that can be handled by this turbine are 0.635 kg/s and 0.363 kg/s respectively. The maximum and minimum pressure ratios for this turbine are 3 and 1.25 respectively.

By employing these maximum and minimum values, and operation pressure ratios ranging from the minimum to the maximum value in increments of 0.25, results are found and put together in Figure 3.3.

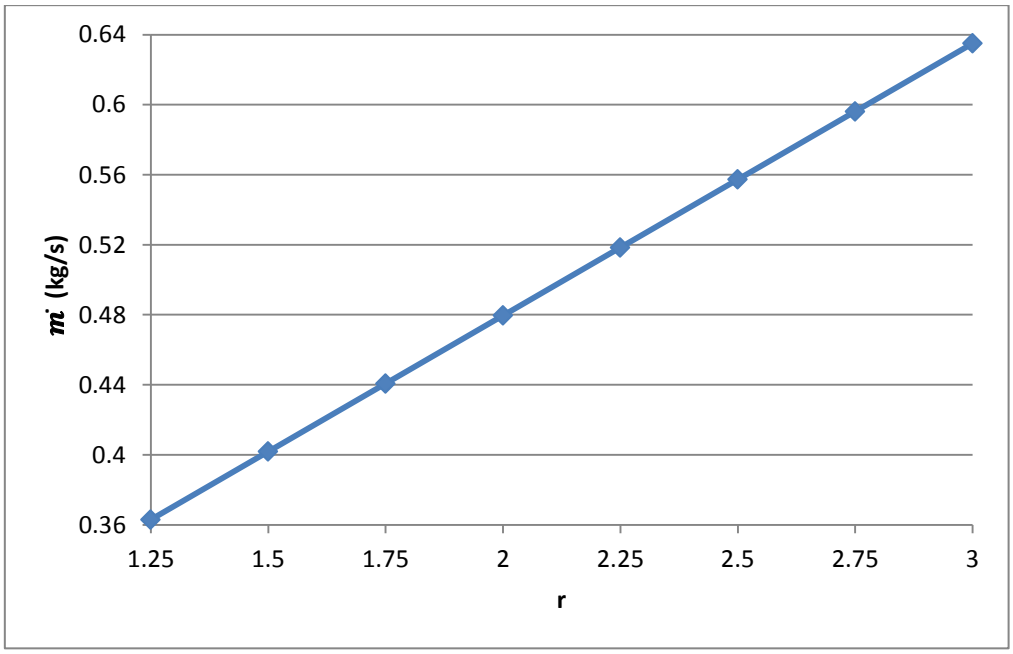

Figure 3.4 Mass flow rate as a function of the input pressure ratio

Figure 3.3 clearly shows how the mass flow rate is directly proportional to the input parameter for the turbine choice at hand. This trend also applies to all the other turbine choices, and can be attributed to the linear form of equation 3.4.7-2.

3.4.8 Steady state and transient operation

A thermodynamic analysis for a control volume can be either steady state or transient. In most cases, a real cycle undergoes transient operation, meaning some significant parameter changes with time. Regularly an analysis is said to be steady state. This simplifies the analysis in terms of complexity and the time needed to solve it, whilst still providing viable conclusions with which to evaluate a cycle or system. Sonntag et al. [26] explains that some investigative models contain specific assumptions that are not always valid. They go on to list a couple of transient model assumptions:

- The control volume remains constant relative to the coordinate frame
- The state of mass within the control volume may change with time, but at any given instant of time, the state is uniform throughout the entire control volume. Alternatively over several identifiable regions that make up the entire control volume.
- The state of the mass crossing each of the areas of flow on the control surface is constant with time although the mass flow rate may be time varying.

A number of first law (of thermodynamics) transient model equations can be found in Sonntag et al. [26]. When considering concentrating solar power systems, the sun's irradiance is in actual fact transient, as it varies throughout the day. Also the mass flow rate through each of the cycles, albeit closed or open, will prove to be transient. This is however a topic for future investigations and will not be covered in this dissertation. Instead, this dissertation considers only a steady state analysis.

3.5 Component parameters

3.5.1 The regenerators

The regenerators are represented by Figure 3.4, which shows all the regenerators' parameters.

In Figure 3.4, the channel width and height are denoted by 'a' and 'b' respectively. 'H' is the total heat exchanger height; 't' is the plate thickness between two channels and L_{reg} is the the total length of the heat exchanger. The hot and cold flows are denoted by the two sets of arrows flowing in and out of the heat exchangers.

3.5.1.1 The number of channels

By using the total height, height per channel and the thickness of the walls between channels, the number of channels to be used in each regenerator can be calculated as:

$$n \geq \frac{H}{t+b} - b \qquad [3.5.1\text{-}1]$$

The top and bottom walls of the regenerator are not included in equation 3.5.1-1.

3.5.1.2 The hydraulic diameter

The hydraulic diameter comes into play when the area of any non-circular channel or shape needs to be determined. It entails that the said shape is related to a circular feature with the same cross-sectional area as the shape itself. In the case of the rectangular regenerator channels under discussion, the rectangular cross-sectional area can be written as:

$$A_{rect} = 2(a+b)L_{reg} \quad [3.5.1\text{-}2]$$

Now recall the area of a circle:

$$A_{circ} = \frac{\pi}{4}D^2 \quad [3.5.1\text{-}3]$$

When the rectangular area is related to the circular area, the circle diameter becomes the hydraulic diameter, as follows:

$$A_{rect} = A_{circ} \quad [3.5.1\text{-}4]$$

$$2(a+b)L_{reg} = \frac{\pi}{4}{D_h}^2 \quad [3.5.1\text{-}5]$$

From this the hydraulic diameter is:

$$D_h = \sqrt{\frac{8(a+b)L_{reg}}{\pi}} \quad [3.5.1\text{-}6]$$

The hydraulic diameter can also be calculated by using a formula proposed by Çengel [51], where

$$D_h = \frac{4A_c}{p} \quad [3.5.1\text{-}7]$$

with:

A_c = cross-sectional area of the rectangle

P = perimeter of the rectangle

Thus when considering Figure 3.4:

$$D_h = \frac{4(ab)}{2(a+b)} = \frac{2ab}{a+b} \quad [3.5.1\text{-}8]$$

When these two equations for hydraulic diameter are equated, we find a way to determine an ideal value for L_{reg} by using the width and height of the channels or by fixing L_{reg} and one of the parameters *a* or *b*, the unfixed parameter can be solved for. This will serve as a control check in the solution for the system.

3.5.2 The receiver

From Reddy and Sendhil Kumar [18], it is found that a modified cavity receiver should be used when an efficient Brayton cycle is required. The motivation behind these findings is the lower convection heat losses experienced by the receiver, which makes it an ideal receiver for solar dish collector

systems. Figure 3.5 shows the modified cavity receiver as suggested by Reddy and Sendhil Kumar [18].

The opening at the bottom of the receiver is called the aperture. The size of this aperture is determined by the flux distribution (local image characteristics of the fuzzy focal solar dish). As seen in Figure 3.5, the inner surface of the modified cavity receiver is completely covered in tightly wound copper tubing. The shape of this tubing can be either circular or rectangular. For the sake of simplicity, only the rectangular-shaped tubing is considered in this analysis. Le Roux et al. [21] considered the influence of the duct shape on the pressure drop through the components. As mentioned earlier, it can be assumed that these tubes form a completely closed hemisphere on the inner surface of the receiver. The convective heat loss from the receiver takes place through the aperture, and it is suggested that the ratio of the inner heat transfer area of the receiver to that of the receiver aperture area should be equal to 8 [16].

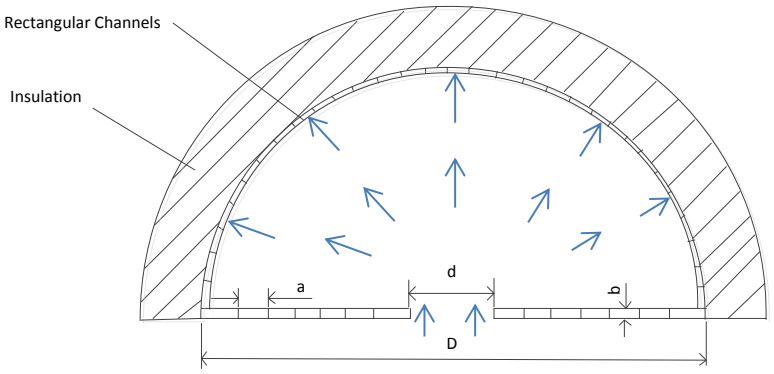

Figure 3.5 Schematic diagram of the modified cavity receiver

In Figure 3.5, 'a' and 'b' again denotes the channel width and height respectively. 'd' is the aperture diameter while 'D' is the total diameter of the modified cavity receiver. Also shown in Figure 3.5 is the direction of heat flowing into the receiver and up to the external channel surface, across which the heat exchange will occur, with the working fluid flowing in the rectangular channels as shown in Figure 3.5.

Reddy and Sendhil Kumar [16] also found that the tilt angle of the receiver influenced the radiation losses. When the tilt angle is zero, meaning the plane passing through the aperture is vertical, the ratio of the contribution of radiation and convection losses is 47:52. When the tilt angle changes to 90°, this ratio becomes 57:43. Thus this ratio between radiation and convection heat loss varies with the inclination of the cavity receiver. From the data taken from this analysis, it is assumed the heat lost by radiation and that lost by convection are equal. It was ultimately concluded that heat loss would be a maximum when the sun is on the horizon and the receiver faces

the sun. This, fortunately, is mostly not the case. The Nusselt number used in this analysis is suggested to be Nu = 20, since the receiver is always between 0 and 90°.

During the calculation of the entropy generation rate in the receiver, the rate of heat loss in the receiver is utilised. This rate of heat loss is made up of convection and radiation heat losses, and can be calculated with an equation found in le Roux et al. [21]:

$$\dot{Q}_0 = 1.396 {Gr_D}^{0.209}(1 + cos\beta)^{0.968}(T_w/T_\infty)^{-0.317}(d/D)^{0.425}(kA_a/D)(T_w - T_\infty) \quad [3.5.2\text{-}1]$$

In the equation above, Gr_D is the Grashof number based in the receiver diameter. The angle β is the inclination angle. T_w is the temperature reached by the wall of the receiver and is set to the maximum system temperature of 1,200 K. T_∞ is the environmental temperature. The small letter 'd' is the diameter of the receiver aperture. Capital 'D' is the diameter of the entire receiver. The area denoted by A_a is the area of the aperture of the receiver.

Reddy and Sendhil Kumar [16] found that for minimum heat loss, the relationship between the modified cavity receiver diameter and the receiver aperture diameter can be simplified as:

$$D = \sqrt{3}d \quad [3.5.2\text{-}2]$$

When considering Figure 3.5, the receiver parameters to be used are the hydraulic diameter of the tubing in the receiver, the total length of the tubing in the receiver and the ratio of the width-to-height of the tubing in the receiver. These parameters are used in the optimisation algorithm to determine the pressure drop in the receiver. These parameters are free to vary with each different analysis, meaning the receiver parameters are different for the same system at various pressure ratios, temperature combinations and turbine choices.

3.6 Constraints and assumptions

As with any numerical analysis conducted in modern-day engineering practice, numerous assumptions are made to help simplify the solution process of a given system. It is of course understandable that the fewer assumptions are made, the higher the quality and feasibility of a set of results will be for that given system. It is for this reason that an engineer must always look at limiting the number of assumptions and finding the perfect balance between simplifications of a solution process (more assumptions), and quality of results (less assumptions).

Another very important practice of engineers is to define some constraints. When considering numerical analysis, constraints serve the same purpose as assumptions in that they simplify the solution process, usually in terms of the boundaries of investigation. Thus the domain or range of any given numerical analysis is controlled by these constraints.

Constraints and assumptions can easily be seen under the same light, but for the purpose of this study, an assumption will be any value or condition set before the solution process which will not

influence the main solution boundaries, and which only consists of a single value. A constraint will be the way in which a set, or range, or domain of values is limited. Thus for a constraint, more values are in use.

Included in Table 3.2 is a summary of all assumptions and constraints for the optimisation under investigation.

- Even though the major regenerator parameters are part of the optimisation algorithm and are solved numerically, some of the values are assumed values, in order to simplify the solution process and time. These parameters are:
    - Total regenerator height (H) is fixed at 1m.
    - The thickness of the plates that split subsequent channels in the regenerator (t) is fixed at 1mm, i.e. 0.001 m.
    - The thermal conductivity of the regenerator material (k_{solid}) is fixed at 401 W/m.K, which is the coefficient of conductivity for pure copper.
    - The length of the regenerator has a maximum value equal to the radius of the parabolic dish. This ensures that every value, at which the regenerator length is optimised, will never be any larger than the parabolic dish radius. This is to keep the total size of the system as small as possible.
    - The temperatures for the cold and hot stream of the regenerators were initially assumed to be fixed temperatures. After the solution for the regenerator efficiencies was completed, these temperatures were investigated, re-evaluated and used in the second run of the process. This ensured that these temperatures, and the air properties read off at them, were feasible.
    - During the investigation of the regenerator efficiencies, a fouling factor for the working fluid was assumed to be 0.004 since this working fluid is air.
- Most receiver parameters are used in the optimisation algorithm as parameters that need to be solved, or optimised; however, the temperature of the receiver outlet is an assumed value. Even though this receiver outlet temperature and its influence is investigated, the maximum value at which it can be fixed is 1,200 K. The motivation for this is the material choice for the receiver ducts/channels, which will start to melt beyond this temperature, resulting in catastrophic failure of the system.
- The copper ducts or tubes, which are closely wound in the receiver, are assumed to be of a flat plate (rectangular) shape. Le Roux et al. [21] investigated both round and rectangular profiles and the influence of the shape on the system as a whole. For the sake of simplicity only one shape is considered in this investigation.

- As mentioned earlier in this report, an exergetic analysis conducted by Petela [48] was originally considered to calculate the amount of heat that can be absorbed by the receiver. It was, however, found that this process is not feasible for the cycle at hand and thus the heat absorbed at the receiver was included in the optimisation algorithm as a parameter.
- The radius of the solar parabolic concentrator dish was assumed to be equal to 5m. This value is used as an input parameter and the same optimisation algorithm can be carried out at other dish radii. This, however, does not fall within the scope of the current investigation.
- As seen in Appendix Ia, a temperature drop of 2K was assumed. This is partly due to the fact that the same value was assumed in a previous and similar investigation by Le Roux et al. [21], and partly because this magnitude influences the optimum solution without dominating it. A closer investigation is suggested for a future study, where the exact magnitude of the temperature drop is found. This investigation will require the length and diameter of each duct in the system, which will enable the more accurate calculation of the temperature and also the pressure drops of the system.
- The values for the various ambient conditions are assumed to be the following:
    - Ambient temperature is fixed at 25°C or 298 K
    - Ambient pressure is fixed at 1 atm, which is 101.325 kPa
    - The temperature of the sun is fixed at 2,470 K. This value is suggested by Bejan [20] to ensure that the entropy generation rate due to scattering can be neglected.
    - The ratio between the constant-pressure- and constant-volume-specific heats, k, is assumed to be 1.4 since the working fluid is air.
- Even though no pipe or duct cross-sections, lengths or surface roughness's are specified, the heat loss through the pipes and ducts can be approximated using the convection heat loss equation similar to that of Equation 3.4.4-43. The mass flow rate can be assumed as 0.386 kg/s which coincides with a pressure ratio of 1.4. The constant-pressure specific heat is taken as 1.005 kJ/kgK and the temperature drop as 2 K. The resultant heat loss then amounts to 800 W or 0.8 kW. When considering a power generation of 40 kW, the heat loss in a pipe or duct can be approximated as 40/0.8 = 2 %. It must once again be noted that the heat loss, temperature and pressure drops in the ducts are direct results of the duct sizing, therefor by changing the hardware setup of the system, i.e. the lengths of the ducting and the structure of the major component assembly, the heat loss, temperature and pressure drop can be influenced accordingly.

Table 3.2 Summary of assumptions and constraints

Consideration	Assumption	Description
Regenerators	H = 1 m	Height of regenerator
	t = 1 mm	Thickness of channel separating plates
	k_{solid} = 401 W/m.K	Coefficient of conductivity for regenerators
	T_{hot}, T_{cold}	Temperatures at which properties are read off
	R_f = 0.004	Fouling factor for air (working fluid)
Parabolic dish	R_{dish} = 5 m	Dish radius fixed at 5m
Temperature drop	T_{drop} = 2 K	Temperature drop in ducts fixed at 2K. However, difference in this value was investigated
Ambient conditions	T_0 = 298 K	Ambient temperature taken as room temperature
	P_0 = 1 atm	Ambient pressure taken as sea-level pressure
	T_{sun} = 2,470 K	Sun temperature assumed to account for scattering
	k = 1.4	Ratio of specific heats for air (working fluid)
Heat loss in ducts	Q_{loss} = 800 W	Heat loss in each of the ducts. Dependent on assumed temperature loss. Kept constant regardless of duct size
Receiver	T_{out} = 1,200 K	Receiver outlet temperature limited to theoretical melting temperature for copper
	Tube shape	Receiver tube shape assumed to be rectangular to simplify solution process
Consideration	**Constraint**	**Description**
Regenerators	L_{rec} <= R_{dish}	Length of regenerators limited to a maximum equal to dish radius
Note: All receiver parameters to be optimised were not constrained in any way		

3.7 Conclusions

In this chapter, the system to be solved was identified as the open-air solar thermal Brayton cycle. This system was modified and mathematically investigated, and all the necessary equations that will be used in the numerical model were identified. The mathematical model includes the entropy generation rates for all of the individual components. The sum of the individual internal entropy generation rates is equal to the external entropy generation rate. Also the maximum amount of net power (work) that can be extracted from the system was linked to the entropy generation rates for the system.

The physical system was discussed in terms of the hardware or components that will be used and all the needed assumptions or pitfalls associated with each of these components were identified and properly discussed.

All assumptions and constraints that will be used in the numerical analysis were set and discussed. The numerical analysis can be found in the next chapter.

4 Numerical method

4.1 Introduction

The numerical method that was used in the set-up of the optimisation algorithm is discussed in this chapter. Different parameters were considered for a number of cases, which are all elaborately explained in the following sections. The procedure that the optimisation algorithm follows is discussed in depth to illustrate the train of thought of the author.

4.2 Optimisation

4.2.1 Parameters influencing the optimisation procedure

For the system at hand a number of different parameters are known, which all influence the optimum system characteristics in one way or another. These are:

- Regenerator and receiver dimensions, such as hydraulic diameters, lengths and width-to-height ratios.
- Choice of temperatures for the compressor inlet and receiver outlet temperatures in the primary cycle
- Choice of turbine

The order in which these parameters are considered and optimised is not structured in any certain way and can be altered to consider the influence of the order on the solution process. This was, however, not done in this analysis.

4.2.2 Optimisation in stages

4.2.2.1 Temperature combinations

Since a central idea of the current investigation is the constraint of fixed temperatures at the compressor inlet and receiver outlet in the primary loop, as seen in Figure 3.2, it is a good idea to investigate the influence of temperatures for these two points, and also the influence of the combination of the two temperatures on the results. The compressor inlet temperature in the primary loop, point 11 in Figure 3.2, is set to a certain value. The optimisation algorithm solves for an optimum T_{11} value while optimising the regenerators and receiver dimensions. The temperatures solved for at the inlet of Compressor 1 for each of the optimum cases, were noted, compared and discussed. The receiver outlet temperature, point 14 in Figure 3.2, was set to values ranging from 1 000K to 1 200K in 50K increments, where 1 200K is the theoretical maximum system temperature at which copper starts to melt, and at which the system would consequently experience major malfunctioning.

The combinations were investigated for feasibility and the valid combinations were considered more closely.

4.2.2.2 Regenerator and receiver dimensions

For the entire system, six different parameters will be optimised. These parameters are as follows:

- $(a/b)_{reg}$ - the ratio of the width to the height of each individual channel in a rectangular regenerator. The width of each channel is also the total width of the regenerator
- D_{hreg} - the hydraulic diameter of the regenerator channels
- L_{reg} - the length of the regenerator
- $(a/b)_{rec}$ - the ratio of the width and height of each individual channel in a rectangular receiver
- D_{hrec} - the hydraulic diameter of the receiver channels
- L_{rec} - the length of the receiver

The parameters for the regenerators are shown graphically in Figure 3.4. The order in which the abovementioned parameters are optimised is once again not fixed and can be varied and re-evaluated. In this analysis, the system parameters were first set at assumed values and a specific pressure ratio ranging from 1.4 to 2.1, with corresponding mass flow rates ranging from 0.3863 to 0.4951 kg/s. These mass flow rates are the result of using the largest possible turbine with the maximum possible mass flow rates.

The first parameter to be optimised was the ratio of width-to-height for the regenerator. Thereafter, the hydraulic diameter and length used for the regenerator were optimised. The three parameters for the receiver were then optimised in the same order as that of the regenerator.

4.2.2.3 Turbine choices

In this analysis, a number of turbines were considered. From a list of about 60 turbines, only the turbines with efficiencies above 74% were considered. For each of these turbine choices the corresponding compressor efficiency was also supplied. From the initial list, only 11 turbines were further considered. These turbines and their properties are shown in Table 4.1.

Table 4.1 Turbines used in analysis

Turbine name	Turbine number	Pressure ratio minimum	Pressure ratio maximum	Mass flow rate minimum (kg/s)	Mass flow rate maximum (kg/s)	Maximum turbine efficiency (%)	Maximum compressor efficiency (%)
GT4202 1.01	42	1.2	3	0.181	0.283	74	77
GT4202 1.15	43	1.2	3	0.204	0.31	74	77
GT4202 1.28	44	1.2	3	0.227	0.329	74	77
GT4202 1.44	45	1.2	3	0.234	0.34	74	77

GT4294R 1.01	46	1.2	3	0.181	0.283	74	78
GT4294R 1.15	47	1.2	3	0.204	0.31	74	78
GT4294R 1.28	48	1.2	3	0.227	0.325	74	78
GT4294R 1.44	49	1.2	3	0.234	0.34	74	78
GT5533R	58	1.2	3.25	0.249	0.454	80	77
GT5541R	59	1.2	3.25	0.249	0.454	80	75
GT6041	**60**	**1.25**	**3**	**0.363**	**0.635**	**78**	**80**

Table 4.1 conveys all of the turbine properties as found in the Garret supercharger catalogue [45]. The minimum and maximum values of the pressure ratios and mass flow rates were used to set up a simple interpolator that supplies the user with the correct mass flow rate at an investigated pressure ratio.

Preliminary tests showed that larger net power outputs were found at larger flow rates. For this reason, it was decided that the GT6041 turbine with the number of 60 in Table 4.1 would be used for further analyses as its range of mass flow rates of operation was the largest and had the highest maximum value.

4.3 Program structure

The code that was used to solve the system for all of the above parameters is included in Appendix I. A basic layout of the code is given below to explain the thought process of the author:

- Set all system parameters, such as environmental conditions and assumed parameters.
- Use a function to determine system mass flow rate and area of the parabolic dish using the initially chosen system parameters.
- Use a second function that inputs the set parameters and mass flow rate to determine the regenerator efficiencies using the ε-NTU method.
- Define all temperature and pressure drops present in both the primary and secondary cycles.
- Assume the pressures at the secondary cycle inlet (point 1 in Figure 3.2), the receiver outlet in the primary cycle (point 14 in Figure 3.2) and the secondary cycle outlet (point 10 in Figure 3.2) to be ambient pressure. Using assumed pressure at point 14, determine remainder of primary cycle pressures using pressure ratio, regenerator and receiver parameters.
- Using the optimised temperature of the receiver outlet (point 14 in Figure 3.2), determine the remainder of the primary cycle temperatures.
- Assume a temperature for the cold stream outlet of Regenerator 2 (point 4 in Figure 3.2).

- Initiate a loop that determines all secondary cycle temperatures while converging to an error of 1e-3 % for the temperature of the cold stream outlet for the second regenerator (point 4 in Figure 3.2).

- Determine entropy values for all of the components and the ducts in between the components.
- Determine objective function using total entropy generation rate.
- Determine remainder of unknowns such as the thermal efficiency of the entire cycle and irreversibilities (both internal and external)
- Set up plots and tables with which results can be compared and discussed.

4.4 Conclusions

The optimisation algorithm to be used was briefly discussed. The parameters that need to be solved with the optimisation algorithm were all identified. The procedure of the optimisation algorithm was deliberated and all stages were discussed at length. The structure of the main analysis of the optimisation algorithm and how the parameters fit into it were also discussed. The use of numerical methods to solve for intricate, multi-parameter single-objective functions once again proved invaluable as a similar analysis would have taken months if only an analytical approach was used. The results from this numerical analysis are all included in the next chapter.

5 Results

5.1 Introduction

The results presented in this chapter serve to properly describe and illustrate the open-air solar thermal Brayton cycle that was considered in this dissertation. First, the results are shown and discussed. Some minor influences on the system are also identified and conclusions are made accordingly. The results are verified with set system values to ensure the validity of the discussed results. A section is included to discuss this validation process. A comparative analysis is conducted on a single regenerator cycle in order to find the major differences and/or similarities. Finally, some conclusions are made by considering the results at hand.

5.2 Full analysis

5.2.1 Relationship between pressure ratio and mass flow rate

As already mentioned, there exists a certain relationship between the pressure ratio for each turbine and its corresponding mass flow rate. This relationship is discussed in Section 3.4.7. The result from this discussion is that the mass flow rate follows a linear relationship as pressure ratio is increased. This is shown graphically in Figure 3.3. For the purpose of standardising all figures and simplifying the understanding of the results, all plots are made as functions of the mass flow rate. However, the profiles of all results are exactly the same if these plots were made as functions of the pressure ratio instead.

5.2.2 The open-air solar thermal Brayton cycle

The inclusion of both regenerators as seen in Figure 3.2 is the accepted norm for the study at hand. An investigation was made into the significance of the second regenerator and its influence on the objective function and efficiency of the cycle.

The objective function, as discussed in Section 3.4.5, is the ultimate value on which the cycle under investigation is evaluated. Nevertheless, there are many other parameters such as efficiency and entropy generation rate from which the conclusions can be elaborated. First, the objective function is also known as the second law net power output from the system as a whole, this includes the primary and secondary cycles, each having a compressor, one or two regenerators and a turbine, which is connected to a generator where the power is eventually generated.

When the optimisation was carried out at the various mass flow rates, the resultant optimum values were all compared. Table 5.1 shows the optimised values for the regenerator parameters that supply the best net power output values. When comparing the respective mass flow rates that go together with these objective function values, it can be seen that a single mass

flow rate exists at which the objective function is a maximum. Turbine 60 from the turbine choice list in Table 4.1 was used in all the analyses below unless stated otherwise.

Table 5.1 Optimum values at various mass flow rates

Mass flow rate (kg/s)	Q_a (kW)	W_{net} (kW)	$(a/b)_{reg}$	$D_{h,reg}$ (m)	L_{reg} (m)	$(a/b)_{rec}$	$D_{h,rec}$ (m)	L_{rec} (m)
0.386	111.6763	13.6008	2.31	0.00383	1	16.31	0.0757	14.7
0.402	102.9557	12.9386	1	0.0111	3.16	10.16	0.0921	15.09
0.417	111.7319	15.1605	3.12	0.00317	1.1	5.134	0.104	11.58
0.433	**111.764**	**15.6402**	**1.97**	**0.00415**	**1.53**	**9.66**	**0.0835**	**9.08**
0.448	109.896	15.2701	1	0.0088	2.827	13.32	0.0753	8.03
0.464	110.7532	15.55	1	0.0078	2.836	15.05	0.0731	7.77
0.48	113.9503	15.5401	1.1	0.00516	2.3	17.05	0.0713	7.659
0.495	110.9698	14.7804	1.15	0.00932	3.91	19.33	0.07	7.45

From Table 5.1 it can be seen that some clear trends appear in the values supplied. First, the net power output, designated Wnet (kW), is the highest at a mass flow rate of 0.433 kg/s, which relates to a pressure ratio of 1.7. The regenerator and receiver parameters all vary with the increase in the mass flow rate. In Table 5.2 the respective entropy generation rates are shown for each of the mass flow rates. The first law of thermodynamics work/power output, the first law efficiency and also the converged Compressor 1 input temperature are shown in Table 5.2. The first law efficiency as in Table 5.2 is determined by dividing the first law net power output, W_{net1}, by the amount of specific heat in the receiver, Q_a:

$$Efficiency\ (first\ law) = \eta = \frac{W_{net1}}{Q_a} \qquad [5.2.2\text{-}1]$$

Table 5.2 Optimum values at various mass flow rates continued

Mass flow rate (kg/s)	Pressure ratio	W_{net1} (kW)	$S_{gen,comp}$ (W/K)	$S_{gen,turb}$ (W/K)	$S_{gen,rec}$ (W/K)	$S_{gen,reg}$ (W/K)	$S_{gen,TOTAL}$ (W/K)	Efficiency (%)	T_{11} (K)
0.386	1.4	19.8964	18.4653	8.9885	51.2511	107.9655	193.5585	17.8161	838.5617
0.402	1.5	23.6528	22.6949	11.4548	46.079	95.5972	182.9414	22.9738	843.705
0.417	1.6	28.4785	26.9912	14.0041	50.4583	94.1932	192.9992	25.4883	816.0997
0.433	**1.7**	**32.4948**	**31.1662**	**16.6344**	**50.1234**	**87.6672**	**193.3059**	**29.0744**	**806.1436**
0.448	1.8	35.9044	35.3029	19.3438	48.7857	80.7369	192.1599	32.6712	799.9255
0.464	1.9	39.6344	39.4591	22.1303	48.9122	75.0923	193.857	35.7862	789.6619
0.48	2	42.841	43.6215	24.9921	50.2321	72.5735	199.3146	37.5963	776.6122
0.495	2.1	45.9936	47.7304	27.9276	48.4006	64.5451	197.4379	41.4469	773.046

The parameters for each of the mass flow rates, as shown in Tables 5.1 and 5.2, are shown graphically in the following figures.

The objective function at each of the investigated mass flow rates is shown in Figure 5.1. Also shown are the first law net power output values, the first law efficiency for each mass flow rate and the net absorbed heat that resulted from the optimisation process.

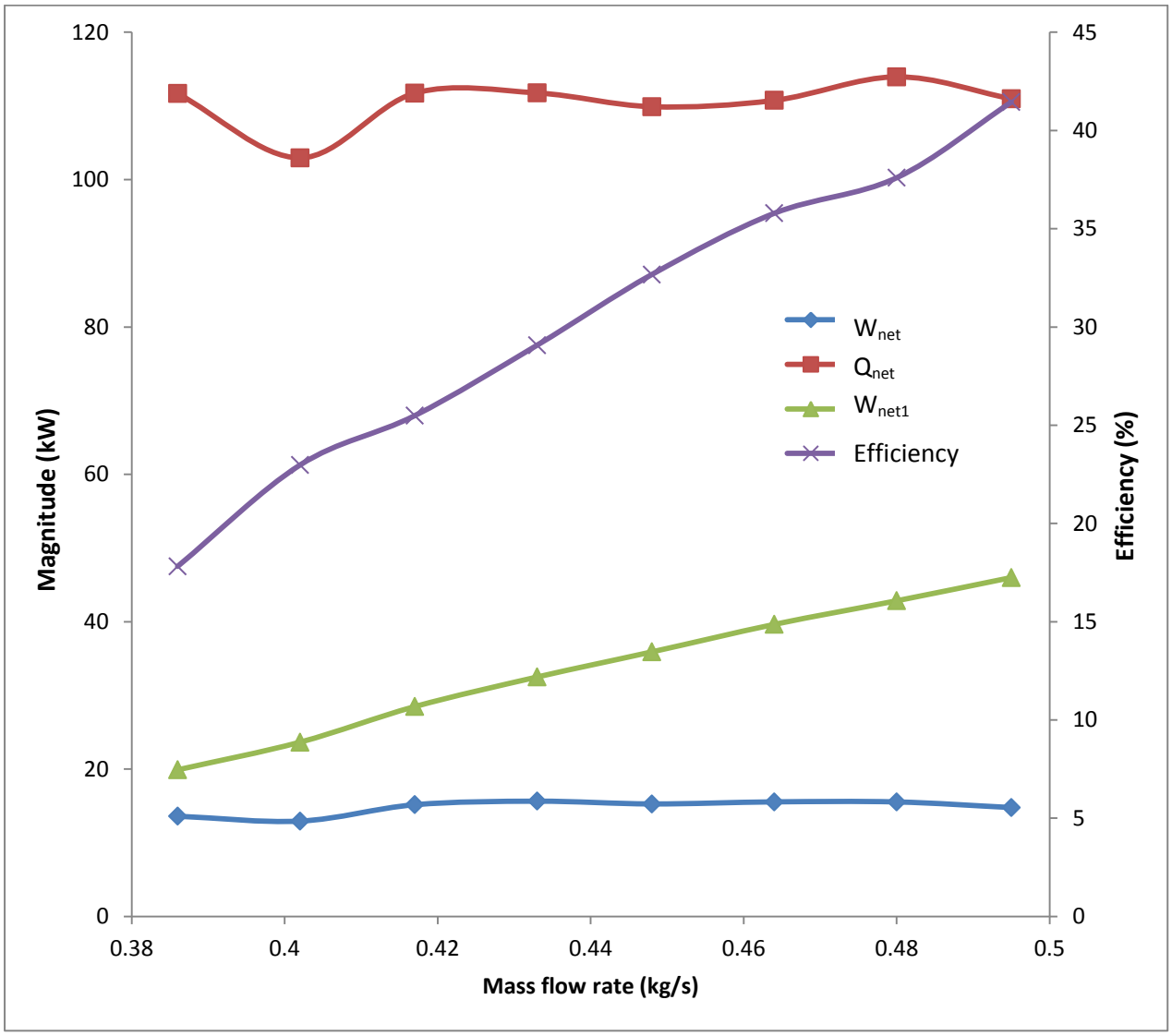

Figure 5.1 Comparison of objective function with major system results

Figure 5.1 indicates how the first law power output continually increases with the increase in mass flow rate. This first law efficiency follows the same trend. The pressure ratio increases as the mass flow rates increase, and the first law power output and efficiency increase as the mass flow rate increases for the system. The objective function is very nearly uniform at all mass flow rates; however, a maximum value exists for which the system is optimised.

Table 5.3 shows by what percentage all the remaining mass flow rates differ from the optimal objective function at a mass flow rate of 0.433 kg/s.

Table 5.3 Percentage difference of objective function

Mass flow rate (kg/s)	Objective function (kW)	% Difference
0.433	**15.6402**	**0**
0.386	13.6008	14.99
0.402	12.9386	20.88
0.417	15.1605	3.16
0.448	15.2701	2.42
0.464	15.55	0.58
0.480	15.5401	0.64
0.495	14.7804	5.82

There is no clear relationship between the difference in mass flow rate and objective function. It is, however, clear that there are two more mass flow rates at which the objective function is quite high, namely 0.464 kg/s and 0.480 kg/s, which differ from the maximised objective function by 0.58 % and 0.64 % respectively.

Entropy generation minimisation is of utmost importance in this analysis, and for this reason, it is clearly broken down in Figure 5.2. The overall trend of the total entropy generation does not vary extensively with the increase in mass flow rate. When this trend is compared with that of the objective function in Figure 5.1 it can be clearly seen how the objective function varies with the change in entropy generation. Theory dictates that in order to optimise a system for maximum net power output, the entropy of the system should be minimised.

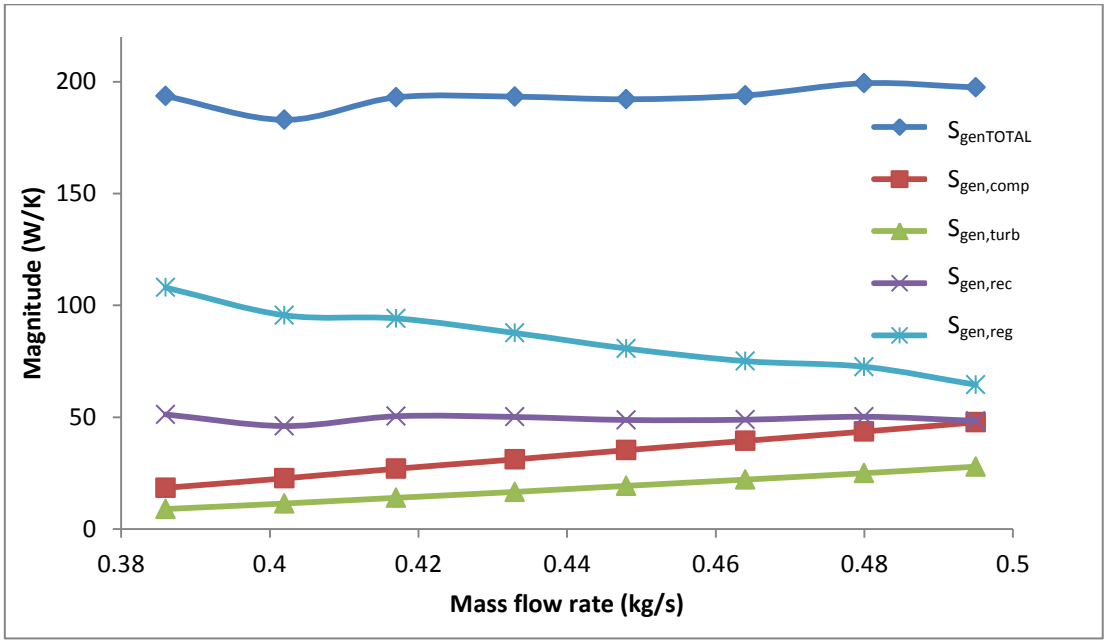

Figure 5.2 Entropy variation with mass flow rate

When comparing Figure 5.1 and 5.2, the maximised objective function does not occur where the entropy generation rate is a minimum. This is caused by the different mass flow rates being

investigated and also the large number of parameters that are different for each of the mass flow rates, and which all have certain influences in the final solution. The contribution of the various components to the overall entropy is also included in Figure 5.2. The contribution of each component is added together with the entropy generated in the ducts to find the overall entropy generation rate. The entropy generation rates in the ducts are deducted from the other entropy generation rates due to the direction of flow and the presence of temperature and pressure losses. The significance of this is discussed in much more detail in Section 5.3.4. From Figure 5.2, it is clear that the compressors' entropy generation rate increases with the increase in mass flow rate. The combined entropy generation rate of the turbines also steadily increases as the mass flow rate increases. This can be attributed to the dependence of the compressors and turbines on the said mass flow rate and on the pressure ratio, and the fact that higher losses occur at higher mass flow rates or pressure ratios, and subsequently, more entropy is generated. The entropy generation rate of the regenerators decreases significantly as the mass flow rate decreases. The receiver entropy generation rate undergoes slight decreases and increases but can be said to stay fairly constant.

The main parameters used in the optimisation algorithm are the width-to-height ratio, length and hydraulic diameter of the rectangular regenerator and receiver channels. The optimised values for these parameters are shown in Table 5.4 and in Figures 5.3, 5.4 and 5.5. It is clear to see from Figure 5.3 that each of the parameters have different profiles with which they vary as the mass flow rate is increased.

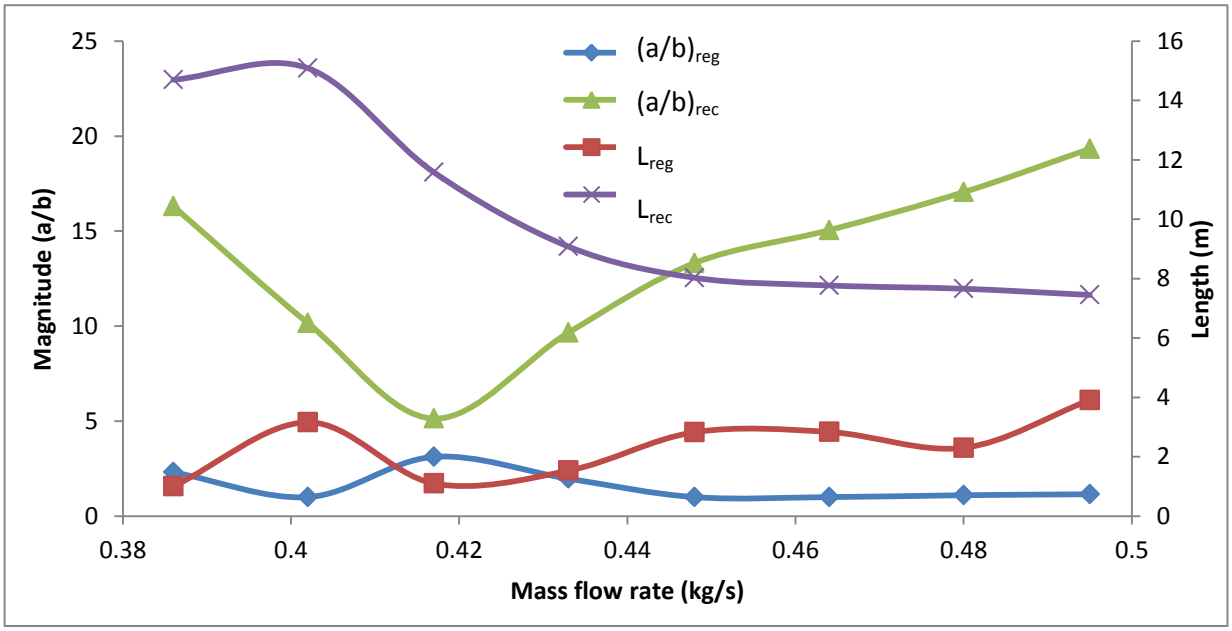

Figure 5.3 Variation in width-to-height ratio and length of the regenerator and receiver

The width-to-height ratio of the regenerator initially decreases as the mass flow rate increases. It then increases for one single increment in mass flow rate whereafter it continually decreases and

reaches a minimum value. The same ratio for the receiver starts off much higher, and then decreases with the increase in mass flow rate up to a mass flow rate of 0.433 kg/s, whereafter it increases with the respective increase in mass flow rate. The length of the regenerators follows a pattern that mirrors that of the regenerator width-to-height ratio. It, however, does not reach a maximum or minimum value but continues to be fairly constant as the mass flow rate increases. The length for the receiver also varies with mass flow rate. Initially, it increases up to a point where the mass flow rate is 0.402 kg/s, whereafter it decreases and it then seems to near a converging value for the last couple of mass flow rates. The variations of the hydraulic diameters for the regenerators and the receiver are shown in Figure 5.4.

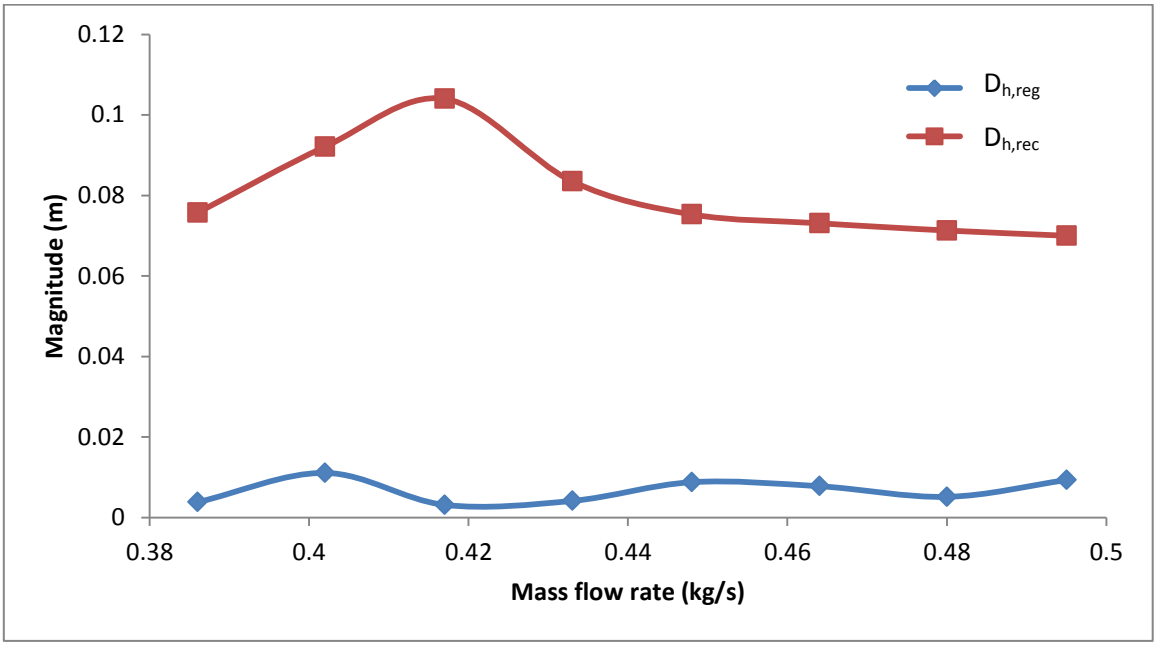

Figure 5.4 Variation in hydraulic diameter for regenerators and receiver

From Figure 5.4, it can be seen that the optimum hydraulic diameter for the regenerators is much smaller in magnitude than that of the receiver. It is also clear to see that this difference slightly decreases as the mass flow rate increases. This is not the case with the hydraulic diameter of the receiver, which initially increases up to a mass flow rate of 0.417 kg/s, whereafter it decreases until it reaches a mass flow rate of 0.480 kg/s. Recall the trends of the width-to-height ratio and length of the receiver as plotted in Figure 5.3. The trend for the hydraulic diameter of the receiver is somewhat similar to that of the trends visible in Figure 5.3, as it seems to resemble a mirror image of the width-to-height ratio of the receiver.

Due to the nature of the optimisation algorithm, only the receiver outlet temperature is fixed at its maximum. The second temperature that is fixed is also an input parameter which undergoes systematic optimisation and is also solved for each cycle set-up. This brings about the occurrence

that the inlet temperature of Compressor 1 yet another optimisation solution. The values of these temperatures can be seen in Table 5.2, and are shown graphically in the Figure 5.5.

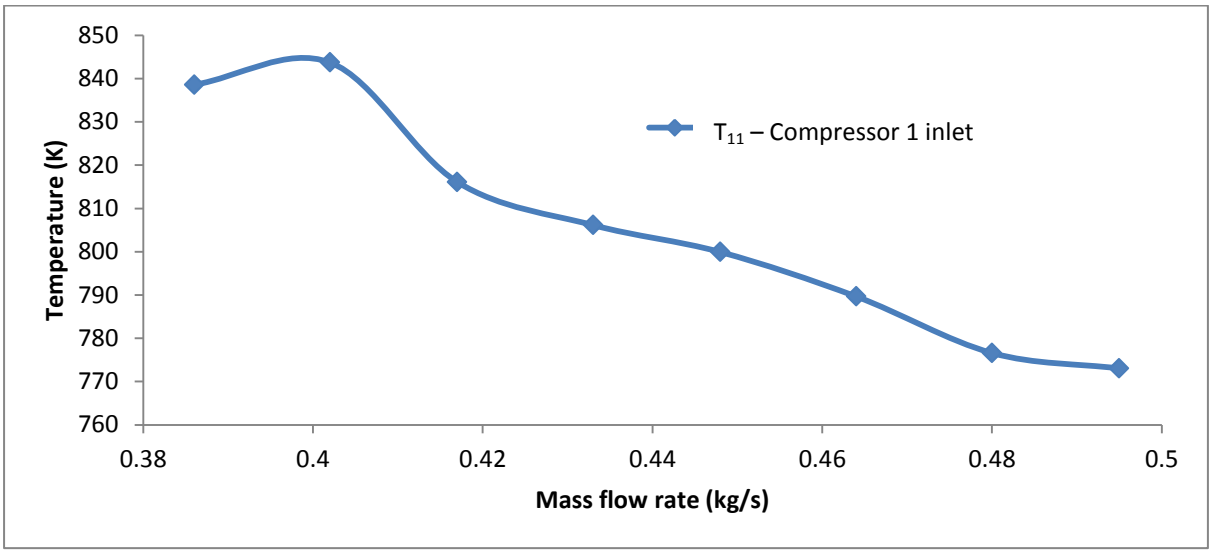

Figure 5.5 Variation in the inlet temperature of Compressor 1 with mass flow rate

In Figure 5.5, it is clear that the inlet temperature of Compressor 1 inlet temperature decreases with the increase in mass flow rate. This would suggest that for a larger difference between T_{11} and T_{14}, a larger mass flow rate follows. Alternatively, when a higher net output is desired, a higher mass flow rate is needed, which means the difference between T_{11} and T_{14} should be as large as possible.

5.3 Validation

During the set-up of the optimisation algorithm, known theory was used to create a system of functions, constraints and stopping criteria. The results found and discussed seem to hold true. It is for this reason that validation is such an important step in the solution process. The validation process in itself entails a series of control checks with which the system results are deemed feasible. These control checks are:

- an investigation into the influence of the assumed temperature drop value used in the optimum solution
- an investigation into the influence of the assumed receiver outlet temperature on the optimum solution
- an investigation into the influence of the choice of turbine on the optimum solution
- an investigation into the influence of the entropy generation rates in the ducts on the optimum solution.

5.3.1 Temperature drop in ducts

The investigation into the temperature drop value assumed in the analysis was conducted by first optimising the system at the assumed value. This is shown in Section 5.2.2. The assumed value of temperature drop was then varied in set increments but for a fixed mass flow rate. Figure 5.6 shows how the objective function and other important parameters vary with temperature drop in the ducts.

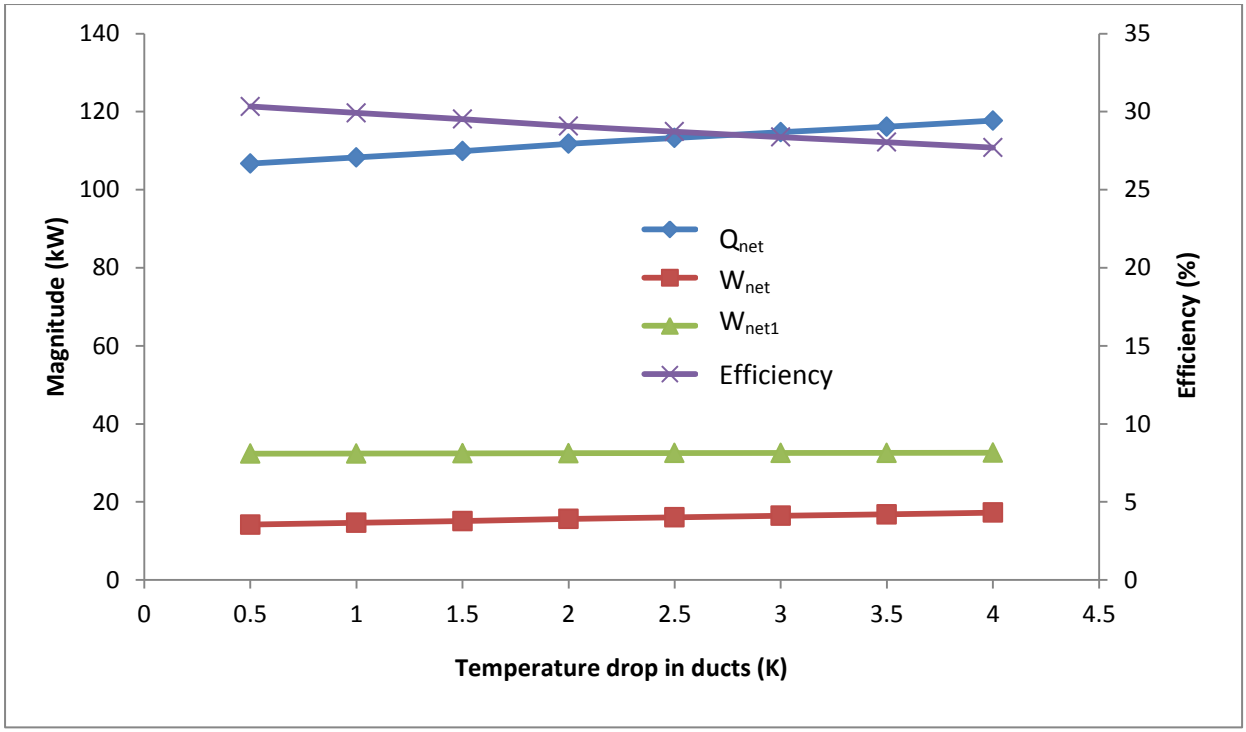

Figure 5.6 Variation of parameters with increase in temperature drop

Figure 5.6 shows how the objective function slightly increases with the increase in temperature drop. The net absorbed heat follows suit as expected. The reason for this is that the optimisation procedure solves T_{11} at increasing values for different temperature drop values. This leads to higher net absorbed heat rates, which consequently lead to higher objective function values. The first law net power output stays constant, which can be attributed to the equations used to determine its magnitude. The efficiency of the cycle decreases at a very small rate as the temperature drop increases. The trends in Figure 5.6 suggest that the assumed temperature drop value could have been increased to supply more net power output; however, this would have been at lower efficiencies. The entropy generation rates follow the same patterns as the objective function and net absorbed heat.

5.3.2 Receiver outlet temperature

The value used for the receiver outlet temperature is the maximum acceptable temperature, namely 1 200K, which is the temperature at which the copper tubing would start melting. To ensure that this assumption was indeed correct, a simple validation was carried out whereby various values of T_{14} were investigated for the optimum solution. The investigation started at a value of 1,000 K and was incremented by 50 K. This was done to determine whether a receiver outlet temperature of less than 1,200 K would provide a larger objective function, whether the receiver outlet temperature should indeed be as large as possible. The resulting graph is shown below and the results are as expected.

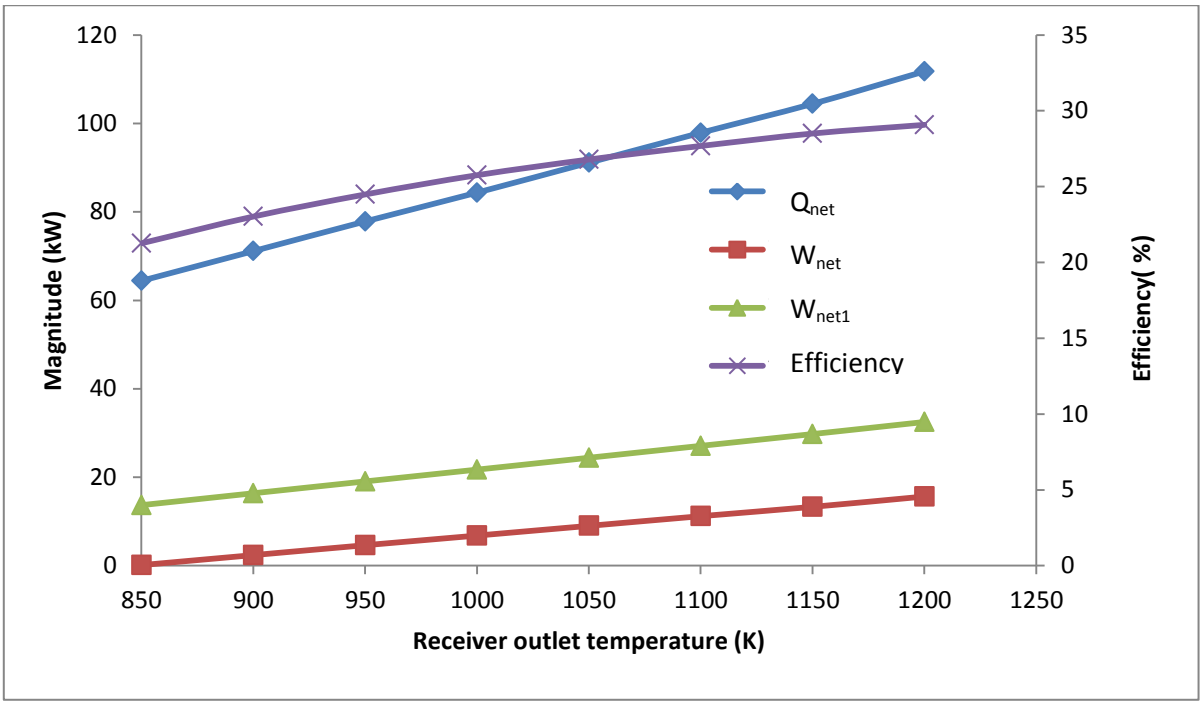

Figure 5.7 Influence of receiver outlet temperature on objective function

From Figure 5.7, it is clear that the larger the receiver outlet temperature is, the larger the objective function becomes. For this reason, the assumption made concerning the receiver outlet temperature is viable. For the cycle and procedure at hand, 1,200 K is the maximum useable value due to the materials used. If future investigations increase the melting temperature of copper or if some other cheaper material is invented with a higher melting temperature the objective function can most certainly reach even higher values.

An investigation was conducted to see what the maximum collector temperature would be if the material limitations were ignored. This temperature was the theoretical maximum where the maximum net power output would result from. The algorithm as set up with a pressure ratio of 1.7, T_0 = 300 K and T_{sun} = 2,470 K.The temperature at the receiver outlet, T14, was not limited and the net

power output was found to increase as the temperature was increased. The thermal efficiency however, converged to a value of 39.3 % at a temperature of 15,100 K. This value is much higher than the aforementioned limit of 1,200 K. The efficiency of 39.3 % is much higher than the 29.1 % found in Table 5.2 for this specific system setup. In Zamfirescu and Dincer [52] it was found that in a Carnot cycle with T_0 = 298 K and T_{sun} = 6,000 K, the maximum temperature at the collector was a little over 2,500 K. These findings may be compared to the 15,100 K, unfortunately though, the relationship cannot be verified as the results come from completely different power generation cycles.

5.3.3 Turbine choice

As mentioned earlier, an initial list of 60 turbines was considered. This list was reduced to the 11 most efficient turbines. From these 11 turbines, the largest turbine sporting the largest mass flow rate was chosen as the test turbine for the optimisation procedure. This is because higher mass flow rates will supply larger objective function values. Figure 5.8 shows how the 11 remaining turbines compare in terms of net absorbed heat, the objective function, the first law net power output and also the first law efficiency.

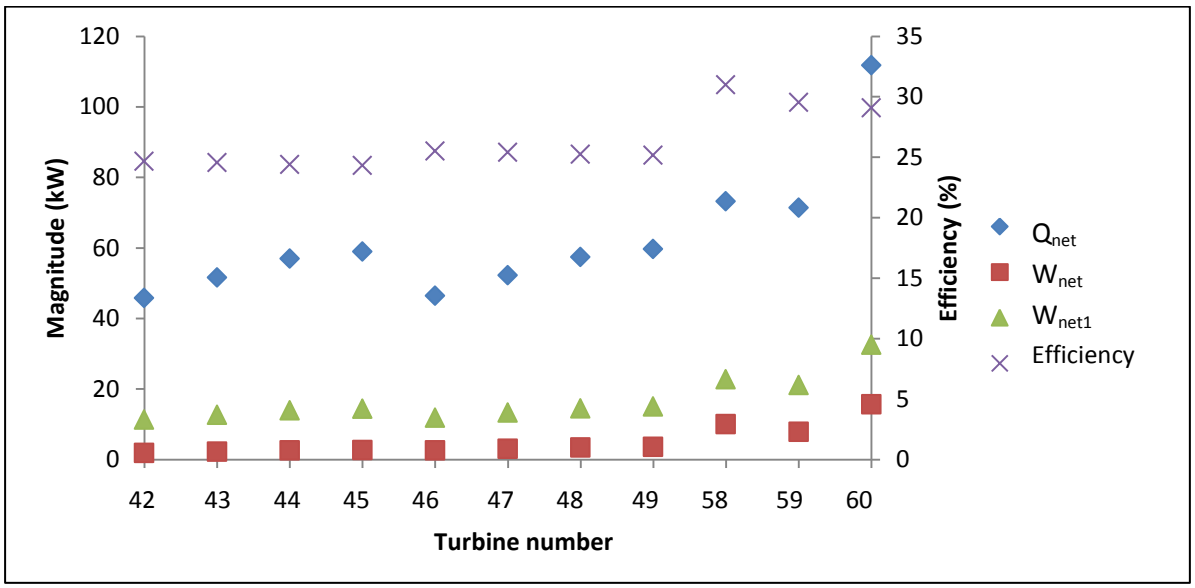

Figure 5.8 Variation of major parameters with choice of turbine

The turbines chosen and illustrated above can be found in the complete turbine list in Appendix II. From Figure 5.8, it is clear that Turbine 60, being the largest turbine available, is indeed the best choice for the system at hand as it has the largest objective function. When considering Figure 3.2, this is the turbine that will be used throughout the cycle to simplify the overall set-up and installation procedure and the specifics of the cycle if they were to be built in the future.

5.3.4 Entropy generation rates in the ducts

A major concern in the optimisation algorithm is the inclusion of the entropy generation rates of the ducts that connect the hardware in the cycle as seen in Figure 3.2.

The optimisation procedure that was followed was done with the assumption that the duct entropy generation cannot be neglected and should be added to the overall entropy generation rate of the system. It makes sense that with even more entropy being generated in the system, the worst-case scenario objective function would be presented. The results from the initial optimisation were used to further investigate the influence of the duct entropy generation rates. As mentioned earlier, the temperature drop in the duct can be varied to change the optimum system. For the purpose of this comparison, only a temperature drop of 2 K is considered. These results are shown in Table 5.4.

Table 5.4 Optimum system results when $S_{gen,duct}$ is added

Mass flow rate	Q_a (kW)	W_{net} (kW)	W_{net1} (kW)	Efficiency (%)	$S_{gen,total}$ (W/K)	$S_{gen,duct}$ %
0.433	111.764	15.6402	32.4948	29.0744	193.3059	4.1568

From Table 5.4 it can be seen that the duct entropy generation rate is a bit more than 4 % of the overall entropy generation rate of the system. This percentage value makes it easier to set up a relation between the total duct entropy generation rate and the influence it has on the system as a whole.

The first auxiliary investigation conducted was for a system where the duct entropy generation rate was neglected. Table 5.5 shows the major system results in comparison with the case where the duct entropy generation rate was added to the overall entropy generation rate.

Table 5.5 Comparison of optimum system results for different $S_{gen,duct}$ actions

$S_{gen,duct}$ action	Mass flow rate	Q_a (kW)	W_{net} (kW)	W_{net1} (kW)	Efficiency (%)	$S_{gen,total}$ (W/K)	$S_{gen,duct}$ percentage	% difference in W_{net}
Added	0.433	111.764	15.6402	32.4948	29.0744	193.3059	4.1568	0
Neglected	0.433	111.764	17.9546	32.4948	29.0744	185.5913	4.1568	12.89029

Table 5.5 clearly shows the large influence of the inclusion of the duct entropy generation rate on the objective function. The net absorbed heat, first law net power output and first law efficiency are not influenced by the addition of the duct entropy generation rate. Since the major concern in this research is the objective function, the results clearly indicate that the initial assumption is

correct. The duct entropy generation rate should be included to ensure that the system is optimised for the worst-case scenario.

As mentioned, the above validation was carried out at a single temperature drop value for the system. It will be good to see what the influence of the addition and exclusion of the duct entropy generation rate is on the objective function at various different temperature drop values. This is a topic for future investigations.

Figure 5.9 shows the magnitude difference in kW as the temperature drop is varied, and Figure 5.10 shows the percentage difference between the two cases.

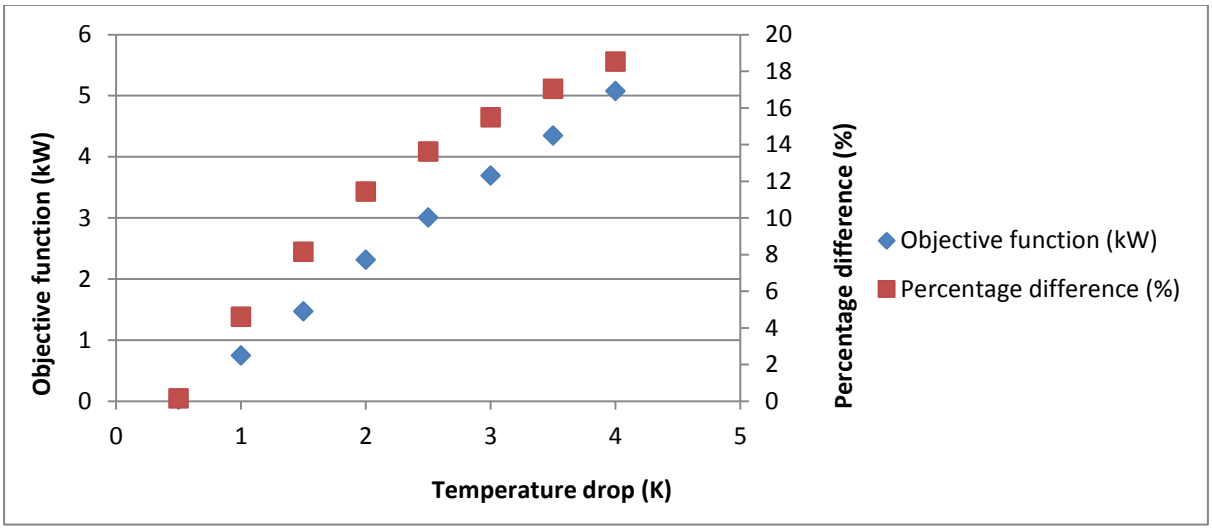

Figure 5.9 Difference in the objective function between adding and neglecting of $S_{gen,T}$ at various temperature drops in kW and percentage values respectively

Figure 5.9 shows how the difference in the objective function increases with the increase in temperature drop. This shows how the assumption made becomes more and more crucial as the temperature drop in the ducts increases. The higher the temperature drop value in the ducts is chosen to be in the analysis, the more kW of power the outlet power or objective function will be overestimated. Thus the error in judgement will increase as the temperature drop in the ducts increases. This same increase is also illustrated in terms of the percentage difference.

This once again shows the magnitude of error or overestimation that can be made when the assumptions are incorrect. The assumption to add the duct entropy generation rate to the total entropy generation rate can be deemed valid with utmost certainty.

5.4 Investigation into the influence of the second regenerator in the open-air solar thermal Brayton cycle

The preceding analysis was repeated for the open-air solar thermal Brayton cycle with the exception that Regenerator 2, as seen in Figure 3.2, was omitted. The analysis results will be discussed hereafter and the significance of the inclusion of Regenerator 2 will be commented upon.

The revised open-air solar thermal Brayton cycle, which contains only one regenerator, is shown in Figure 5.10. The numbering system used in the cycle was altered to simplify the optimisation algorithm and this new numbering system is clearly visible in Figure 5.10.

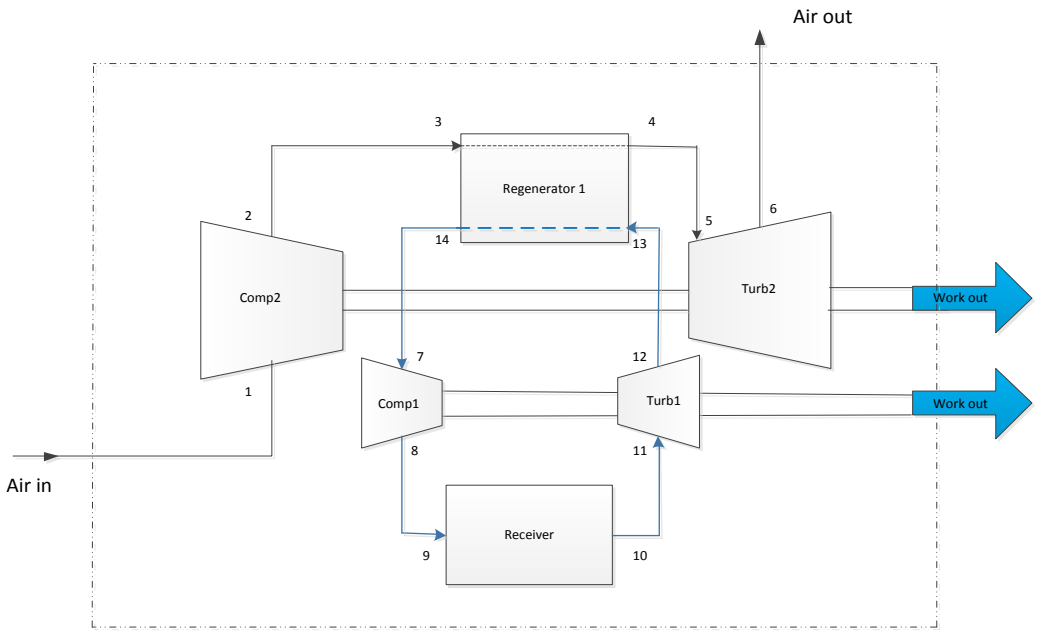

Figure 5.10 Revised open-air solar thermal Brayton cycle

The analysis procedure and system constraints were kept similar to that of the double Brayton cycle, which was analysed earlier. The key differences come to light when the behaviour of the objective function is considered.

Figure 5.11 defines the relationship between the system objective function, the net absorbed heat at the receiver, the first law net power output and also the first law efficiency as functions of the mass flow rate.

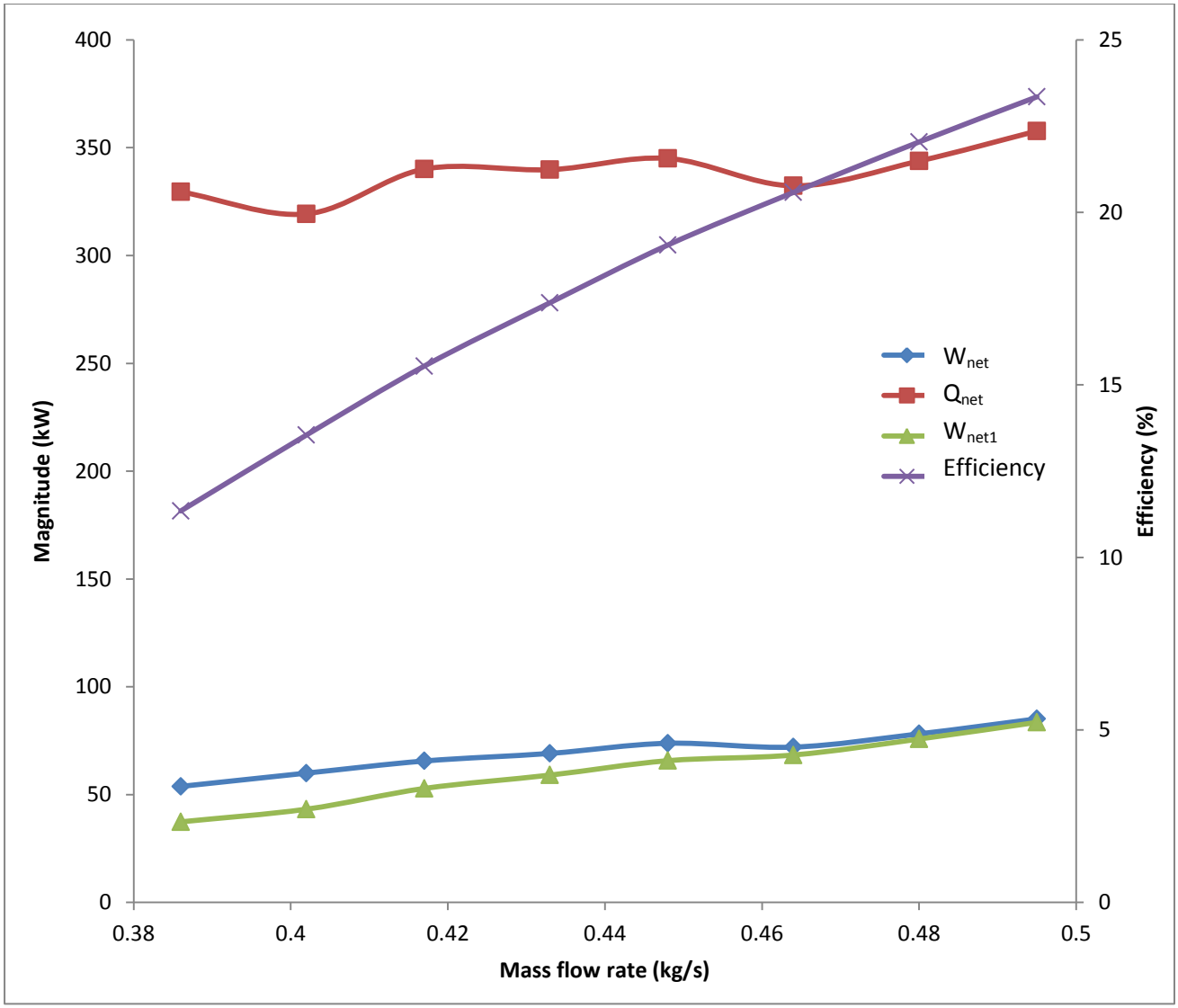

Figure 5.11 Objective function and other main parameters as functions of the mass flow rate

When the mass flow rate is increased gradually from 0.386 kg/s (r=1.4), it is clear that the objective function (defined as W_{net}) continually increases. At a mass flow rate of 0.448 kg/s, an initial optimum is found where the objective function is at its maximum. However, when the mass flow rate is in excess of 0.464 kg/s, the objective function, net absorbed heat, first law net power output and first law efficiency all increase with the increase in mass flow rate. The mass flow rate in Figure 5.11 only reaches 0.495 kg/s for the sake of simplicity, however, this trend continues to the maximum mass flow rate that can be handled by the turbine model being used.

Even though there is no clear optimum mass flow rate for the system, the trend is still of use. For this specific cycle, it is now possible to determine what range of net power will be extracted from the system when the mass flow rate is fixed. This becomes useful when the turbine and compressor models are fixed beforehand. In Figure 5.12, the variations in the different entropy

generation rates are shown as functions of the mass flow rate in a) magnitude given in kW/K and b) percentages of the total entropy generation rate.

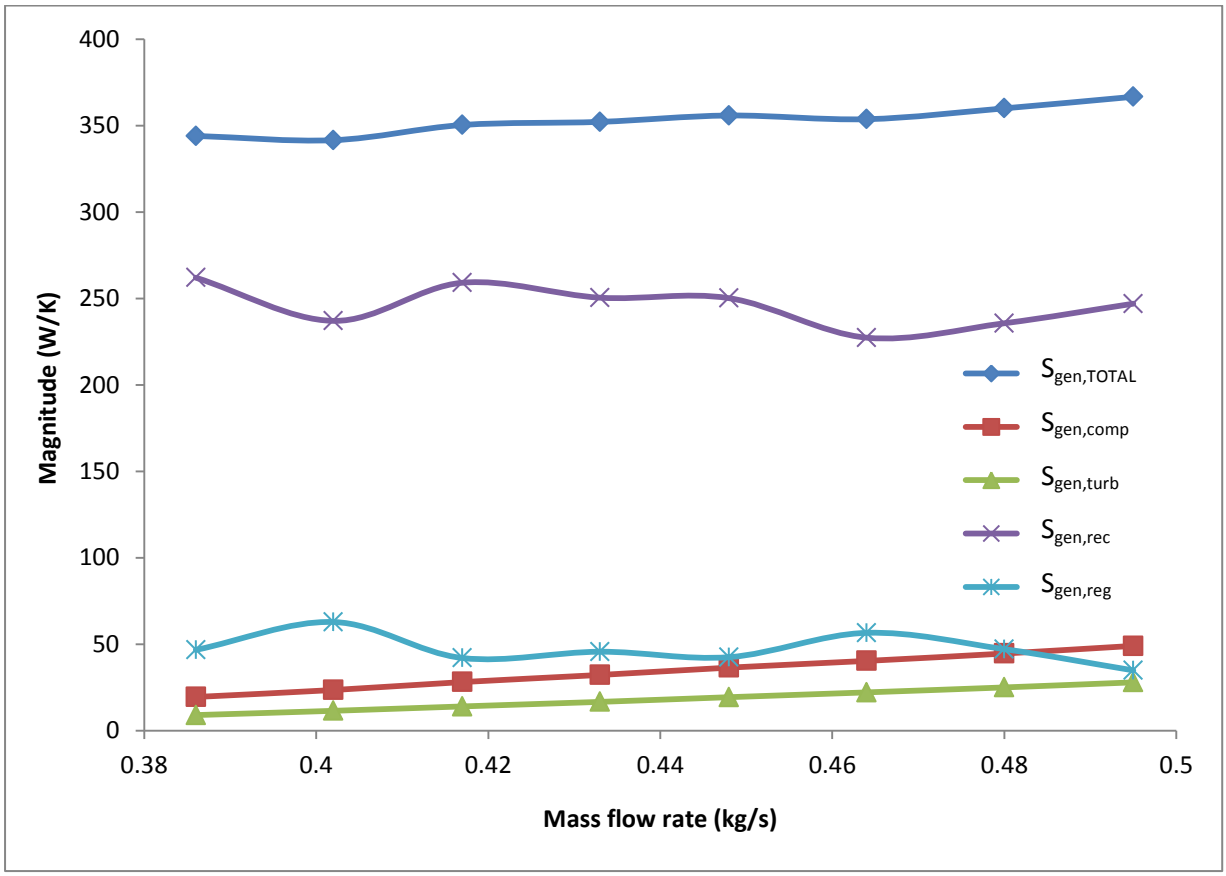

Figure 5.12a) Entropy generation rate as a function of the mass flow rate

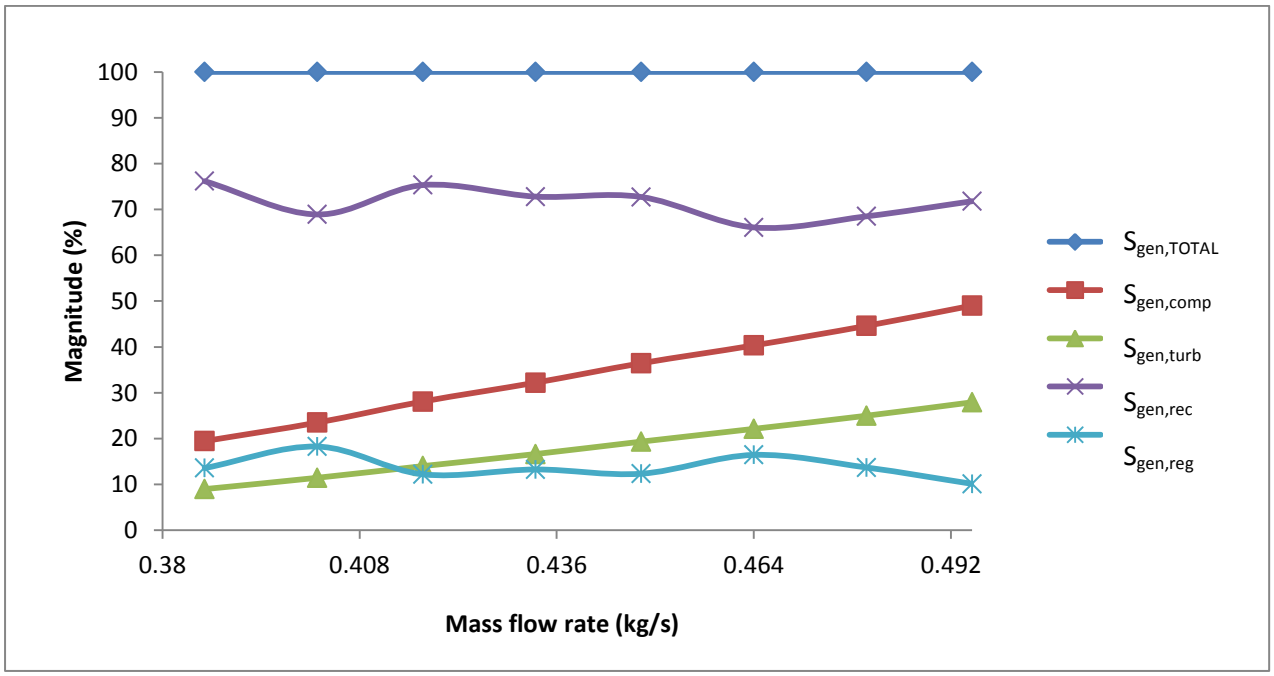

Figure 5.12b) Entropy generation rate as a function of the mass flow rate (given as in percentages of the total entropy generation rate)

From Figure 12a) and 12b) it is clear that the amount of entropy generated in the cycle will always be the highest in the receiver. The compressor and turbine entropy generation rates continually increase as the mass flow rate increases with the compressor entropy generation rate always larger than that of the turbine. The regenerator entropy generation rate seems to mirror that of the receiver. Even though it is significantly less, it increases when the receiver entropy generation rate decreases, and vice versa.

The overall entropy generation rate continually increases for the increase in mass flow rate. It is expected that the optimum objective function will be where the entropy generation rate is at its smallest; however, this is not the case as multiple parameters (see Section 4.2.1.) are optimised simultaneously. Because of this, the total entropy generation rate and objective function (second law of thermodynamics' net power output) as seen in Figure 5.12b) do not follow similar graph profiles.

The optimised regenerator parameters vary with no clear relationship. This is also the case with the optimised receiver parameters.

From Figure 5.13, it is clear how the length of the regenerator is always at its maximum, which is equal to the radius of the parabolic dish. The regenerator height-to-width ratio displays an erratic behaviour and is not included in the graph. It oscillates for mass flow rate from 0.402 to 0.480 kg/s. Its behaviour can be studied in future analyses.

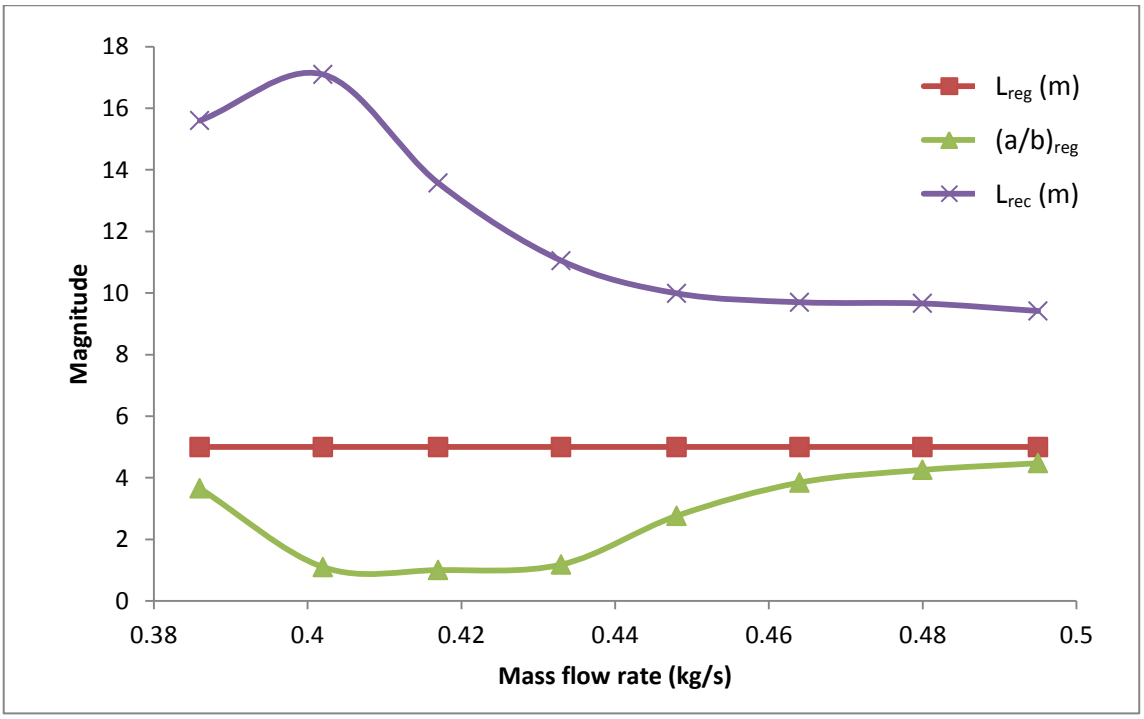

Figure 5.13 Regenerator and receiver parameters as function of the mass flow rate

The hydraulic diameters for the regenerator and receiver are shown in Figure 5.14. The hydraulic diameter of the regenerator is more or less constant throughout the entire mass flow rate range,

where-as the receiver hydraulic diameter substantially increase up to a mass flow rate of 0.402 kg/s, where-after it decreases as the mass flow rate increases. The hydraulic diameter of the receiver is much larger than that of the regenerator for all mass flow rates under investigation.

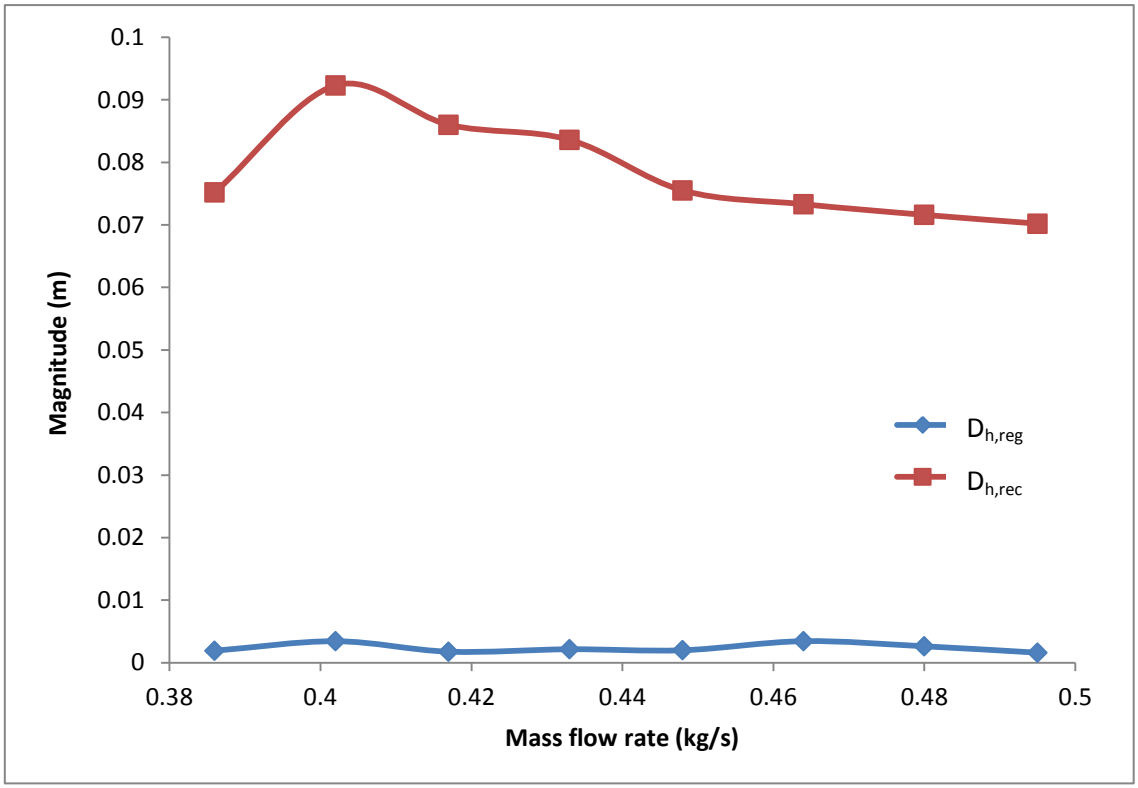

Figure 5.14 Regenerator and receiver parameters as function of the mass flow rate continued

5.5 Comparison between cycles

When the cycles of Figures 3.2 and 5.10 are compared, some major differences come to light. Because the major deliverable of this investigation is the objective function of the cycles, it makes perfectly good sense to compare the two on the same graph. The behaviour of the objective functions with increase in the mass flow rate is shown in Figure 5.15.

It is very easy to see how the cycle containing only one regenerator provides more second law net power output than the original cycle with the two regenerators. Prior to the optimisation phase, it was thought that the second regenerator, as seen in Figure 3.2, would increase the output of the entire cycle as it increases the temperature of the working fluid before it enters the primary regenerator from which the working fluid receives most of its energy.

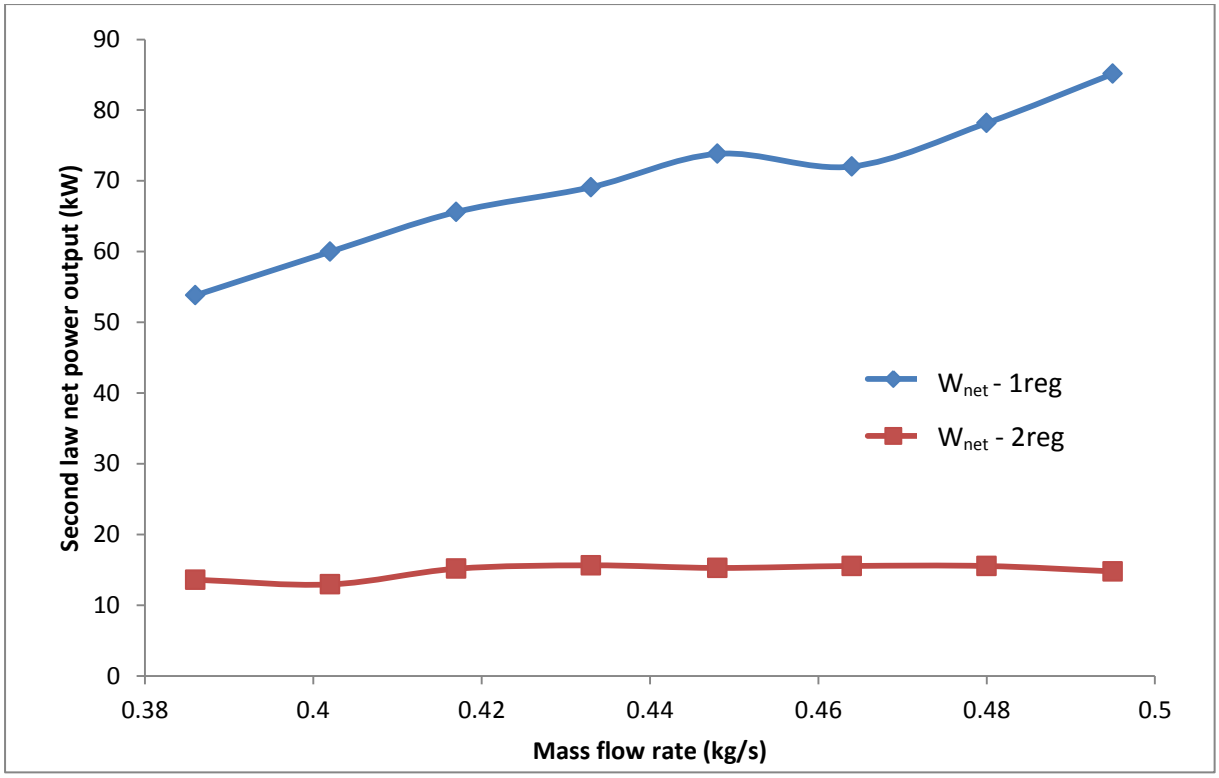

Figure 5.15 Objective functions as functions of the mass flow rate

The reason for this misjudgement can be seen in Figure 5.16. The simpler cycle containing only one regenerator satisfies the same criteria and constraints as the original double Brayton cycle, however, the resulting temperatures and pressures, as solved by the optimisation algorithm, produce a higher net absorbed heat at the receiver. This higher net absorbed heat then ensures a much higher second law net power output, or objective function value.

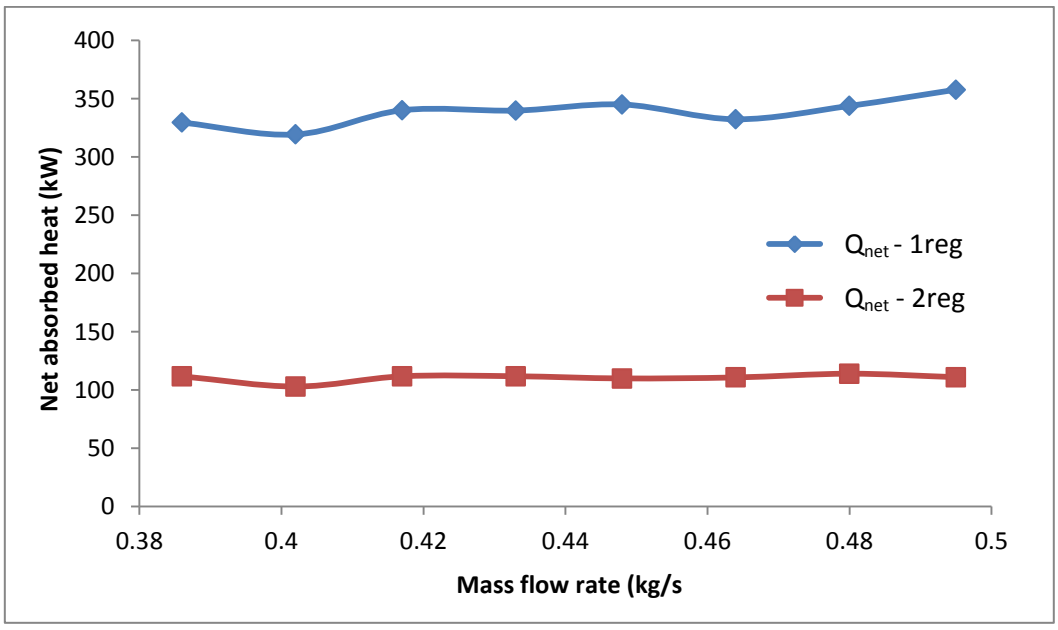

Figure 5.16 Net absorbed heats as functions of the mass flow rate

When the efficiencies of the cycles are compared, another conclusion is drawn on the relevance and influence of the second regenerator in the cycle. As seen in Figure 5.17, the efficiency for the original double Brayton cycle, containing two regenerators, is much higher than that of the single regenerator cycle. It can now be concluded that the purpose of the second regenerator is merely to increase the efficiency at which power is generated, but not to increase the physical amount of power that is generated.

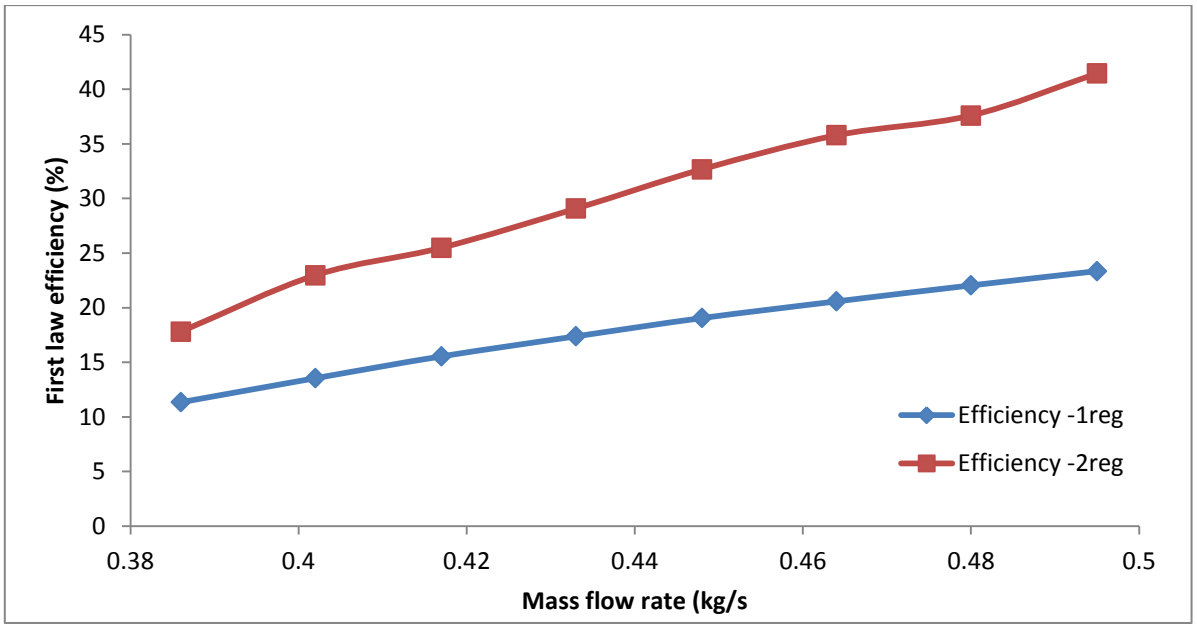

Figure 5.17 First law efficiencies as functions of the mass flow rate

Perhaps the most important conclusion to be drawn from the difference in efficiencies as in Figure 5.17 is that the higher efficiency of the double Brayton cycle suggests it will perform better for longer. This brings about the realisation that even though the single Brayton cycle produces considerably more power, the cycle will not be able to produce this net power output as long as the double Brayton cycle produces its own net power output.

Taking the cost of operation and maintenance into consideration, this makes the choice between the two cycles very easy. It will be a much better choice to use the double Brayton cycle. Even though it would not produce as much net power as the single Brayton cycle, it would do so for much longer. Thus in the long run, the net power output supply from the double Brayton cycle is superior. As this is an investigation into optimising the performance characteristics of the open-air solar thermal Brayton cycle, it can be assumed that the single cycle is a very bad choice since it will lack in performance.

5.6 Irreversibilities

Another factor that can be used to clearly and effectively illustrate the system characteristics is the irreversibility. The system as a whole delivers a certain amount of external irreversibility determined by using the inlet and outlet conditions of the system. None of the internal components are considered when external irreversibilities are under consideration. The second type of irreversibility worth mentioning is the internal irreversibility of the system. This irreversibility is the most inclusive as it considers all internal components such as compressors, turbines, regenerators and the receiver, and the respective irreversibilities these components produce. The internal irreversibility of the system is merely the sum of all the separate component irreversibilities.

First, consider the variation of the internal irreversibility of both the single and double cycles as functions of the mass flow rate. Figure 5.18 shows how the internal irreversibility of the single Brayton cycle steadily increases as the mass flow rate increases. This can be attributed to the increasing amounts of entropy being generated in the internal system components as the mass flow rate increases. The internal irreversibility for the double Brayton cycle follows a quite different profile, as it stays mostly constant for all mass flow rates with small fluctuations occurring at mass flow rates of 0.402 and 0.480 kg/s.

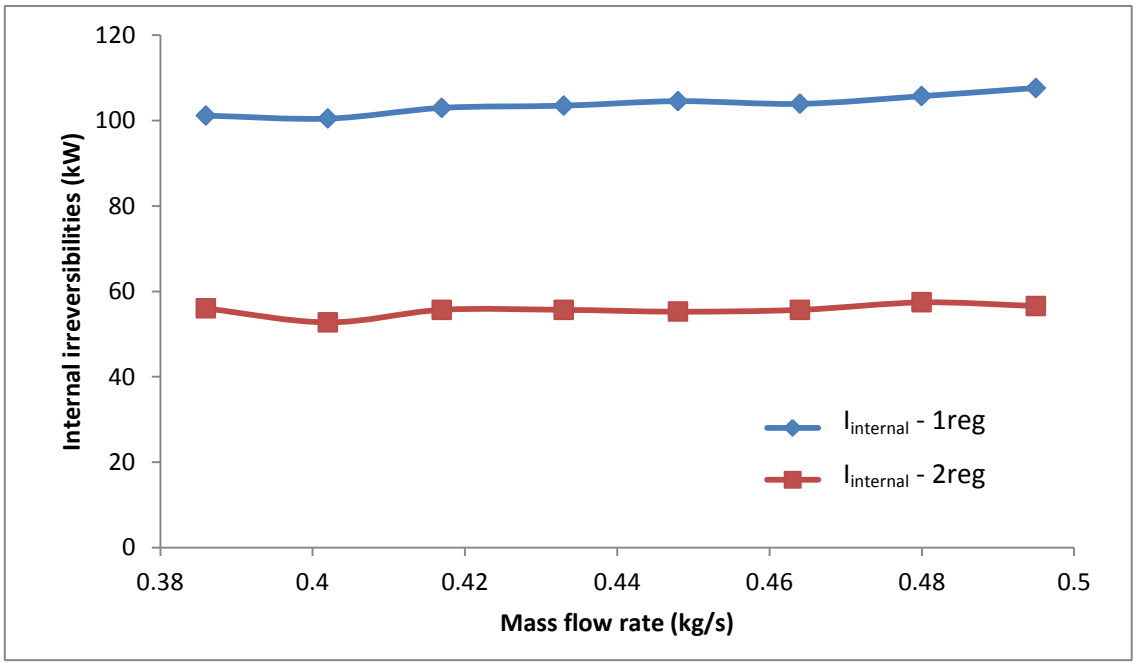

Figure 5.18 Internal irreversibilities as functions of the mass flow rate

The external irreversibilities of the single and double Brayton cycles are plotted in Figure 5.19 as functions of the mass flow rate. Unlike the internal irreversibilities, the external irreversibilities have clear trends for both the single and the double Brayton cycle. For both cycles, the irreversibilities increase as the mass flow rate increases. The external irreversibility of the double cycle increases at

almost a constant rate for each increment in mass flow rate. The external irreversibility of the single cycle increases and decreases as the mass flow rate increases, but the overall trend is an increase in the external irreversibility.

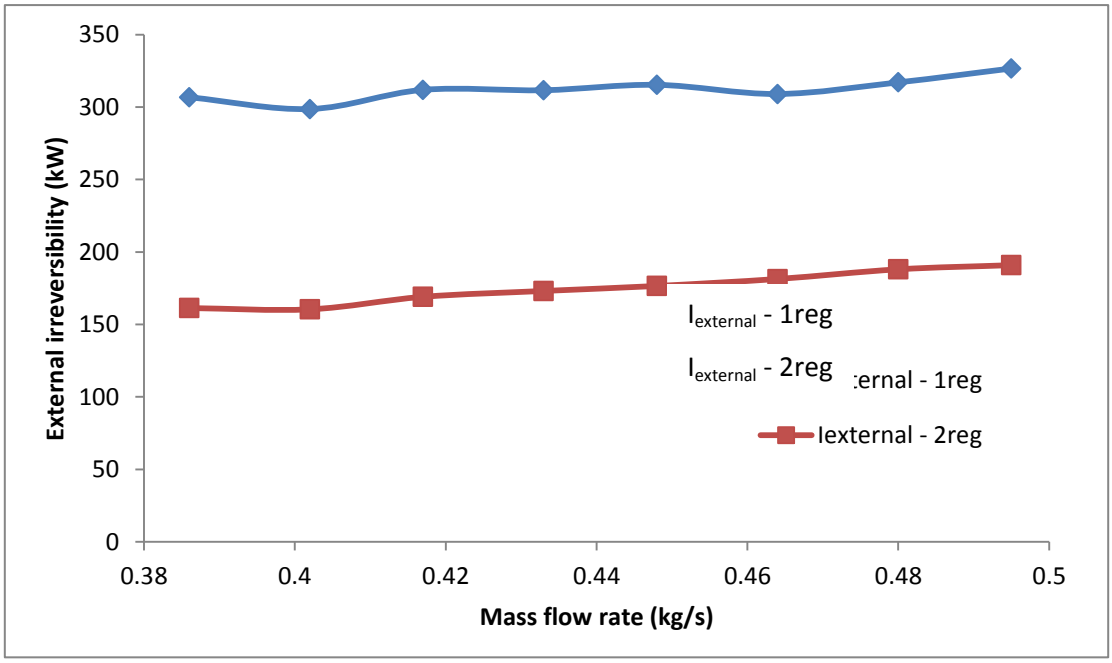

Figure 5.19 External irreversibilities as functions of the mass flow rate

Next consider the plot of external irreversibility as a function of the internal irreversibility as seen in Figure 5.20.

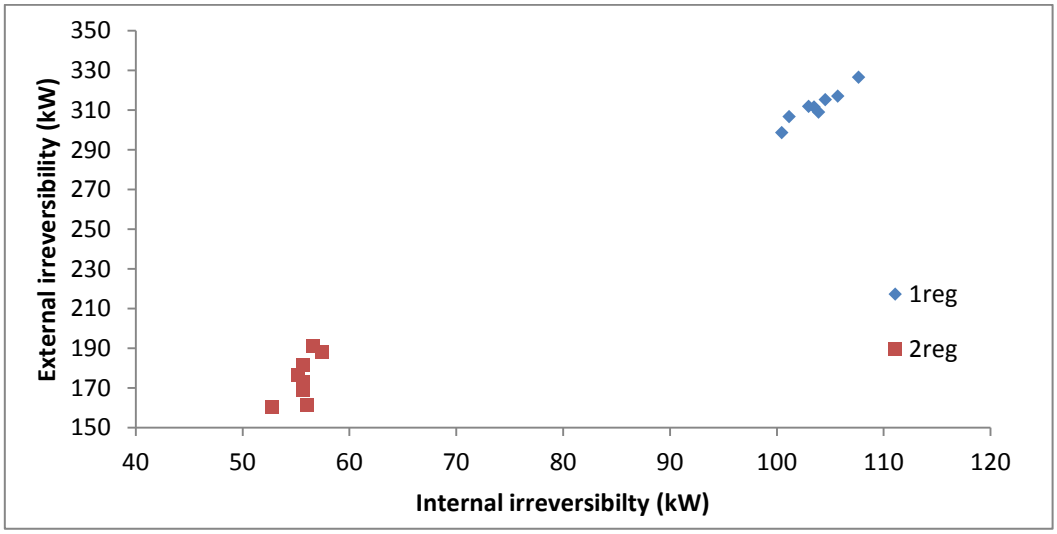

Figure 5.20 Comparison of the external and internal irreversibilities for both the single and double cycles

The irreversibilities of both the single and double cycles are considered here. It is easy to see how the irreversibilities form dense groups of plots. This shows that there must be some value with which the irreversibilities can be compared to investigate the trend that seems to appear.

At this point in the investigation, it is acceptable to introduce a variable, denoted C_W, which is the ratio of the external irreversibility to the internal irreversibility of each of the cycles. This ratio can be seen in Figure 5.21.

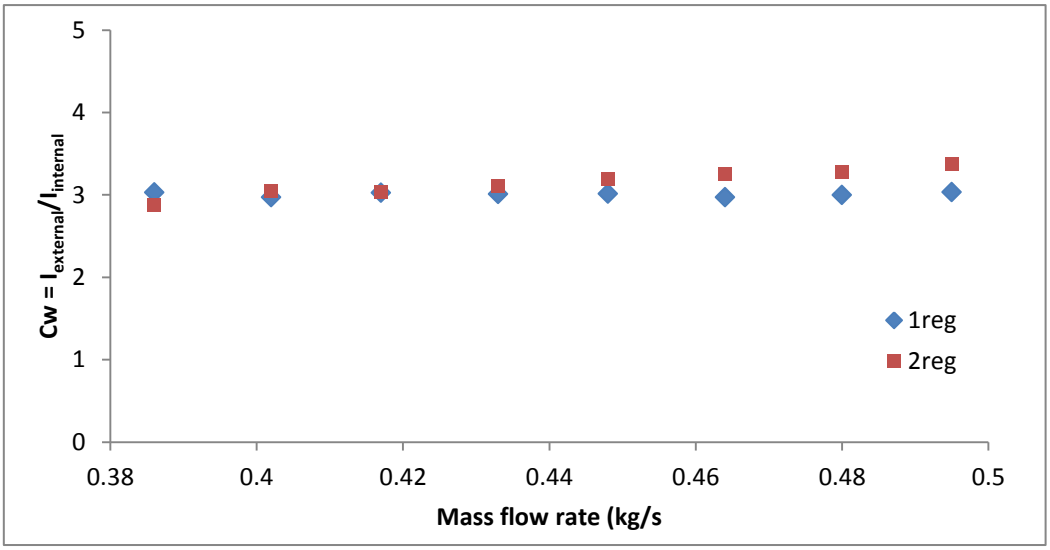

Figure 5.21 Ratio of the external irreversibility to the internal irreversibility

Figure 5.21 shows how C_W is nearly a constant value at all mass flow rates. The variation of C_W for the double Brayton cycle is significant, with C_W ranging from just below 3 to almost 3.5. The variation for the single Brayton cycle is not as excessive, with all values located close to 3. This result can be presented in the form of an equation as:

$$C_w = \frac{I_{external}}{I_{internal}} \approx 3 \qquad [5.6.\text{-}1]$$

This result is also validated by the work of Le Roux et al. [21].

5.7 Pressure drop through the receiver

An investigation was conducted into the influence of the pressure drop through the receiver on the objective function. Figure 5.22 shows how the pressure drop through the receiver varies with the change in pressure drop.

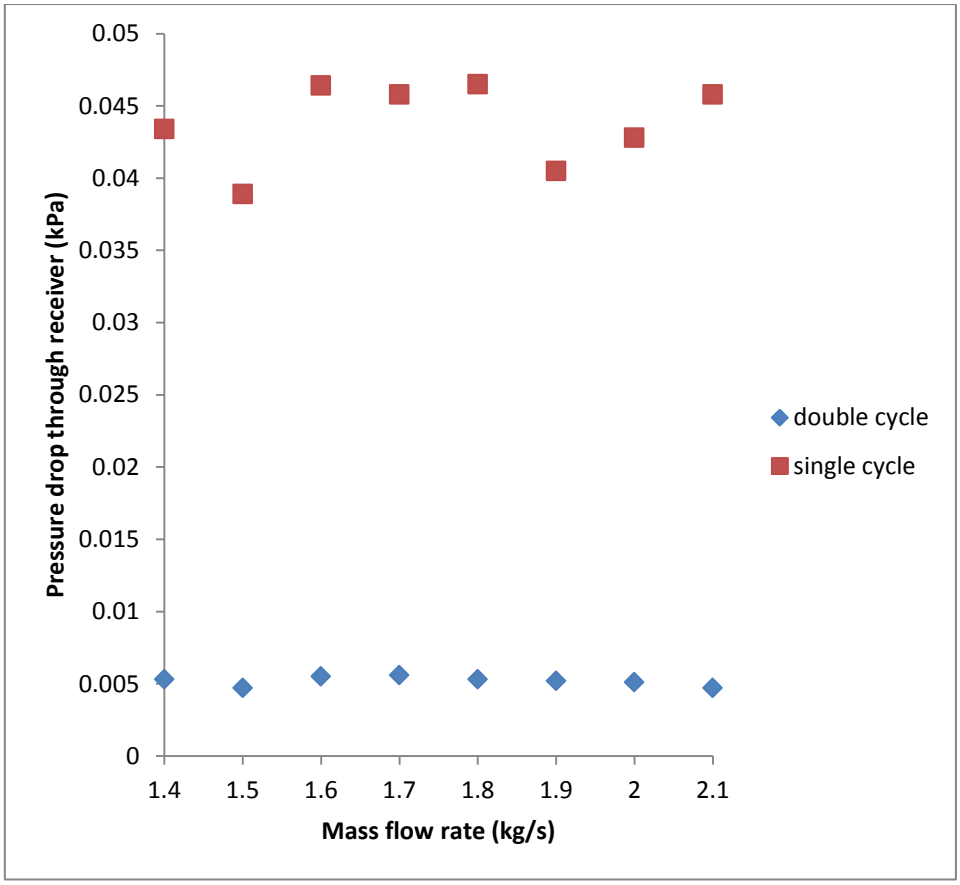

Figure 5.22 Pressure drop through the receiver as a function of the mass flow rate for both the single and double cycles

From Figure 5.22, it is clear how the pressure drop through the receiver in the single cycle differs from that in the double cycle. Both the profile and the magnitude differ significantly. The pressure drop through the receiver in the single cycle is between 9 and 10 times larger than that of the pressure drop in the double cycle receiver. Worth mentioning are the receiver parameters that have been optimised by the optimisation algorithm and their respective relationships with the pressure drop through the receiver.

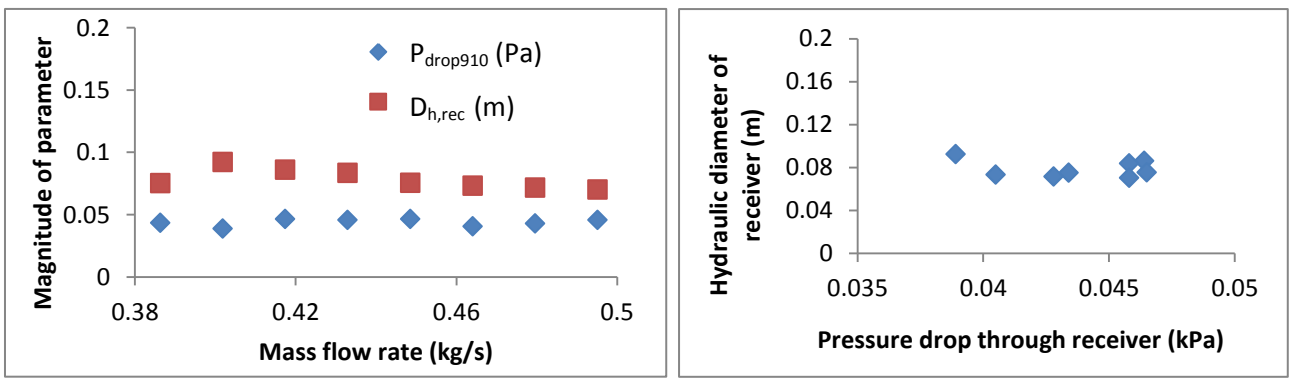

Figure 5.23 Receiver parameters as functions of the mass flow rate and pressure drop through the receiver for the single cycle

For both the single and double Brayton cycle receiver parameters as shown in Figure 5.23 and Figure 5.24, the receiver parameters do not follow clear trends. This verifies what is expected, namely that there is no clear relationship between the pressure drop through the receiver and the receiver parameters individually, but when the parameters' combined effect is considered, the existing relationships appear.

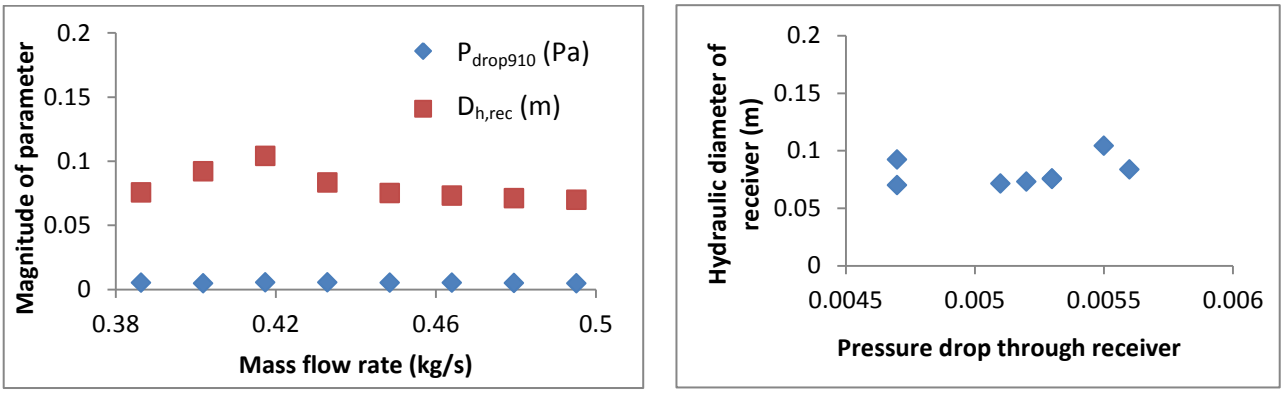

Figure 5.24 Receiver parameters as functions of the mass flow rate and pressure drop through the receiver for the double cycle

5.8 Pressure drop through the regenerators

The pressure drops through the hot and cold streams of Regenerator 1 and 2 in the double Brayton cycle are calculated with equations 3.4.4-4, -11, -14 and -24. The influence of the pressure drops through these regenerators on the net absorbed heat and also on the net power output is investigated to verify the validity of the optimisation results.

It is well known from theory that a system with higher pressure drop will deliver lower net power output values. It is for this simple reason that the regenerator parameters were optimised so that the losses through the regenerators were minimised. Following this statement, it is expected that both the single and double Brayton cycle will perform worse at higher levels of pressure drop.

The following graphs show how the net absorbed heat differs for the single and double Brayton cycles at pressure drops that are the same value as the present analysis, 10 times as large as present and also 20 times as large as present. Consider Figure 5.25 where the net absorbed heat at the receiver is plotted against the mass flow rate, at various magnitudes of pressure drop. The plot against mass flow rate is used because the results have already been verified and may thus be used with confidence. The results show that for both the single and double Brayton cycles, the pressure drop through the system should be as small as possible.

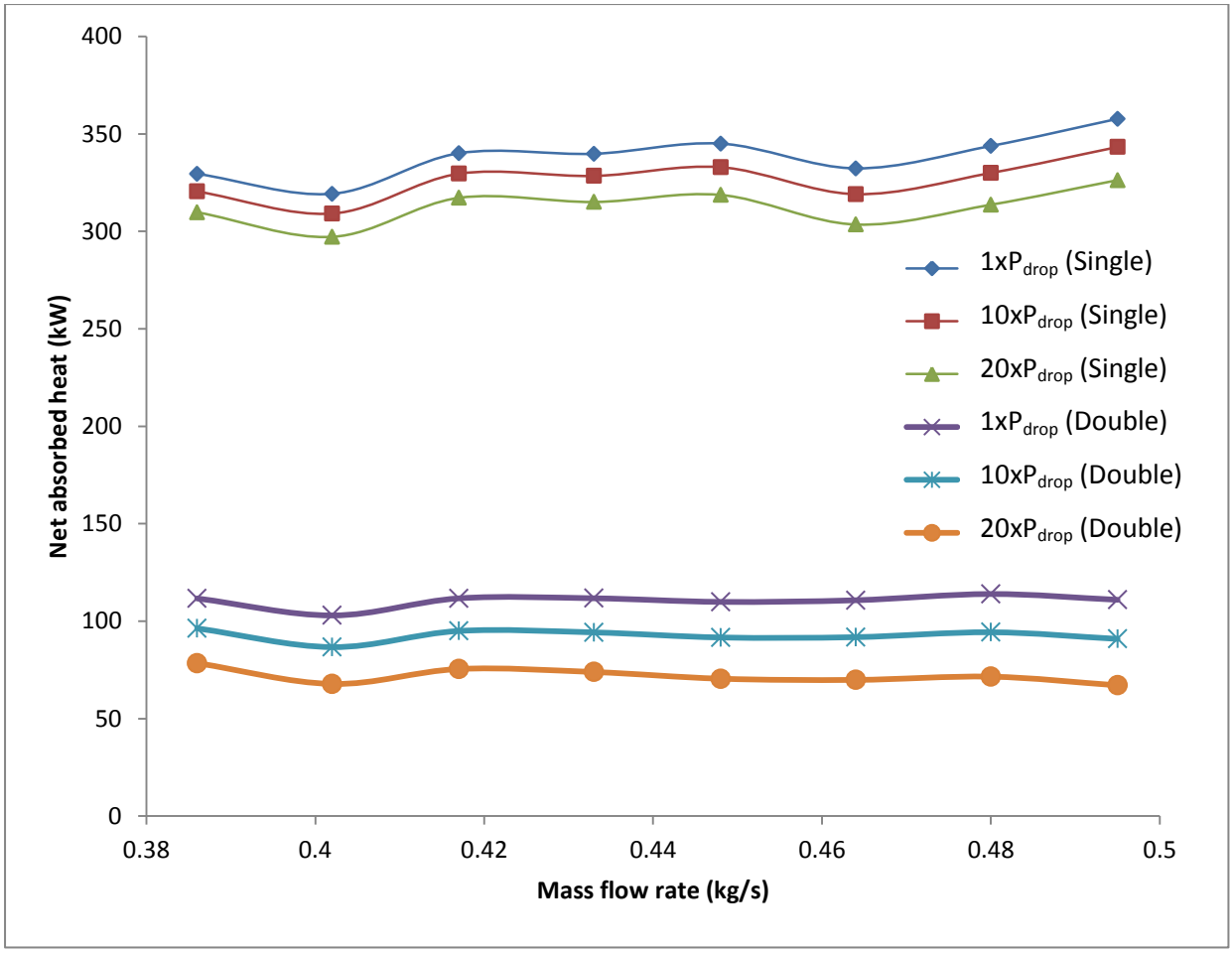

Figure 5.25 Net absorbed heat as a function of the mass flow rate at various pressure drop magnitudes of both single and double Brayton cycles

For the case of 10 times (10x) and 20 times (20x) the magnitude of the pressure drop, the optimisation algorithm was used to solve the systems when all pressure drops were 10x and 20x larger, and consequently smaller values of net absorbed heat were found.

As for the net power output, another similar plot was made and can be seen in Figure 5.26. The same expected trends appear as in Figure 5.25. The net power output of the system becomes smaller as the mass flow rate in the cycle increases.

In both Figure 5.25 and Figure 5.26, it is clear that the level of influence of the increase in pressure drop on the system decreases as the physical amount of either the net absorbed heat or the net power output increases. Thus a system generating more power with more heat being absorbed at the receiver will be influenced less than small power generation systems.

The values of pressure drop investigated, namely 10x and 20x, are very large and not descriptive of what would happen in real-life applications. Nevertheless, the trends that appear in Figures 5.26 and 5.26 show how the system design in terms of pressure drop could influence the overall system performance. The conclusion can now be made that smaller pressure drops are

always better, but the importance of having the pressure drop as small as possible becomes less of an issue as the system delivery size becomes larger.

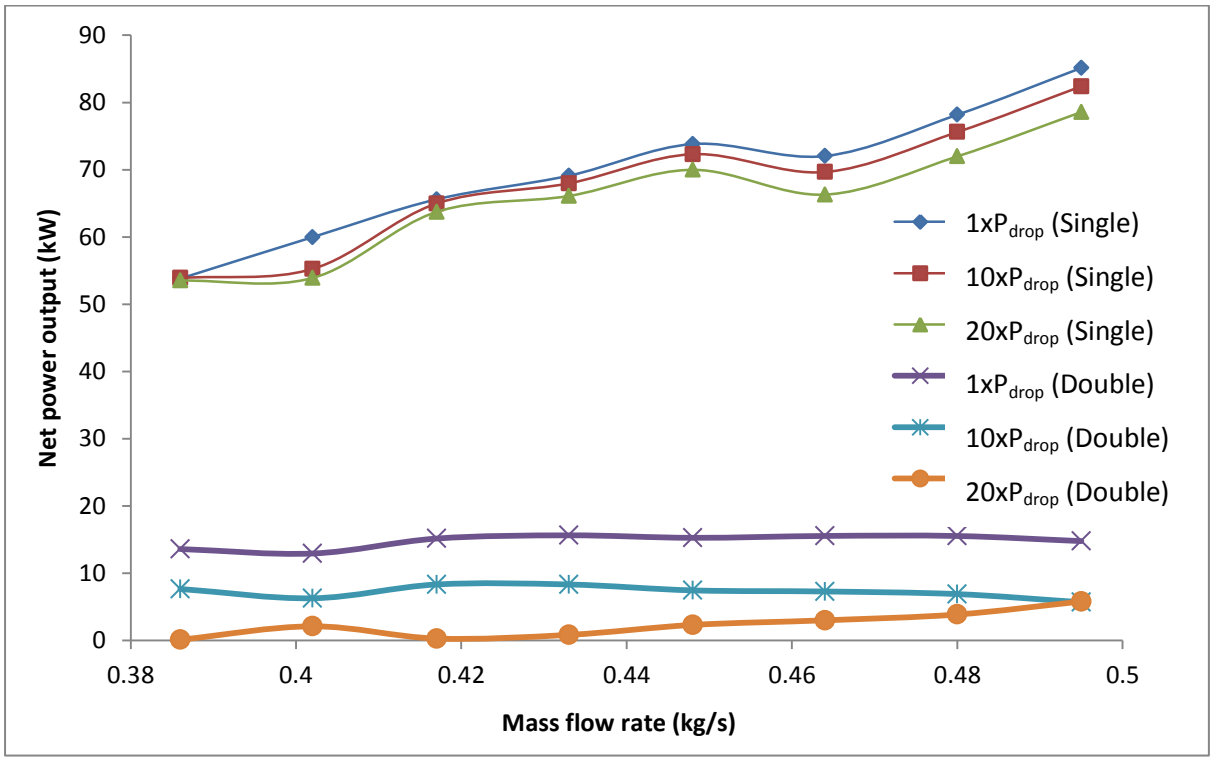

Figure 5.26 Net power output as a function of the mass flow rate at various magnitudes of pressure drop for both the single and double Brayton cycles

5.9 Conclusions

The objective function is the ultimate value on which the cycle under investigation is evaluated. An investigation was made into the significance of the second regenerator and the influence it has on the objective function and efficiency of the cycle. The optimisation was conducted at the various mass flow rates and the resultant optimum values were all compared.

When comparing the respective mass flow rates that go together with these objective function values, it can be seen that a single mass flow rate exists at which the objective function is a maximum, namely at a mass flow rate of 0.433 kg/s.

The regenerator and receiver parameters all vary with the increase in the mass flow rate. The first law net power output continually increases with the increase in mass flow rate. This first law efficiency follows the same trend. The reason for this trend is that the pressure ratio for the cycle dictates the mass flow rate at which the cycle is investigated.

There is no clear relationship between the variations in mass flow rate and objective function. The entropy generation rates for all components are shown and discussed and it was found that the entropy generation rate for the regenerators was the dominant source of entropy generation.

The variation in the regenerator and receiver parameters with the increase in mass flow rate was found and discussed and no clear relationship was found. The behaviour of the variation of these parameters is unstructured.

The change in the inlet temperature of Compressor 1 for the double Brayton cycle was investigated and found to continually decrease as mass flow rate increases.

Validation was carried out to verify the validity of the results for the double Brayton cycle. The investigation into the temperature drop value assumed in the analysis was conducted by first optimising the system at the assumed value. The objective function increased slightly with the increase in temperature drop. The first law net power output stayed constant at various temperature drop values, which can be attributed to the equations used to determine its magnitude. It was found that the value at which the temperature drop was assumed was viable.

The receiver outlet temperature was varied and the optimum was found to be the maximum, namely 1,200 K. For this reason, the assumption concerning the receiver outlet temperature is viable without any doubt.

From the 11 turbines investigated, the largest turbine having the largest mass flow rate was chosen as the test turbine for the optimisation procedure. It became clear that the largest turbine was indeed the best choice for the system at hand as it produced the largest objective function.

The absolute value of the entropy generation rate in the ducts should be added to the overall entropy generation rate in order to produce the worst-case scenario. It was found that if the duct entropy generation rate was only 4% of the overall entropy generation rate, it could make a difference of almost 13% on the objective function.

The single regenerator Brayton cycle was also investigated. It was found that when the mass flow rate was increased gradually from 0.386 kg/s, the objective function (defined as W_{net}) continually increased accordingly. Because of this, the total entropy generation rate and objective

function (second law of thermodynamics' net power output) did not follow similar graph profiles. It was found that both cycles experienced minimum entropy generation rate at a mass flow rate that was slightly larger than 0.4 kg/s.

The two investigated cycles were thoroughly compared. The cycle containing two regenerators seems to be superior to the single cycle with only one regenerator. The simpler cycle containing only one regenerator satisfies the same criteria and constraints as the original double Brayton cycle, however, the resulting temperatures and pressures, as solved by the optimisation algorithm, produce a higher net absorbed heat at the receiver. The efficiency of the original double Brayton cycle, containing two regenerators, is much higher than that of the single regenerator cycle. This leads to the conclusion that the double cycle will perform its needed task for much longer than the single cycle. For this reason, the double open-air solar thermal Brayton cycle is deemed the best choice for the problem at hand.

6 Final conclusions and recommendations

In the initial analysis, it was decided that the Brayton cycle was the best choice for the problem at hand. The advantages of the Brayton cycle include lower pressure ratios, more types of applications and the simplicity of the working fluid, which in this case is air. These advantages would significantly decrease the set-up and operation costs for the power generation cycle that was being optimised. Most of the disadvantages, such as the pressure losses, receiver size and irreversibilities, were included in the optimisation algorithm and were solved in conjunction with the normal power generation cycle.

The modified cavity receiver as suggested by Reddy and Sendhil Kumar [18], was deemed to be the best method of collecting the necessary solar radiation for the power cycle under discussion.

The optimal collector shape was shown to be the parabolic dish collector with factors such as physical size and complexity aiding in the decision-making process.

The combination of the open-air solar thermal Brayton cycle, the parabolic dish collector and the modified cavity receiver was investigated by Le Roux et al. [21]. The results in this dissertation discuss a similar and simpler than cycle than the double Brayton cycle as shown in Figure 3.2. As an added analysis tree, the aforementioned double cycle was also simplified to incorporate only one regenerator. The analyses for the two cycles were properly discussed and compared. An exergetic analysis was completed for the chosen power cycles. The generation of entropy was investigated and possible minimisation strategies were described and conducted. The origin of irreversibilities and losses was investigated and these irreversibilities and losses were included in the numerical analysis of the systems.

The physical system was discussed in terms of the hardware or components that would be used and all the needed assumptions or pitfalls associated with each of these components were identified and properly discussed.

The optimisation algorithm used was discussed. The parameters that were solved with the optimisation algorithm were all identified. The procedure of the optimisation algorithm was deliberated and all stages were discussed at length. The structure of the main analysis of the optimisation algorithm and how the parameters fit into it were also discussed.

The temperature drop in the ducts was investigated to determine the significance of the physical value of temperature drop and its influence on the total system performance. It was found that the assumed value of 2 K was feasible and fit for integration into the optimisation algorithm.

The receiver outlet temperature was varied and it was found that the main factor limiting higher net power outputs was the physical maximum temperature of the materials to be used, which in this case, was copper and was assumed to start melting at 1,200 K.

The 11 turbine choices under investigation showed that the largest turbine in the list was the best choice for the problem at hand. This is due to the fact that this turbine operated in the highest mass flow rate range, which led to the highest objective function values being supplied by this turbine.

The presence of the entropy generation rates in the ducts was investigated and it was found that these entropy generation rates should be included in the analysis, rather than being omitted. This allowed for the overall system result to be more feasible and applicable to modern-society investigations.

As the objective function value was the main parameter on which the cycles were evaluated, care was taken to correctly identify the analytical equations and import them into the numerical optimisation algorithm. A further analysis was conducted to investigate the influence and significance of the second regenerator in the cycle. The analysis was conducted at various mass flow rates and the resultant optimum values were all compared. The receiver parameters showed no clear relationship to the varying mass flow rate of the system. The regenerator parameters included in the optimisation algorithm all varied with the change in mass flow rate.

The first law net power output continually increased as the mass flow rate increased. The first law efficiency followed the same trend. This was caused by the dependency of the mass flow rate on the pressure ratio of the system, and the fact that increasing pressure ratios dictated increasing first law parameters.

There was no clear relation between the mass flow rate and the objective function, also known as the second law net power output. A combination of the entropy generation rates, irreversibilities, physical system parameters and the mass flow rate seemed to be responsible for the unstructured

variation in the objective function values. The entropy generation in the regenerators was the dominant source of the total entropy generation rate in the system.

The absence of the second regenerator in the single cycle explained why the objective function value was so much higher in the single cycle (due to the lower total entropy generation rate). The efficiency of the single cycle was found to be much lower than that of the original double cycle, and this phenomenon could also be attributed to the presence of the second regenerator and the more efficient reuse of waste heat in the double Brayton cycle.

It is now concluded that the double open-air solar thermal Brayton cycle is the best choice for the aforementioned problem. When technology and materials research further improve in the future, some additional alterations can be made to the double Brayton cycle as discussed in the report, and this will almost certainly lead to an even better supply of net power output from a solar thermal source. The efficiency at which this power is produced can be increased with future investigations.

7 References

[1] U.S. DoE. 2000. “The History of Solar,” *Energy efficiency and Renewable Energy*.

[2] "Solar cooking" [Online] Available: http://www.solarcooking.org [Accessed: 31 May 2012].

[3] "The history of solar cooking" [Online] Available: http://www.americanhistory.si.edu [Accessed: 31 May 2012].

[4] “Why Solar Engineering.” [Online] Available: http://www.engineering.com. [Accessed: 31 January 2012].

[5] Chen, L., Zhang, W. & Sun, F. 2007. “Power, efficiency, entropy-generation rate and ecological optimization for a class of generalised irreversible universal heat-engine cycles”. *Applied Energy.* vol. 84, pp. 512–525.

[6] Shah, R.K. 2005. “Compact heat exchangers for micro-turbines”. *Micro gas turbines*. Paper 2. pp. 2.1–2.18.

[7] Kreith, F. & Kreider, J. F.1978. *Principles of solar engineering*. Colorado: Hemisphere.

[8] Bejan, A. 1982. *Entropy generation through heat and fluid flow*. Colorado: John Wiley.

[9] Stine, B.S. & Harrigan, R.W. 1985. *Solar energy: Fundamentals and design*. New York: John Wiley.

[10] Kennedy, C.E. & Price, H. 2005. "Progress in development of high-temperature solar-selective coating". *2005 International Solar Energy Conference*. Aug 6-12

[11] Shuai, Y., Xia, X. & Tan, H. 2008. “Radiation performance of dish solar concentrator/cavity receiver systems”. *Solar Energy*. vol. 82. pp. 13–21.

[12] Prakash, M., Kedare, S.B. & Nayak, J.K. 2009. “Investigations on heat losses from a solar cavity receiver”. *Solar Energy*. vol. 83. pp. 157–170.

[13] Duffie, J.A. & Beckman, W.A. 1991. *Solar engineering of thermal processes.* New York. John Wiley

[14] Heller, P., Pfänder, M., Denk, T., Tellez, F., Valverde, A., Fernandez, J. & Ring, A. 2006. Test and evaluation of a solar powered gas turbine system. *Solar Energy, 80, p. 1225-1230*

[15] Bertocchi, R., Karni, J. & Kribus, A. 2004. Experimental evaluation of a non-isothermal high temperature solar particle receiver. *Energy*, 29, p. 687-700

[16] Reddy, K.S. & Sendhil Kumar, N. 2007. “Comparison of receivers for solar dish collector system”. *Energy Conversion and Management*. vol. 49. no. 4. pp. 812–819.

[17] Reddy K.S. & Sendhil Kumar, N. 2006. “Numerical investigation of natural convection heat loss in modified cavity receiver for fuzzy focal solar dish concentrator”. *Solar Energy.* vol. 81. pp. 846–855.

[18] Reddy K.S. & Sendhil Kumar, N. 2009. “An improved model for natural convection heat loss from modified cavity receiver of solar dish concentrator”. *Solar Energy.* vol. 83. pp. 1884–1892.

[19] Yilmaz, M., Sara, O.N. & Karsli, S. 2001. “Performance evaluation criteria for heat exchangers based on second law analysis”. *Exergy, an International Journal*. vol. 1. no. 4. pp. 278–294.

[20] Bejan, A. 1997. *Advanced Engineering Thermodynamics*. 2nd Ed. Durham: John Wiley.

[21] le Roux, W.G., Bello-Ochende, T. & Meyer, J.P. 2011. “Thermodynamic optimisation of the integrated design of a small-scale solar thermal Brayton cycle”. *International Journal of Energy Research*.

[22] Hesselgreaves, J.E. 2000. “Rationalisation of second law analysis of heat exchangers”. *International journal of Heat and Mass Transfer*. vol. 43. no. 22. pp. 4189–4204.

[23] Narenda, S., Kaushik S.C. & Misra, R.D. 2000. “Exergetic analysis of a solar power system”. *Renewable Energy*. vol. 19. pp. 135–143.

[24] Jubeh, N.M. 2005. “Exergy Analysis and Second Law Efficiency of a Regenerative Brayton Cycle with Isothermal Heat Addition”. *Entropy*. vol. 7. no. 3. pp. 172–187.

[25] Dundas, R.E. *Sawyer’s Gas Turbine Engineering Handbook Volume 1: Design of the Gas Turbine Engine*. Gas Turbine Publications inc.

[26] Sonntag, R.E., Borgnakke, C. & van Wylen, G.J. 2003. *Fundamentals of Thermodynamics*. 6th Ed. New York: John Wiley.

[27] Spliethoff, H. & Schuster, A. 2006. “The Organic Rankine Cycle – Power Production from Low Temperature Heat” Institute for Energy Systems. Technische Universität München.

[28] Müller, N. 2002. “Performance analysis of Brayton and Rankine cycle microsystems for portable power generation” *Power*. pp. 1–10.

[29] Kapooria, R.K., Kumar, S. & Kasana, K.S. 2008. “An analysis of a thermal power plant working on a Rankine cycle: A theoretical investigation”. *Journal of Energy In Southern Africa.* vol. 19. no. 1. pp. 77–83.

[30] Nice, K. “How Stirling engines work”. [Online]. Available: http://www.howstuffworks.com/stirling-engine.html [Accessed: 28 June 2012].

[31] [Online].Available: http://peswiki.com [Accessed: 10 Oct 2013]

[32] Allan, S.D. “World’s largest solar installation to use Stirling engine technology”. [Online]. Available: http:/2005/08/11/9600147_Edison_Stirling_largest_solar/ [Accessed: 28 June 2012].

[33] Bowyer, J.M. 1984. “The Kinematic Stirling Engine as an Energy Conversion Subsystem for Paraboloidal Dish Solar Thermal Power Plants”. *Jet Propulsion Laboratory Report*. vol. JPL 84–30.

[34] Martini, W.R. 1980. *Stirling Engine Design Manual*. May. NASA CR-135382.

[35] Urieli, I. & Berchowitz, D. 1983. *Stirling Cycle Engine Analysis*. New York: Hayden and Sons.

[36] Roos, C. 2008. “Concentrating solar collectors”. *Solar Engineering. Spring 2008*.

[37] Kalogirou, S.A. 2004. *Solar thermal collectors and applications.* vol. 30. no. 3. pp. 231–295.

[38] Zamfirescu, C., Dincer, I., Stern, M. and Wagar, W.R. 2012. "Exergetic, environmental and economic analysis of small-capacity concentrated solar-driven heat engines for power and heat cogeneration." *International Journal of Energy Research.* Vol. 36. p 397-408

[39] Sharma, N., Sharma, P., Irwin, D. and Shenoy, P. 2011b. "Predicting Solar Generation from Weather Forecasts Using Machine Learning." *In Proceedings of Second IEEE International Conference on Smart grid Communicati*on.*(SmartGridComm)*

[40] Fluri, T.P. 2009. The potential of concentrating solar power in South Africa. *Energy Policy,* 37, p. 5075-5080

[41] DME, Department of Minerals and Energy, Republic of South Africa. 2010. *Solar Energy.* [Online]. Available: http://www.dme.gov.za/energy/renew_solar.stm [Accessed: 20 July 2010]

[42] Odeh, S.D., Morrison, G.L. & Behnia, M. 1994. “Thermal analysis of parabolic trough solar collectors for electric power generation”. *Manufacturing Engineering*.

[43] Brooks, M. 2005. “Performance of a parabolic trough solar collector”. *Journal of Energy In Southern Africa*. vol. 17. no. 3. pp. 71–80.

[44] TREC [Online]. Available: http://www.trec-uk.org.uk/images/solar_two_barstow.jpg [Accessed: 20 November 2013].

[45] Garret. “Garret by Honeywell”. 2009. [Online]. Available: http://www.turbobygarret.com [Accessed: 05-Jun-2012].

[46] Ordóñez, J.C. & Bejan, A. 2000. “Entropy generation minimization in parallel-plates counter flow heat exchangers”. *Power*. no. 24. pp. 843–864.

[47] Hartley, J.G. 2001. “Power Generation Cycle Analysis”. *Georgia Institute of Technology*.

[48] Petela, R. 2003. “Exergy of undiluted thermal radiation”. *Solar Energy.* vol. 74. no. 6. pp. 469–488.

[49] Petukhov, B. 1970. “Heat transfer and friction in turbulent pipe flow with variable physical properties”, *Advances in Heat Transfer*. vol. 6. pp. 503–564.

[50] Gnielinski, V. 1976. “New equations for heat and mass transfer in turbulent pipe and channel flow”. *International Chemical Engineering*. vol. 16. pp. 359–368.

[51] Çengel, Y.A. 2006. *Heat and Mass Transfer*. 3rd ed. Nevada. Reno: McGraw-Hill.

[52] Zamfirescu, C. and Dincer, I. 2009. "How mush exergy one can obtain from incident solar radiation?". *Journal of Applied Physics.*105, 044911

[53] Bejan, A., 1996. Method of entropy generation minimization, or modelling and optimization based on combined heat transfer and thermodynamics. Rev Gén Therm, 35, p. 637-646.

Appendices

I Matlab codes

a Main code for double regenerator cycle

This is the code that was employed to calculate all the necessary parameters for the cycle during the optimisation process.

```
close all
clear all
clc

% Stage 1: Define system characteristics to be optimised

%%%%%%% Collector Dish Radius %%%%%%
Rdish = 5;

%%%%% Regenerator Properties %%%%%%%
abreg = 2.31;          % abreg ranges from 1 to 25
Dhreg = 0.00383;       % Dhreg ranges from 0.001 to 0.1
Lreg = 1;              % Lreg ranges from 1 to 3
abrec = 16.31;         % abrec ranges from 1 to 10
Dhrec = 0.0757;        % Dhrec ranges from 0.001 to 0.1
Lrec = 14.7;           % Lrec ranges from 1 to 10

F = [abreg, Dhreg, Lreg, abrec, Dhrec, Lrec];

%%%%%%%%% Pressure Ratio %%%%%%%%%%
r = 1.4;               % r ranges from 0 to 3

%%%%%%%%%% Turbine Number %%%%%%%%%%
mt = 60;

%%%%% Temperatures to be fixed %%%%%%
T14 = 1200;
T11 = 700;

%%%%%% Temperature drop in ducts %%%%%%
Tdrop = 2;

%%%%%%%%% Dish surface area %%%%%%%%%
Tsun = 2470;
depth = Rdish/2;
Ddish = 2*Rdish;
ff = (Ddish^2)/(16*depth);
aaa = 1/(4*ff);
```

```
Area_dish = (pi*((aaa^2*Ddish^2 + 1)^(3/2))-1)/(6*aaa^2);% spherical
dish area

%% Stage 2: Determine mdot from pressure ratio
[mdot,turb_eff,comp_eff] = garret(mt,r);

%% Stage 3: Determine convective porperties
rho_cold1 = 0.381375;
rho_hot1 = 0.2803;
rho_cold2 = 0.5862;
rho_hot2 = 0.4981;
[eff_reg1,eff_reg2,f_cold1,f_cold2,f_hot1,f_hot2,mplate1,mplate2] =
convection_props(F,mdot);

%% Stage 4: Solve cycle unknowns (Temperatures & Pressures)
R = 287;
Cp = 1040;
mu = 4.6e-5;
rho = 0.3008;
P1 = 101325;
T0 = 300;
T1 = T0;

d = 1; % used to investigated the influence of 1x, 10x and 20x the
normal pressure drop in ducts

Pdrop23 = 0.001*d;
Pdrop1213 = Pdrop23;

Pdrop34 =
((f_cold2*F(3)/(F(2))^5)*8*(mplate2^2)*(F(1)^2)/((F(1)+1)^4)/rho_col
d2)/(P1*r*(1-Pdrop23)*1000);

Pdrop45 = 0.004*d;
Pdrop56 =
((f_cold1*F(3)/(F(2))^5)*8*(mplate1^2)*(F(1)^2)/((F(1)+1)^4)/rho_col
d1)/(P1*r*(1-Pdrop45)*1000);

Pdrop67 = 0.004*d;
Pdrop1811 = 0.004*d;
Pdrop1415 = Pdrop67;
Pdrop89 = 0.001*d;
Pdrop1617 = Pdrop89;

Pdrop910 =
(f_hot2*F(3)/(F(2))^5*8*mplate2^2*F(1)^2/(F(1)+1)^4/rho_hot2)/(P1*10
00);
```

```
Pdrop171 =
(f_hot1*F(3)/(F(2))^5*8*mplate1^2*F(1)^2/(F(1)+1)^4/rho_hot1)/(P1*(1
-Pdrop1617)*1000);

k = 1.4;

P10 = P1;
P9 = P10*(1 + Pdrop910);
P8 = P9*(1 + Pdrop89);
P7 = r*P8;
P6 = P7*(1 + Pdrop67);
P5 = P6*(1 + Pdrop56);
P4 = P5*(1 + Pdrop45);
P3 = P4*(1 + Pdrop34);
P2 = P3*(1 + Pdrop23);

Kcomp = (P2/P1).^((k-1)/k);
T2 = T1.*(1+(Kcomp-1)./comp_eff);
T3 = T2 - Tdrop;

P14 = P1;                % assumed value
P14new = P14;
errorP14 = 1;

while errorP14 > 1e-3
P14 = P14new;
P15 = P14*(1 - Pdrop1415);
P16 = P15/r;
P17 = P16*(1 - Pdrop1617);
P18 = P17*(1 - Pdrop1718);
P11 = P18*(1 - Pdrop1811);
P13 = P14 + (0.79*log(4*mdot*F(4)/mu/(F(4)+1)^2/(F(5))-1.64)^-
2)*(8*(mdot^2)*(F(4)^2)/rho/(F(4)+1)^4)*(F(6)/(F(5)^5));
P12 = P13*(1 + Pdrop1213);

T15 = T14 - Tdrop;
Kturb = r.^((k-1)/k);
T16 = T15*(1-turb_eff.*(1-(1./(Kturb))));
T17 = T16 - Tdrop;


Pcomp1 = P12/P11;
iteration = 0;
error2 = 1;
while error2 > 1e-3
    T12 = T11*(1+((((Pcomp1).^((k-1)/k))-1)/comp_eff));
    T13 = T12 - Tdrop;
    Qa = mdot*1145*(T14 - T13);
    T4 = 700;
    error = 1;
```

```
    while error > 1e-3
        T5 = T4 - Tdrop;
        T6 = T5 + eff_reg1*(T17-T5);
        T7 = T6 - Tdrop;
        T8 = T7.*(1-turb_eff.*(1-1/Kturb));
        T9 = T8 - Tdrop;
        T4new = T3 + eff_reg2*(T9 - T3);
        error = norm(T4new - T4)/norm(T4new);
        T4 = T4new;
    end
    T10 = T9 - eff_reg2*(T9-T2);
    T18 = T17-eff_reg1*(T17-T5);
    T11new = T18 - Tdrop;
    error2 = norm(T11new-T11)/norm(T11new);
    T11 = T11new;
    iteration = iteration + 1;
end

P14new = P13*(1-0.04);

errorP14 = abs(P14new-P14)/P14;
end


T = [T1 T2 T3 T4 T5 T6 T7 T8 T9 T10 T11 T12 T13 T14 T15 T16 T17
T18];

%% Stage 5: Determine all entropy generation rates
Sgencomp1 = -mdot*1007*log(T1/T2) + mdot*R*log(P1/P2);
Sgencomp2 = -mdot*1007*log(T11/T12) + mdot*R*log(P11/P12);
Sgencomp = Sgencomp1 + Sgencomp2;

Qloss = 2;
Qloss23 = Qloss;
Sgenduct23 = mdot*1007*log(T3/T2) - mdot*R*log(P3/P2) + Qloss23/T0;
Sgenduct1213 = mdot*1007*log(T13/T12) - mdot*R*log(P13/P12) +
Qloss23/T0;

Qloss45 = Qloss;
Sgenduct45 = mdot*1145*log(T5/T4) - mdot*R*log(P5/P4) + Qloss45/T0;

Qlossreg1 = Qloss;
Qlossreg2 = Qloss;
Sgenreg1 =
mdot*1070*(log((T6*T18)/(T5*T17))*((P6*P18)/(P5*P17))^((1-k)/k)) +
Qlossreg1/T0;
Sgenreg2 = mdot*1070*(log((T4*T10)/(T3*T9))*((P4*P10)/(P3*P9))^((1-
k)/k)) + Qlossreg2/T0;
Sgenreg = Sgenreg1 + Sgenreg2;
```

```
Qstar = Qa;
Tstar = Tsun;
GrD = 5.663E6;
beta = pi./2;
Tw = 1200;
d = sqrt(4*Area_dish/pi);
D = sqrt(3).*d;
k2 = 0.024;
Aa = Area_dish/8;
Qdot0 = 1.396.*(GrD.^0.209).*(1+cos(beta)).^0.968.*(Tw./T0).^-
0.317.*(d./D).^0.425.*(k2.*Aa./D).*(Tw-T0);
Sgenrec = -Qstar./Tstar + Qdot0./T0 + mdot.*Cp.*log(T14./T13)-
mdot.*R.*log(P14./P13);

Qloss67 = Qloss;
Sgenduct67 = mdot*1145*log(T7/T6) - mdot*R*log(P7/P6) + Qloss67/T0;
Sgenduct1415 = mdot*1145*log(T15/T14) - mdot*R*log(P15/P14) +
Qloss67/T0;
Sgenduct1811 = mdot*1145*log(T11/T18) - mdot*R*log(P11/P18) +
Qloss67/T0;

Qloss89 = Qloss;
Sgenduct89 = mdot*1070*log(T9/T8) - mdot*R*log(P9/P8) + Qloss89/T0;
Sgenduct1617 = mdot*1070*log(T17/T16) - mdot*R*log(P17/P16) +
Qloss89/T0;

Sgenturb1 = -mdot*1145*log(T7/T8) + mdot*R*log(P7/P8);
Sgenturb2 = -mdot*1145*log(T15/T16) + mdot*R*log(P15/P16);
Sgenturb = Sgenturb1 + Sgenturb2;

Sgenparts = Sgencomp + Sgenreg + Sgenrec + Sgenturb;
Sgenducts = Sgenduct23 + Sgenduct45 + Sgenduct67 + Sgenduct89 +
Sgenduct1811 + Sgenduct1213 + Sgenduct1415 + Sgenduct1617;

%%%%%%%%%%%%%%%%%%%%%%%%%%%%%%%%%%%
Sgen = Sgenparts + (-1)*Sgenducts;
%%%%%%%%%%%%%%%%%%%%%%%%%%%%%%%%%%%
Sgenductperc = abs(Sgenducts/Sgenparts)*100;
display(Sgenductperc)

% objective function
W = -T0*Sgen + (1-(T0/Tstar))*Qstar + mdot*Cp*(T1-T10) +
mdot*T0*1007*log(T10/T1);

Wc = mdot*1016*(T2-T1) + mdot*753*(T12-T11);
Wt = mdot*1081*(T7-T8) + mdot*1169*(T15-T16);
Wnet1 = Wt - Wc; % Turbine work - Compressor work
```

```
Wnet = abs(W);

%% Stage 6: Determine system irreversibilities
Icomp1 = T0*Sgencomp1;
Icomp2 = T0*Sgencomp2;
Icomp = Icomp1 + Icomp2;
Ireg1 = T0*Sgenreg2;
Ireg2 = T0*Sgenreg1;
Ireg = Ireg1 + Ireg2;
Irec = T0*Sgenrec;
Iturb1 = T0*Sgenturb1;
Iturb2 = T0*Sgenturb2;
Iturb = Iturb1 + Iturb2;
Iinternal = Icomp + Ireg + Iturb + Irec;
Iexternal = mdot.*Cp.*(T1 - T10) - mdot.*T0.*Cp.*(T1./T10);
Iexternal = Iexternal*(-1);

%% Stage 7: Determine thermal efficiencies
th_eff1 = Wnet1/Qa;

%% Stage 8: Check system solution for validity
tempcheck(T)
sgencheck_2reg(Sgencomp1,Sgencomp2,Sgenreg1,Sgenreg2,Sgenrec,Sgentur
b1,Sgenturb2);
```

b Main code for single regenerator cycle

This is the code that was employed to calculate all the necessary parameters for the cycle during the optimisation process.

```
close all
clear all
clc

% Stage 1: Define system characteristics to be optimised

%%%%%%% Collector Dish Radius %%%%%%
Rdish = 5;

%%%%% Regenerator Properties %%%%%%%
abreg = 29.4;          % abreg ranges from 1 to 25
Dhreg = 0.0016;        % Dhreg ranges from 0.001 to 0.1
Lreg = 5;              % Lreg ranges from 1 to 3
abrec = 4.472;         % abrec ranges from 1 to 10
Dhrec = 0.0702;        % Dhrec ranges from 0.001 to 0.1
Lrec = 9.416;          % Lrec ranges from 1 to 10
F = [abreg, Dhreg, Lreg, abrec, Dhrec, Lrec];

%%%%%%%%% Pressure Ratio %%%%%%%%%%
r = 2.1;               % r ranges from 0 to 3

%%%%%%%%%% Turbine Number %%%%%%%%%%
mt = 60;

%%%%% Temperatures to be fixed %%%%%%
T10 = 1200;
T7 = 800;

%%%%%% Temperature drop in ducts %%%%%%
Tdrop = 2;

%%%%%%%%% Dish surface area %%%%%%%%%
Tsun = 2470;
depth = Rdish/2;
Ddish = 2*Rdish;
ff = (Ddish^2)/(16*depth);
aaa = 1/(4*ff);
Area_dish = (pi*((aaa^2*Ddish^2 + 1)^(3/2))-1)/(6*aaa^2);   %
spherical dish area

%% Stage 2: Determine mdot from pressure ratio
[mdot,turb_eff,comp_eff] = garret(mt,r);

%% Stage 3: Determine convective porperties
rho_cold1 = 0.381375;
rho_hot1 = 0.2803;
rho_cold2 = 0.5862;
rho_hot2 = 0.4981;
[eff_reg1,eff_reg2,f_cold1,f_cold2,f_hot1,f_hot2,mplate1,mplate2] =
convection_props(F,mdot);
```

```
%% Stage 4: Solve cycle unknowns (Temperatures & Pressures)
R = 287;
Cp = 1040;
mu = 4.6e-5;
rho = 0.3008;
P1 = 101325;
T0 = 300;
T1 = T0;

Pdrop23 = 0.001*20;
Pdrop89 = Pdrop23;

Pdrop34 =
((f_cold1*F(3)/(F(2))^5)*8*(mplate1^2)*(F(1)^2)/((F(1)+1)^4)/rho_col
d1)/(P1*r*(1-Pdrop23)*1000);

Pdrop45 = 0.004*20;
Pdrop147 = 0.004*20;
Pdrop1011 = Pdrop45;
Pdrop1213 = 0.001*20;

Pdrop1314 =
(f_hot1*F(3)/(F(2))^5*8*mplate1^2*F(1)^2/(F(1)+1)^4/rho_hot1)/(P1*(1
-Pdrop1213)*1000);

k = 1.4;

P6 = P1;
P5 = r*P6;
P4 = P5*(1 + Pdrop45);
P3 = P4*(1 + Pdrop34);
P2 = P3*(1 + Pdrop23);

Kcomp = (P2/P1).^((k-1)/k);
T2 = T1.*(1+(Kcomp-1)./comp_eff);
T3 = T2 - Tdrop;

P10 = P1;                % assumed value
P11 = P10*(1 - Pdrop1011);
P12 = P11/r;
P13 = P12*(1 - Pdrop1213);
P14 = P13*(1 - Pdrop1314);
P7 = P14*(1 - Pdrop147);

P9 = P10 + (0.79*log(4*mdot*F(4)/mu/(F(4)+1)^2/(F(5))-1.64)^-
2)*(8*(mdot^2)*(F(4)^2)/rho/(F(4)+1)^4)*(F(6)/(F(5)^5));
P8 = P9*(1 + Pdrop89);

Pcomp1 = P8/P7;

error = 1;
while error > 1e-3
    T8 = T7*(1+((((Pcomp1).^((k-1)/k))-1)/comp_eff));
    T9 = T8 - Tdrop;
    Qa = mdot*1145*(T10 - T9);
```

```
    T11 = T10 - Tdrop;
    Kturb = r.^((k-1)/k);
    T12 = T11*(1-turb_eff.*(1-(1./(Kturb))));
    T13 = T12 - Tdrop;
    T14 = T13-eff_reg1*(T13-T3);
    T7new = T14 - Tdrop;
    error = norm(T7new-T7)/norm(T7new);
    T7 = T7new;
end

T4 = T3 + eff_reg1*(T13-T3);
T5 = T4 - Tdrop;
T6 = T5.*(1-turb_eff.*(1-1/Kturb));

T = [T1 T2 T3 T4 T5 T6 T7 T8 T9 T10 T11 T12 T13 T14];

%% Stage 5: Determine all entropy generation rates
Sgencomp1 = -mdot*1007*log(T1/T2) + mdot*R*log(P1/P2);
Sgencomp2 = -mdot*1007*log(T7/T8) + mdot*R*log(P7/P8);
Sgencomp = Sgencomp1 + Sgencomp2;

Qloss = 2;
Qloss23 = Qloss;
Sgenduct23 = mdot*1007*log(T3/T2) - mdot*R*log(P3/P2) + Qloss23/T0;
Sgenduct89 = mdot*1007*log(T9/T8) - mdot*R*log(P9/P8) + Qloss23/T0;

Qlossreg1 = Qloss;
Sgenreg1 =
mdot*1070*(log((T4*T14)/(T3*T13))*((P4*P14)/(P3*P13))^((1-k)/k)) +
Qlossreg1/T0;

Qstar = Qa;
Tstar = Tsun;
GrD = 5.663E6;
beta = pi./2;
Tw = 1200;
d = sqrt(4*Area_dish/pi);
D = sqrt(3).*d;
k2 = 0.024;
Aa = Area_dish/8;
Qdot0 = 1.396.*(GrD.^0.209).*(1+cos(beta)).^0.968.*(Tw./T0).^-
0.317.*(1./sqrt(3)).^0.425.*(k2.*Aa./D).*(Tw-T0);
Sgenrec = -Qstar./Tstar + Qdot0./T0 + mdot.*Cp.*log(T10./T9)-
mdot.*R.*log(P10./P9);

Qloss45 = Qloss;
Sgenduct45 = mdot*1145*log(T5/T4) - mdot*R*log(P5/P4) + Qloss45/T0;
Sgenduct1011 = mdot*1145*log(T11/T10) - mdot*R*log(P11/P10) +
Qloss45/T0;
Sgenduct147 = mdot*1145*log(T7/T14) - mdot*R*log(P7/P14) +
Qloss45/T0;

Qloss1213 = Qloss;
Sgenduct1213 = mdot*1070*log(T13/T12) - mdot*R*log(P13/P12) +
Qloss1213/T0;
```

```
Sgenturb2 = -mdot*1145*log(T5/T6) + mdot*R*log(P5/P6);
Sgenturb1 = -mdot*1145*log(T11/T12) + mdot*R*log(P11/P12);
Sgenturb = Sgenturb1 + Sgenturb2;

Sgenparts = Sgencomp + Sgenreg1 + Sgenrec + Sgenturb;
Sgenducts = Sgenduct23 + Sgenduct45 + Sgenduct89 + Sgenduct147 +
Sgenduct1213 + Sgenduct1011;

% %%%%%%%%%%%%%%%%%%%%%%%%%%%%%%%%%%
Sgen = Sgenparts + (-1)*Sgenducts;
% %%%%%%%%%%%%%%%%%%%%%%%%%%%%%%%%%%
Sgenductperc = abs(Sgenducts/Sgenparts)*100;
display(Sgenductperc)

% objective function
W = -T0*Sgen + (1-(T0/Tstar))*Qstar + mdot*Cp*(T1-T6) +
mdot*T0*1007*log(T6/T1);

Wc = mdot*1016*(T2-T1) + mdot*753*(T8-T7);
Wt = mdot*1081*(T5-T6) + mdot*1169*(T11-T12);
Wnet1 = Wt - Wc; % Turbine work - Compressor work

Wnet = abs(W);

%% Stage 6: Determine system irreversibilities
Icomp1 = T0*Sgencomp1;
Icomp2 = T0*Sgencomp2;
Icomp = Icomp1 + Icomp2;
Ireg1 = T0*Sgenreg1;
Ireg = Ireg1;
Irec = T0*Sgenrec;
Iturb1 = T0*Sgenturb1;
Iturb2 = T0*Sgenturb2;
Iturb = Iturb1 + Iturb2;
Iinternal = Icomp + Ireg + Iturb + Irec;
Iexternal = mdot.*Cp.*(T1 - T6) - mdot.*T0.*Cp.*(T1./T6);
Iexternal = Iexternal*(-1);

%% Stage 7: Determine thermal efficiencies
th_eff1 = Wnet1/Qa;

%% Stage 8: Check system solution for validity
tempcheck(T)
sgencheck_1reg(Sgencomp1,Sgencomp2,Sgenreg1,Sgenrec,Sgenturb1,Sgentu
rb2);
```

c The 'garret' function

The 'garret.m' function was set up to take the turbine choice and the pressure ratio, and use a data file named 'garret_long.csv', which contains the maximum and minimum values of pressure ratio and mass flow rate for each of the turbines, and to use these values and the input (operation) pressure ratio to find the operation mass flow rate through interpolation.

```
function [mdot,turb_eff,comp_eff] = garret(mt,r)

G = csvread('garret_long.csv',0,1); % read data from Garret.pdf %

TN = G(:,1);          % Turbine Number
PRRmin = G(:,2);      % Pressure Ratio minimum
PRRmax = G(:,3);      % Pressure Ratio maximum
MFRmin = G(:,6);      % Mass Flow Rate minimum
MFRmax = G(:,7);      % Mass Flow Rate maximum
MTE = G(:,8);         % Maximum Turbine Efficiency
MCE = G(:,9);         % Maximum Compressor Efficiency

OMFR = ((MFRmax(mt)-MFRmin(mt))./(PRRmax(mt)-PRRmin(mt))).*(r -
PRRmin(mt)) + MFRmin(mt);% Optimal Mass Flow Rate

MCE = MCE(mt);
MTE = MTE(mt);

mdot = OMFR;
turb_eff = MTE/100;
comp_eff = MCE/100;

end
```

d The 'convection props' function

The 'convection_props.m' function is used to determine the regenerator efficiencies by employing the ε-NTU method.

```
function
[eff_reg1,eff_reg2,f_cold1,f_cold2,f_hot1,f_hot2,mplate1,mplate2] =
convection_props(X,mdot)

H = 1;
t = 0.001;
ksolid = 401;

% Regenerator 1
% Cold side 5-6 - assume values to be at 928K ~ 655degC
Pr_cold1 = 0.7067;
k_cold1 = 0.063614;
Cp_cold1 = 1126;

mu_cold1 = 3.99E-5;

mplate1 = (2*mdot/H*(t + X(2)/1000/X(1)/2*(X(2)+1)));

Re_cold1 = (4*mplate1*X(1))/(mu_cold1*X(2)*((X(1) + 1)^2));

f_cold1 = (0.79*log(Re_cold1) - 1.64)^-2;

Nu_cold1 = (f_cold1/8)*Pr_cold1*(Re_cold1-
1000)/(1+(12.7*((f_cold1/8)^0.5)*((Pr_cold1^(2/3))-1)));

h_cold1 = k_cold1*Nu_cold1/X(2);

% Hot side 17-18 - assume values to be at 1260K ~ 987degC
Pr_hot1 = 0.7253;
k_hot1 = 0.07816;
Cp_hot1 = 1182;

mu_hot1 = 4.8E-5;

Re_hot1 = (4*mplate1*X(1))/(mu_hot1*X(2)*((X(1) + 1)^2));

f_hot1 = (0.79*log(Re_hot1)-1.64)^-2;

Nu_hot1 = f_hot1/8*Pr_hot1*(Re_hot1-
1000)/(1+12.7*(f_hot1/8)^0.5*(Pr_hot1^(2/3)-1));

h_hot1 = k_hot1/X(2)*Nu_hot1;

% Regenerator 2 (choose different temps for hot and cold
% Cold side 3-4 - assume values to be at 603K ~ 330degC
Pr_cold2 = 0.6936;
k_cold2 = 0.045998;
Cp_cold2 = 1051;

mu_cold2 = 3.03E-5;
```

```
mplate2 = mplate1;

Re_cold2 = (4*mplate2*X(1))/(mu_cold2*X(2)*((X(1)+ 1)^2));

f_cold2 = (0.79*log(Re_cold2) - 1.64)^-2;

Nu_cold2 = f_cold2/8*Pr_cold2*(Re_cold2-
1000)/(1+12.7*(f_cold2/8)^0.5*(Pr_cold2^(2/3)-1));

h_cold2 = k_cold2/X(2)*Nu_cold2;

% Hot side 9-10 - assume values to be at 709K ~ 436degC
Pr_hot2 = 0.6960;
k_hot2 = 0.052188;
Cp_hot2 = 1078;

mu_hot2 = 3.37E-5;

Re_hot2 = (4*mplate2*X(1))/(mu_hot2*X(2)*((X(1) + 1)^2));

f_hot2 = (0.79*log(Re_hot2)-1.64)^-2;

Nu_hot2 = f_hot2/8*Pr_hot2*(Re_hot2-
1000)/(1+12.7*(f_hot2/8)^0.5*(Pr_hot2^(2/3)-1));

h_hot2 = k_hot2/X(2)*Nu_hot2;

% e-NTU
Rf = 0.0004; % fouling factor for air

Aplate1 = X(3)*X(2)*(X(1)+1)*(1+1/X(1));
Aplate2 = Aplate1; % can be made different to Aplate1

U1 = (1/h_cold1 + 2*Rf + X(3)/ksolid + 1/h_hot1)^-1;
U2 = (1/h_cold2 + 2*Rf + X(3)/ksolid + 1/h_hot2)^-1;

NTU1 = U1*Aplate1/(mplate1*Cp_cold1);
NTU2 = U2*Aplate2/(mplate2*Cp_cold2);

c1 = Cp_cold1/Cp_hot1;
c2 = Cp_cold2/Cp_hot2;

eff_reg1 = (1-exp(-NTU1*(1-c1)))/(1-c1*exp(-NTU1*(1-c1)));
eff_reg2 = (1-exp(-NTU2*(1-c2)))/(1-c2*exp(-NTU2*(1-c2)));

if eff_reg1 > 1
    display('eff_reg1 not valid')
end

if eff_reg2 > 1
    display('eff_reg2 not valid')
end
```

e The "sgencheck_2reg" function

The 'sgencheck_2reg.m' function checks the double regenerator cycle for discrepancies in terms of the entropy generation rates that are determined. If any of these values are output as negative the user is notified of where the problem is so that the temperature and pressure values at this position can be corrected.

```
function [] =
sgencheck_2reg(Sgencomp1,Sgencomp2,Sgenreg1,Sgenreg2,Sgenrec,Sgentur
b1,Sgenturb2)
Sgencomp = Sgencomp1 + Sgencomp2;
Sgenreg = Sgenreg1 + Sgenreg2;
Sgenturb = Sgenturb1 + Sgenturb2;

if Sgencomp1 < 0
    display('No solution - Comp1 fail');
end

if Sgencomp2 < 0
    display('No solution - Comp2 fail');
end

if Sgencomp < 0
    display('No solution - Comp TOTAL fail');
end

if Sgenreg1 < 0
    display('No solution - Reg1 fail');
end

if Sgenreg2 < 0
    display('No solution - Reg1 fail');
end

if Sgenreg < 0
    display('No solution - Reg TOTAL fail')
end

if Sgenrec < 0
    display('No solution - Rec fail');
end

if Sgenturb1 < 0
    display('No solution - Turb1 fail');
end

if Sgenturb2 < 0
    display('No solution - Turb2 fail');
end

if Sgenturb < 0
    display('No solution - Turb TOTAL fail');
end
end
```

f The "sgencheck_1reg" function

The 'sgencheck_1reg.m' function checks the single regenerator cycle for discrepancies in terms of the entropy generation rates that are determined. If any of these values are output as negative the user is notified of where the problem is so that the temperature and pressure values at this position can be corrected.

```
function [] =
sgencheck_1reg(Sgencomp1,Sgencomp2,Sgenreg1,Sgenrec,Sgenturb1,Sgentu
rb2)
Sgencomp = Sgencomp1 + Sgencomp2;
Sgenreg = Sgenreg1;
Sgenturb = Sgenturb1 + Sgenturb2;

if Sgencomp1 < 0
    display('No solution - Comp1 fail');
end

if Sgencomp2 < 0
    display('No solution - Comp2 fail');
end

if Sgencomp < 0
    display('No solution - Comp TOTAL fail');
end

if Sgenreg1 < 0
    display('No solution - Reg1 fail');
end

if Sgenreg < 0
    display('No solution - Reg TOTAL fail')
end

if Sgenrec < 0
    display('No solution - Rec fail');
end

if Sgenturb1 < 0
    display('No solution - Turb1 fail');
end

if Sgenturb2 < 0
    display('No solution - Turb2 fail');
end

if Sgenturb < 0
    display('No solution - Turb TOTAL fail');
end
end
```

II Turbine options

The initial list of 60 or more turbines as found in the Garret by Honeywell [45] turbocharger catalogues was considered, and these turbine options are shown in Table II.1. From this initial list of turbine options, the 11 turbines for investigation as in Table 4.1 were taken. These 11 turbines are shown in bold in Table II.1.

Table II.1 Initial list of turbine options

	Turbine number	Pressure ratio minimum	Pressure ratio maximum	Mass flow rate minimum (kg/s)	Mass flow rate maximum (kg/s)	Maximum turbine efficiency (%)	Maximum compressor efficiency (%)
GT1241	1	1.3	2.75	0.036	0.052	65	76
GT1544	2	1.25	3.75	0.032	0.047	62	76
GT1548	3	1.25	3	0.034	0.06	62	72
GT2052	4	1.25	3	0.054	0.085	70	77
GT2056	5	1.2	3	0.045	0.079	65	78
GT2252	6	1.15	3	0.064	0.119	68	78
GT2259	7	1.25	3	0.064	0.106	70	76
GT2554R	8	1.18	2.95	0.06	0.112	65	71
GT2560R	9	1.18	2.95	0.06	0.112	65	73
GT2854R	10	1.12	2.95	0.03	0.121	75	71
GT2859R	11	1.12	2.95	0.03	0.121	75	76
GT2860R 62	12	1.12	2.95	0.03	0.121	78	71
GT2860RS 0.64	13	1.3	2.95	0.083	0.132	72	76
GT2860RS 0.86	14	1.2	2.95	0.106	0.159	72	76
GT2871R	15	1.2	2.95	0.076	0.132	60	76
GT2876R 0.64	16	1.3	2.95	0.083	0.132	62	76
GT2876R 0.86	17	1.2	2.95	0.098	0.159	62	76
GT3071R 0.63	18	1.3	2.9	0.102	0.151	72	78
GT3071R 0.82	19	1.25	2.9	0.113	0.174	72	78
GT3071R 1.09	20	1.18	2.9	0.132	0.204	72	78
GT3076R 0.63	21	1.28	2.95	0.102	0.155	72	77
GT3076R 0.82	22	1.22	2.95	0.113	0.178	72	77
GT3076R 1.06	23	1.2	2.95	0.132	0.204	72	77
GT3271	24	1.2	3	0.094	0.151	64	77
GT35R 0.63	25	1.3	2.85	0.113	0.174	70	79
GT35R 0.82	26	1.25	2.85	0.121	0.204	70	79
GT35R 1.06	27	1.25	2.85	0.151	0.242	70	79
GT3582R 0.63	28	1.3	2.85	0.113	0.174	70	78
GT3582R 0.82	29	1.25	2.85	0.121	0.204	70	78
GT3582R 1.06	30	1.25	2.85	0.151	0.242	70	78
GT3776	31	1.2	2.85	0.159	0.249	68	77
GT4088R 0.85	32	1.15	2.95	0.136	0.242	70	78

GT4088R 0.95	33	1.15	2.95	0.151	0.253	70	78
GT4088R 1.06	34	1.12	2.95	0.159	0.265	70	78
GT4088R 1.19	35	1.12	2.9	0.166	0.28	70	78
GT4088 1.19	36	1.25	3	0.174	0.295	68	74
GT4088 1.34	37	1.2	2.95	0.174	0.302	68	74
GT4094R 0.85	38	1.125	2.95	0.136	0.242	70	77
GT4094R 0.95	39	1.12	2.95	0.151	0.253	70	77
GT4094R 1.06	40	1.12	2.95	0.159	0.265	70	77
GT4094R 1.19	41	1.12	2.9	0.166	0.28	70	77
GT4202 1.01	**42**	**1.2**	**3**	**0.181**	**0.283**	**74**	**77**
GT4202 1.15	**43**	**1.2**	**3**	**0.204**	**0.31**	**74**	**77**
GT4202 1.28	**44**	**1.2**	**3**	**0.227**	**0.329**	**74**	**77**
GT4202 1.44	**45**	**1.2**	**3**	**0.234**	**0.34**	**74**	**77**
GT4294R 1.01	**46**	**1.2**	**3**	**0.181**	**0.283**	**74**	**78**
GT4294R 1.15	**47**	**1.2**	**3**	**0.204**	**0.31**	**74**	**78**
GT4294R 1.28	**48**	**1.2**	**3**	**0.227**	**0.325**	**74**	**78**
GT4294R 1.44	**49**	**1.2**	**3**	**0.234**	**0.34**	**74**	**78**
GT4708 0.96	50	1.5	3	0.219	0.325	69	79
GT4708 1.08	51	1.45	3	0.227	0.355	69	79
GT4708 1.23	52	1.35	3	0.227	0.378	69	79
GT4708 1.39	53	1.2	3	0.227	0.423	69	79
GT4718 0.96	54	1.5	3	0.219	0.325	69	78
GT4718 1.08	55	1.45	3	0.227	0.355	69	78
GT4718 1.23	56	1.35	3	0.227	0.378	69	78
GT4718 1.39	57	1.2	3	0.227	0.423	69	78
GT5533R	**58**	**1.2**	**3.25**	**0.249**	**0.454**	**80**	**77**
GT5541R	**59**	**1.2**	**3.25**	**0.249**	**0.454**	**80**	**75**
GT6041	**60**	**1.25**	**3**	**0.363**	**0.635**	**78**	**80**

Seen below is a turbine map taken from the Garret by Honeywell catalogue for a random turbine to illustrate how the turbine selection was made. This turbine is the GT5533R. These maps were used in the set-up of the turbine property tables.

Figure II.1 Turbine map for the GT5533R turbine

In the above turbine map, the minimum and maximum values for the operation pressure ratio for the turbine are seen at the left-most and right-most ends of the solid line, located in the middle of the graph respectively. The top- and bottom-most points on this same line were taken as the maximum and minimum values for the turbine mass flow rate respectively. The interpolation function in Appendix Ic finds the mass flow rate of operation for any given pressure ratio that falls within these maximum and minimum values. Also shown in Figure II.1 is the maximum isentropic efficiency that can be achieved by this given turbine within its range of operation.

As for the island of operation as found in Figure II.2, the design or choice of any turbine should be made such that the points of operation, i.e. the choices of pressure ratio and their respective mass flow rates, fall within the solid line island. The closer to the centre of an island the design points are, the better. When considering Figure II.2, it can also be seen that the solid lines in the island denote isentropic efficiencies for the compressors that are to be used in conjunction with the turbines. It is from these islands that the maximum isentropic efficiencies of all the compressors for each of the turbine choices were taken and used in the optimisation algorithm.

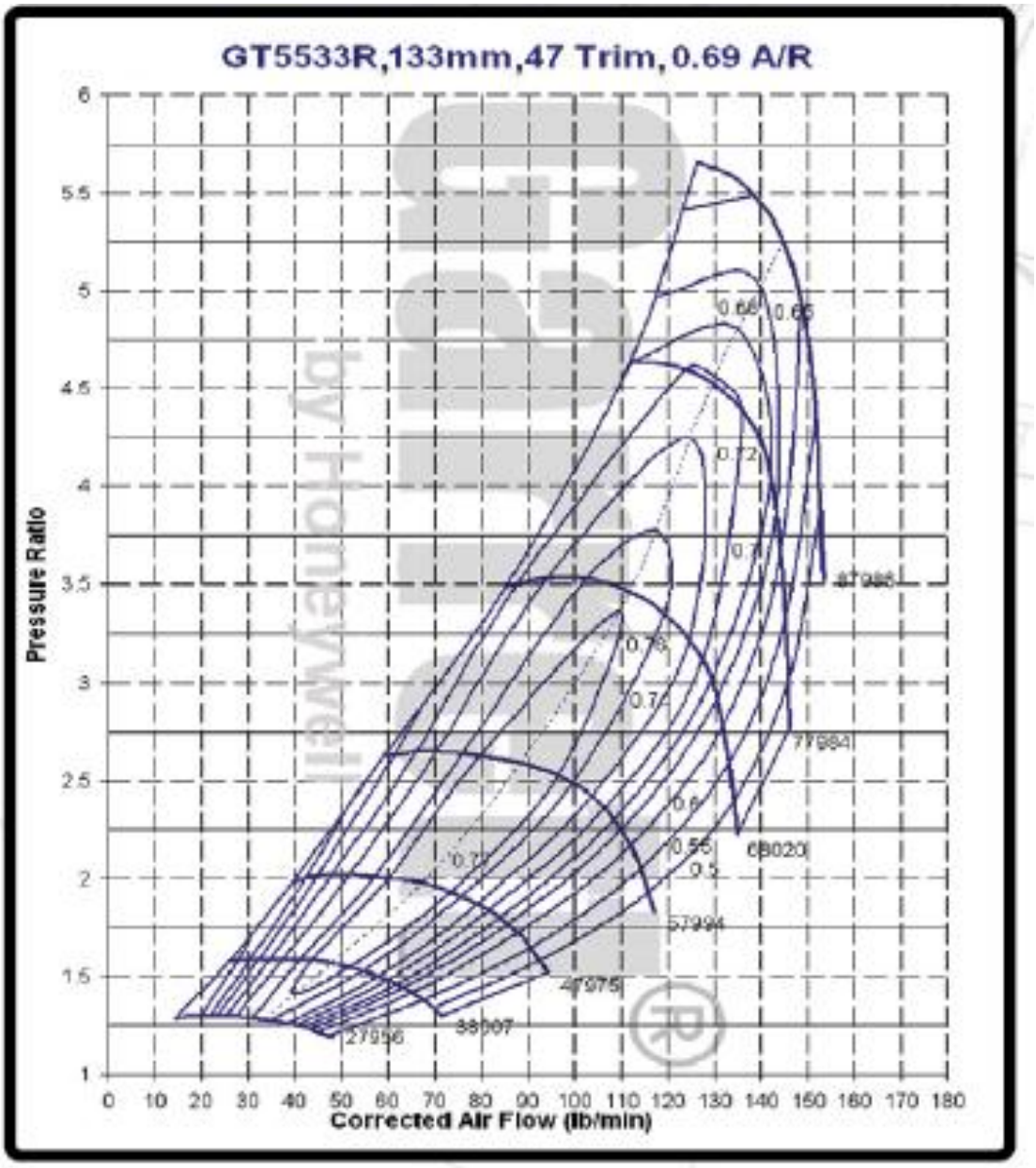

Figure II.2 Operation island for the GT5533R turbine